Characterization and Application of Large Disposable Shaking Bioreactors

Von der Fakultät für Maschinenwesen der
Rheinisch-WestfälischenTechnischen Hochschule Aachen
zur Erlangung des akademischen Grades eines Doktors der
Ingenieurwissenschaften genehmigte Dissertation

vorgelegt von

Keyur Raval

aus

Rajkot, Indien

Berichter: Universitätsprofessor Dr.-Ing. J. Büchs
Universitätsprofessor Dr.-Ing. U. Renz

Tag der mündlichen Prüfung: 14. April 2008

Diese Dissertation ist auf den Internetseiten der Hochschulbibliothek online verfügbar.

Acknowledgement

I am highly indebted to my parents and my Guru Shree Jayantikaka for shaping up my life from childhood to date and helping me to build up internal strength.

I feel great pleasure in expressing my gratitude to my guide Professor Dr.-Ing. Jochen Büchs for his expert guidance and constant encouragement throughout the period of the project work. I am extremely indebted for his motivation, professional acumen and precious time that he devoted for successful completion of my project work. He was and still remains a father figure in my life.

I express my heartiest thanks to my colleagues Cyril Peter, Andreas Daub and Arnd Knoll who were always there not only for technical brain storming but also at vital moments of my life.

Last but not least, I am very thankful to my wife, Ritu; who is always there to hold and support me during the most painful moments of my life.

Kurzfassung

In dieser Forschungsarbeit wird die Anwendung eines geschüttelten Bioreaktorsystems im Pilotmaßstab dargestellt. Diese sehr einfache, vielfältige und allgemein verwendbare Technologie wurde mit zylinderförmigen Einwegreaktoren kombiniert, um sie zu einer idealen Wahl für die Kultivierung von Pflanzen-, Tier- und Insektenzellkulturen zur Produktion im Pilotmaßstab zu machen. Die zylinderförmigen Reaktoren der Größe 2L, 20L und 50L wurden in Bezug auf wichtige Betriebseigenschaften wie Mischen, Leistungseintrag, Wärmeübertragungsrate und Sauerstofftransferrate eingehend charakterisiert. Die vollständige Vermischung der Flüssigkeit wurde innerhalb weniger Sekunden bei einer Schüttelfrequenz von 80 U/min erreicht. Die Leistungsaufnahme von Flüssigkeiten, deren physikalische Eigenschaften sich nicht drastisch mit der Temperatur verändern, wurde durch die Temperaturmethode gemessen. Die Methode wurde modifiziert, um die Änderungen physikalischer Eigenschaften der Flüssigkeiten mit der Temperatur zu berücksichtigen, wie z.B. die Viskosität und die Dichte. Betriebsbedingungen, in denen eine sehr schlechte Vermischung beobachtet werden konnte, wurden identifiziert und der Leistungseintrag des Reaktorsystems dimensionslos beschrieben. Hohe Wärmeerzeugungsraten wurden in 20L- und 50L-Reaktoren, besonders für Schüttelfrequenzen über 230 U/min beobachtet. Experimente zeigten eine maximale Zunahme der Flüssigkeitstemperatur für Wasser und für ein 80%-Glycerol-Wasser-Gemisch von 16 K bzw. 30 K bei 300 U/min. Während eine vollständige Belüftung für langsam wachsende Tier- und Insektenzellkulturen nicht zwingend erforlich ist, ist eine vollständige Belüftung mit Umgebungsluft jedoch besonders für Hochzelldichte-Kultivierungen schnell wachsender Pflanzenzellkultursysteme wie z.B. *Nicotiana tabacum* notwendig, um eine Temperaturbeanspruchung zu vermeiden. Die Sauerstofftransferrate wurde durch die gut erforschte Sulfitoxidationsmethode gemessen. Die maximalen Sauerstofftransferraten, die im 20L- und 50L-Reaktor gemessen wurden, waren 0.032 mol/L/h bzw. 0.028 mol/L/h. Der Stofftransferkoeffizient wurde mit der Energiedissipation korreliert. Die Maßstabsvergrößerung eines Produktionsprozesses für ein therapeutisches Protein, basierend auf *Nicotiana tabacum* Pflanzenzellsuspensionskultur, wurde erfolgreich vom 250mL-Schüttelkolben zum 50L Einwegbioreaktor durchgeführt. Die Maßstabsvergrößerung zum 2L-Einwegbioreaktor für einen Prozess zur Kultivierung tierischer Zellen, basierend auf hybridoma-cmyc Zellen, war ebenfalls erfolgreich.

Abstract

Application of a shaking bioreactor system at pilot-scale level is presented in this research work. This very simple, versatile and widely used technology was combined with the cylindrical disposable reactors to make it an ideal choice for cultivation of plant, animal and insect cell cultures for pilot-scale production. Cylindrical reactors of size 2L, 20L and 50L were thoroughly characterized in terms of important engineering parameters such as mixing, power consumption, heat transfer rate and oxygen transfer rate. Complete mixing of fluid was achieved within few seconds at shaking frequencies as low as 80 rpm. Power consumption for fluids whose physical properties do not vary drastically over temperature was measured by the temperature method. The method was extended to incorporate changes in fluid physical properties such as viscosity, density etc. over temperature. Operating conditions where poor mixing might be observed were identified and a non-dimensional description of power consumption is given for the reactor system. High rates of heat generation were observed in 20L and 50L reactors especially for shaking frequencies higher than 230 rpm. Experiments revealed maximum of 16 K and 30 K increase in fluid temperature for water and a 80% glycerol/water mixture at 300 rpm, respectively. Although thorough ventilation may not be mandatory for slow growing animal and insect cell culture, a thorough ventilation of the surrounding atmosphere is mandatory, especially for high cell density cultivation of fast growing plant cell culture systems e.g. *Nicotiana tabacum* suspension culture to avoid any temperature stress. Oxygen transfer rate was measured by a well researched sulfite oxidation method. The maximum value of oxygen transfer rate measured in 20L and 50L reactors were 0.032 mol/L/h and 0.028 mol/L/h, respectively. Mass transfer coefficient was correlated with respect to energy dissipation. A therapeutic protein production process based on relatively less hydro-mechanical stress sensitive and one of the fastest growing *N. tabacum* plant cell suspension culture was successfully scaled-up from a 250 mL shake flask culture to 50L cylindrical disposable shaking bioreactor. The cell growth and protein production was comparable to that observed in other bioreactor systems. An animal cell culture process based on hybridoma-cmyc cells was also scaled-up successfully to a 2L cylindrical disposable shaking bioreactor.

Table of contents

1. Introduction and objectives 1
2. Literature review 6
2.1. Shaking bioreactors 6
2.1.1. Mixing and power consumption 6
2.1.2. Mass transfer characteristics of shaking bioreactors 7
2.1.3. Ventilation in shaking bioreactors 9
2.2. Application of disposable shaking bioreactors 9
3. Theory 13
3.1. Conventional temperature method 13
3.2. Extended temperature method 13
3.3. Oxygen transfer rate measurement 15
3.3.1. The sulfite system 15
3.3.2. Online oxygen transfer rate measurement 16
3.3.3. Calibration of the oxygen sensor 17
3.3.4. Material balance on oxygen at steady-state (in the rinsing phase) 18
3.3.5. Material balance in measuring phase 20
3.4. Ventilation in shake flasks 23
4. Materials and methods 25
4.1. Hydrophilic shake flasks 25
4.2. Hydrophobic shake flasks 25
4.3. Mixing performance 25
4.4. Measurement of power consumption 26
4.4.1. Torque method 26
4.4.2. Conventional temperature method 28
4.4.3. Extended temperature method 30
4.5. Determination of overall heat transfer coefficient *(UA)* 30
4.5.1. Characterization without lateral air flow 30
4.5.2. Characterization with lateral air flow 30
4.5.3. Measurement of heat transfer area 32
4.6. Determination of oxygen transfer rate (*OTR*) 32
4.7. Determination of the ventilation through aluminum foil in shake flasks 34
4.8. Biological experiments 35
4.8.1. Maintenance of plant cell suspension culture in shake flask 35

4.8.2. Cultivation of *N. tabacum* suspension culture at large-scale 35
4.8.3. Hybridoma cell culture cultivation 36
4.9. Analytical methods 38
4.9.1. Determination of fresh weight and dry weight of plant cell culture 38
4.9.2. Determination of extracellular sugar concentration in plant cell culture 38
4.9.3. Determination of phosphate concentration in plant cell culture 38
4.9.4. Determination of Human Serum Albumin (HSA) produced by plant cell cultures of *N. tabacum* 38
5. Results and discussion 40
5.1. Effect of hydrophobicity on power consumption 40
5.2. Mixing performance and critical shaking frequency 42
5.3. Power consumption in disposable shaking bioreactors 43
5.3.1. Comparison of the temperature method and the torque method 43
5.3.2. Extended temperature method 46
5.4. Non-dimensional description of power consumption 52
5.5. Heat transfer characteristics 58
5.5.1. Necessity to characterize the bioreactors in terms of heat transfer 58
5.5.2. Characterization of *UA* without lateral air flow 59
5.5.3. Characterization of *UA* with lateral air flow 63
5.5.4. Estimation of outside heat transfer coefficient 66
5.6. Mass transfer characteristics of disposable shaking bioreactors 68
5.6.1. Oxygen transfer rate 68
5.6.2. Correlation for volumetric mass transfer coefficient 70
5.7. Application 74
5.7.1. Scale- up of plant cell culture process 74
5.7.1.1. Ventilation in shake flasks 75
5.7.1.2. Cultivation of *N tabacum* cell culture in different bioreactors 78
5.7.2. Scale-up of animal and insect cell culture 81
6. Conclusion 83
7. References 84
Appendix A: Dimensionless numbers 89
Appendix B: Symbols 90
Appendix C: Greek symbols 93
Appendix D: Proposed level of hydro-mechanical stress generation 94

1. Introduction and objectives

In today's biopharmaceutical industry, a good technology portfolio, a strong intellectual property position and access to capital do not guarantee success (1). Flexibility, cost effectiveness, and time to market are becoming key issues as well (1-4). Biopharmaceutical companies are all in a race to get their products to market as quickly as possible so as to attain the largest possible market share. Timely market penetration can make the difference between a blockbuster drug and one that barely makes a profitable return on R&D expenditures (5). The potential losses in revenue resulting from delays in product approval can be considerable; it is often reported that for a moderately successful drug (one with annual sales of $350 million) each day's delay to market incurs a loss of $1 million (6). It is also known that biopharmaceutical products have high failure rates (7). Therefore, decision of future expansion of any product development process becomes bottleneck as this decision must be made quite early during product development stage. Such decisions are difficult to change later due to regulatory constraints (2, 8). Hence, to achieve an acceptable return on investment, biopharmaceutical companies focus on cutting down the cost of drug development and improving the overall time-to-market. Therefore, companies are moving rapidly towards "Disposable" processing units. There was a time in the not-too-distant past when all processing from laboratory scale to production scale was dedicated to glass, hard plastic and stainless steel components. Supporting such equipments required labour, money, time and effort. For example, the bioprocessing unit must be assembled, sterilized and cleaned, which requires supplies, labour and downtime. Later, the equipments being used must be validated, maintained and stored. With rigid, reusable components such as glass and stainless steel, cross-contamination becomes an added risk (9). On the other hand, apart from flexibility, disposable units have the following advantages

Safety: Single-use bags and components eliminate the risk of cross-contamination

Efficiency: No need of assembling, sterilizing, cleaning and validation

Space savings: Empty systems can be stored in a small space

Productivity: With less down time and fewer time consuming duties the other important issues such as researching, developing, discovering and producing can be met quickly. Moreover, use of disposable equipment also allows for quick change over

between products, which is invaluable in the clinical phase of development, when often multiple products are evaluated simultaneously. A key factor determining the speed to market of disposables-based processes is associated with the decision of when to build the manufacturing facility (9). The simpler construction of disposables-based plants implies that shorter implementation time can be realized which allows for more detailed process optimization before moving into construction. Further, shorter construction time may allow for earlier entry to market and at a lower risk due to the smaller investment involved (2, 9).

Much effort has been made for economic evaluation of disposables-based processing and compared with other traditional bioprocessing methods (9). Novais et al. compared several important parameters such as capital investment, running cost, utilities cost, net present value etc. for disposable option and conventional option using a case study of therapeutic protein production by *E. coli* (9). The initial capital investment for a disposables option was substantially reduced to 60% of that for a conventional option. Utilities cost halved due to absence of operations like CIP (Cleaning-In-Place) and SIP (Sterilization-In-Place). However, disposables-based running costs increased by 70% of those of the conventional option. Despite the higher value, the net present value of the disposable plant was positive and within 25% of that for the conventional plant. The net present value was identical to that of a conventional plant when a nine months reduction in time to market arising from the adoption of a disposables-based approach was incorporated in the model of Novais et al. (9). However, authors assumed that the two cultivation options had the same yield of biomass and therapeutic protein production. The net present value was also calculated for the disposables option when there was a 25% reduction in biomass yield and protein expression yield encountered. Results revealed that while biomass yield was 25% less, there was only a slight drop in the net present value to 91% of that of the base case but a 25% lower protein expression level had a high impact on the net present value, decreasing to 83% of the base case.

Because of these tremendous advantages, the disposables-based option is widely accepted in today's biopharmaceutical industries.

Although disposable bioreactors were studied mainly in the late nineties, its very first concept and use was reported decades ago by Falch et al. (10). They cultivated bacterial and fungal cultures in 300 mL shaking tetrahedron plastic bags with 50 mL filling volume. The authors reported that the cell growth was not limited because of

hydrophobic nature of the bags and cells did not attached to the wall of plastic. Because of the limitations of the shaking machines available, the experiments were carried out at 130 rpm shaking frequency and 4.1 cm shaking diameter. However, it took three decades to identify the potential of the disposables-based process concept till late nineties. The numbers of disposable bioreactors available now in the market are increasing in leaps and bounds. Some of the successful trade names are, CELLine, Wave Bioreactors, CellMaker Lite2, XDR bioreactors, CellPharm, miniPerm etc. However, most of the bioreactros have limited fluid handling capacity, except Wave bioreactors, CellMaker Lite2 and XDR bioreactors. XDR and Wave bioreactors are available in the size of 2L to 1000L, whereas the size of the CellMaker Lite 2 ranges from 1L to 50L. In spite of numerous bioreactors available, the Wave bioreactors are most successful in biopharmaceutical industry. The Wave bioreactors were developed by Singh et al. (11). Singh et al. reported successful scale-up of a number of processes based upon plant, animal, insect cell culture as well as virus cultures up to 100L in Wave bioreactors. Although other disposable bioreactors except Wave bioreactors were also available in the market in late nineties but all of them had problems in scale-up, therefore, could not be used for pilot-scale production. Table 1.1 compares costs associated for production of Secreted Associated Phosphatase (SEAP) in various disposable bioreactor systems as well as standard stirred tank fermentors (12). Table 1.1 indicates that the production cost of SEAP is minimum for Wave bioreactors. There are numerous papers available about successful cultivation of a range of cell lines in Wave bioreactors. In spite of their ease of handling the Wave bioreactors possess following major disadvantages,

Ill-defined operating conditions: Wave bioreactors are not defined in terms of very important scale-up parameters such as mixing, power consumption and hydro-mechanical stress generation. There is a report of measurement of oxygen transfer rate in Wave bioreactors but it is limited to only a few operating conditions and for only a few reactor sizes. In bio-pharmaceutical industries the large scale production (>1m^3) is still performed in standard stirred tank reactors. Therefore, it may not be easy to scale-up the process from Wave bioreactors to standard stirred tank fermentors because of the ill-defined operating conditions.

Thin Wave bags prone to wear and tear: The Wave bags are relatively thin as compared to standard carboys, which make them an ideal choice as it saves much space. But these bags become more prone to punctures, which may cause severe accidents especially, when working with virus cultures.

Cultivation system	**CELLine 1000**	**miniPerm-classic kit**	**Cell-Pharm-100(BR 130)**	**Wave Cellbase 20 SPS (1L[***])**	**Wave Cellbase 20 SPS (2L[***])**	**Standard stirred tank (2L[***])**
SEAP activity (U)	1156	1102.5	495	5160	10320	4120
Investment costs[*] (SFr)	15,000	16270	4095	30,000	30,000	73,320
Cultivation system	**CELLine 1000**	**miniPerm-classic kit**	**Cell-Pharm-100(BR 130)**	**Wave Cellbase 20 SPS (1L[***])**	**Wave Cellbase 20 SPS (2L[***])**	**Standard stirred tank (2L[***])**
Costs per batch (SFr)	250	272	69	500	500	1222
Running costs (SFr)	750	478	305	526	1052	877
Cultivation unit costs (SFr)	540	130	1150	295	590	0
Personal costs (SFr)	1160	1160	1200	1160	2320	2000
Cost[**] per 1000 units SEAP (SFr)	2336	1850	5503	481	432	995

[*]Cultivation system and peripheral systems e.g. CO_2 incubator etc.

[**]Calculation is based upon 60 experiments. Costs associated with energy, cell culture laboratory and analytical systems not included.

[***]Working volume

Table 1.1: Comparison of production cost of SEAP in various disposable bioreactor systems along with a standard stirred tank reactor system. Courtsey of Eibl et al. (12).

Costs: The Wave bioreactors are expensive because of their monopoly in the disposables-based bioprocess market.

In contrast to such an expensive bioreactor, large shaking bioreactors presented in Figure 1.1 give a promising choice for cell culture systems from laboratory scale to pilot scale.



Figure 1.1: A 50L (to the left) and a 20L (to the right) large disposable shaking bioreactor mounted on a commercially available RC-6 shaker from Kühner AG, Switzerland. The shaker has a fixed shaking diameter of 5 cm and can operate at shaking frequencies from 0 to 400 rpm.

In this research work, a type of disposable bioreactor is introduced, which is based on the shaking technology (see Figure 1.1). The sizes of the bioreactors used are 2L, 20L and 50L. The main objectives of the research work are:

- Characterization of mixing performance and identification of operating conditions where poor mixing is observed.
- Characterization of disposable shaking bioreactors in terms of power consumption and heat transfer.
- Investigation of mass transfer characteristics of large disposable shaking bioreactors.
- Application of the large disposable shaking bioreactors to available cell culture systems.

2. Literature review

2.1. Shaking bioreactors

Shake mixing has been widely used at small scale level in biotechnology laboratories and industries for the screening of valuable micro-organisms and in basic bioprocess development experiments. Their simple operation, easy handling and low cost are some of the major advantages (13).

2.1.1. Mixing and power consumption

The mixing characteristics of conical shake flasks were pioneered by Sumino et al. (14, 15). They used a temperature method for the determination of power consumption in small shake flasks of size 250 mL. Shake mixing in conical shaking flasks of size up to 5L is extensively studied by Büchs et al. (16-19). Büchs et al. used different shaking diameters (1.25 to 7 cm) and different shaking frequencies (100 to 400 rpm) with varying liquid viscosities up to 200 mPa·s. The authors also used filling volumes in the range of 5% to 20% of the total flask volume. Büchs et al. derived following dimensionless equation between modified Newton number (*Ne'*) and Reynolds number (*Re*),

$$Ne' = 70 \cdot Re^{-1} + 25 \cdot Re^{-0.6} + 1.5 \cdot Re^{-0.2} \qquad 2.1$$

where following condition of axial Froude number (Fr_a) must be satisfied,

$$Fr_a > 0.4 \qquad 2.2$$

where, $Ne' = \frac{P}{\rho \cdot n^3 \cdot d^4 \cdot V_L^{1/3}}$, $Re = \frac{\rho \cdot n \cdot d^2}{\eta}$ and $Fr_a = \frac{(2 \cdot \pi \cdot n)^2 \cdot d_0}{2 \cdot g}$,

where,

Ne' Modified Newton number (-)

Re Reynolds number (-)

Fr_a Axial Froude number (-)

P Power consumption (W)

ρ Density of fluid (kg/m^3)

n Shaking frequency (1/s)

d Maximum Inside diameter of the vessel (m)

V_L Filling volume (m^3)

η Dynamic viscosity of fluid (Pa·s)

d_0 Shaking diameter (m)

However, different geometries of conical shake flasks and cylindrical shaking vessels may make it difficult to extrapolate the experimental results to large shaking bioreactors. On the other hand, Kato et al. (20) reported mixing performance of cylindrical shaking vessels of size from 0.5L up to 12L, where liquid height to vessel diameter ratio was kept constant. However, the operating conditions were limited for all the characterization experiments. The measurements of Kato et al. were carried out in cylindrical vessels for shaking frequencies of 100-200 rpm, while the shaking diameter was kept in the range of 1 to 4 cm. Kato et al. derived following dimensionless equation for power consumption in cylindrical shaking vessels,

$$Ne = 934 \cdot Fr^{\frac{3}{2}} \cdot Re^{-\frac{1}{4}} \cdot \left(\frac{d_0}{d}\right)^{\frac{3}{2}} \quad 2.3$$

$$P = Ne \cdot \rho \cdot n^3 \cdot d^5 \quad 2.4$$

$Fr_r = \frac{n^2 \cdot d}{g}$ and $Re = \frac{\rho \cdot n \cdot d_0^{\,2}}{\eta}$

where following equation must be satisfied,

$$0.135 \cdot Re^{0.166} < Fr < 0.135 \cdot Re^{r\text{-}0.176} \quad 2.5$$

where,

Ne Newton number (-)

g Gravitational acceleration (m^2/s)

2.1.2. Mass transfer characteristics of shaking bioreactors

Mass transfer characteristics of conical shaking bioreactors are studied by various authors. It is thoroughly investigated over a wide range of operating conditions by Maier et al. (21). Following table describes the operating conditions used by various authors.

Authors	**Flask size (ml)**	**Filling volume (% of flask vol.)**	**Shaking speed (rpm)**	**Shaking diameter (mm)**
Haarde & Zehner (22)	S/SB (250, 1000)	5%-20%	50-330	Not mentioned
Henzler & Schedel (23)	S (1000)	5%-20%	150-400	25, 50
Van Suijdam et al. (24)	S/SB (500)	8%-40%	230, 320	25
Veglio et al. (25)	S (300)	33%-50%	150-250	32
Veljkovic et al. (26)	S (300, 500, 1000)	5%-20%	0-400	20
Maier et al. (21)	S (50-1000)	4%-16%	50-500	12.5-100

Table 2.1: Investigation of mass transfer characteristic in shake flasks by various authors. **S** denotes conical shake flask and **SB** denotes conical shake flask with baffles.

Maier et al. used a sulfite oxidation method for measurement of oxygen transfer rate in shaking bioreactors of a size up to 1L at different filling volumes and shaking diameters. They developed a “two sub-reactor model” for the gas-liquid mass transfer in shaking bioreactors. According to this model, the mass transfer characteristics in shaking flasks can be divided into a film reactor and a stirred tank reactor. The experimentally found volumetric mass transfer coefficient was then compared with the model and can be described as follows,

$$k_L a \sim V_L^{-0.83} \cdot n^{1.16} \cdot d_0^{0.38} \cdot d^{1.92} \qquad 2.6$$

where,

$k_L a$ Volumetric mass transfer coefficient (1/s)

V_L Filling volume (mL)

n Shaking frequency (1/min)

d_0 Shaking diameter (cm)

d Maximum inside diameter of the flask (cm)

Kato et al. investigated the oxygen transfer rate by a dynamic gassing-in method in cylindrical shaking vessels of diameter 12 cm and 15 cm with a liquid height to diameter ratio of 0.5, 1, and 1.5 (27). The shaking frequencies used were in the range

of 100 to 200 rpm and the shaking diameter was kept in the range of 1 to 4 cm. Mass transfer occurred mainly on the surface of the bulk liquid and, hence, it was characterized in terms of power consumption as follows,

$$k_L a \sim P_V^{0.4} \cdot H^{-0.6} \cdot d^{-0.25} \qquad 2.7$$

where,

$k_L a$ Volumetric mass transfer coefficient (1/s)

P_V Power consumption per unit volume (W/m^3)

H Height of the fluid inside the vessel (m)

d Maximum inside diameter of the vessel (m)

2.1.3. Ventilation in shaking bioreactors

Henzler & Schedel (23) measured the mass transfer resistance of sterile shake flask closures. Based on their basic model, Mrotzek et al. (28) developed an extended model for determination of resistance of sterile closures in shake flasks of different sizes. Mrotzek et al. used sterile plugs made of cotton, paper, urethane foam and fibreglass along with caps made of aluminium and silicon. The authors found that the mass transfer resistance was mainly dependent on neck geometry, flask closure and its packing density.

2.2. Application of disposable shaking bioreactors

In fact, Millard et al. (29) investigated recombinant protein expression based on *E.coli* cultures in 2L polyethylene beverage bottles. The notches at the bottom of the bottle served as baffles. At low filling volumes (0.25L) the cell growth and protein expression was almost double as compared to that found in 2L baffled shake flasks. At high filling volumes (1L) the cell growth and protein expression was similar to that found in 2L baffled shake flasks. Millard et al. (29) currently employ these 2L beverage bottles for protein expression because of their ease of handling and reduction in labour and time. Müller et al. (30) also cultivated HEK-293 EBNA and CHO-DG44 cell lines in 1L borosilicate square shaking bottles. They employed different filling volumes at 2.5 cm shaking diameter. The live cell count was 2 to 3 times higher than that obtained in normal 2L spinner flasks. Müller et al. (30) observed optimal cell growth and viability at 30-40% filling volume, 130 rpm and 2.5 cm shaking diameter. Use of these simple though highly efficient shaking bioreactors is not limited to 2L scale only. Liu et al. (31,

32) already showed the potential of large cylindrical shaking bioreactors for the cultivation of animal and insect cell cultures at pilot scale.

Liu et al. (31) were the first to scale-up production processes based on the animal and insect cell lines in disposable large shaking bioreactors. They successfully cultivated hybridoma cells, CHO cells and insect cell lines Sf-9 and H-5. Normal batch, fed-batch, semi-continuous and continuous operation modes were used. Liu et al. used different sizes of cylindrical disposable shaking bioreactors ranging from 3L to 50L. In all the cases the cell growth was better than that obtained by spinner flasks or standard fermentors. Sf-9 and H-5 cells have a higher oxygen demand than mammalian cells. A maximum viable cell density of $14 \cdot 10^6$ cells/mL was achieved in 20L bioreactor with 4L filling volume during cultivation of Sf-9 cells (Figure 2.1). Singh et al. reported a maximum cell density of $4.75 \cdot 10^6$ cells/mL during a fad-bath process based on baculovirus/Sf-9 cells in a 20L Wave bioreactor system with 1L Bio-Whittaker X-press insect cell medium. Similarly an expression system containing Baculovirus/H-5 was scaled-up successfully in 20L shaking bioreactor with a maximum viable cell density of $7 \cdot 10^6$ cells/mL. The maximum cell density of the same baculovirus/H-5 system attained in spinner flask and standard 3L jar fermentor was $3 \cdot 10^6$ cells/mL and $2.5 \cdot 10^6$ cells/mL, respectively.

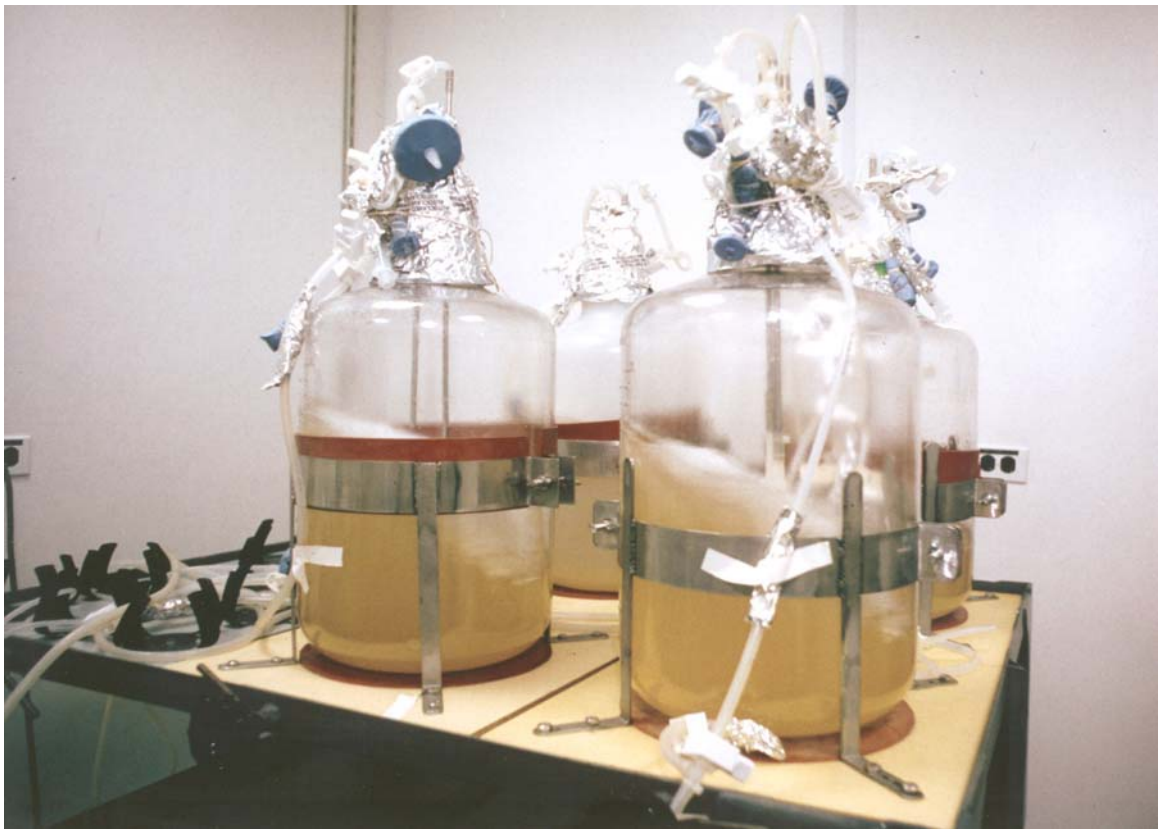

Figure 2.1: Insect cells (Sf-9) cultured in 20L polypropylene bioreactors. Culture volume: 7L. Shaking diameter 5 cm. This photo is a courtesy of Dr. Liu (personal gift).



Figure 2.2: Hybridoma cells cultured in a 50L polypropylene bioreactor: culture volume 36L. Shaking diameter 5 cm. This photo is a courtesy of Dr. Liu (personal gift).

Liu et al. (31) also evaluated the IgG production using hybridoma cells in shaking bioreactors ranging from 3L to 50L size using a semi-continuous mode (Figure 2.2). The experiments were conducted with an 11% exchange of the culture broth per day with fresh medium. IgG production reached 150 mg/L per day while maintaining $2 \cdot 10^6$ viable cells/mL. A maximum of 250 mg/L of IgG was produced in the same process after termination of the daily exchange of broth with the fresh medium. A continuous process for the IgG production was maintained for 70 days in a 50L shaking disposable bioreactor with 14.5L filling volume.

A cultivation of CHO cells in a 20L disposable bioreactor with 5L filling volume is shown in Figure 2.3. CHO cells were also grown in a fed-batch mode in a 50L shaking bioreactor with a maximum viable cell count of $6 \cdot 10^6$ cells/mL. The maximum viable CHO cell count obtained in a fed-batch process in a 20L Wave bioreactor was $4.5 \cdot 10^6$ cells/mL at 6L filling volume (11). Shaking bioreactors of 20L and 50L scale with a working volume of 5-10L and 30-35L, respectively are routinely employed by Liu et al. (31) (at Roche Discovery Technologies Department in NJ, USA) to grow suspension adapted mammalian (e.g., CHO, HEK293), insect cells and Hel A and B cells for recombinant protein expression and live cell production to support high through put drug screening programs at pilot- scale level.



Figure 2.3: CHO cells cultured in 20L polycarbonate bioreactors. Culture volume 5L. Shaking diameter 5 cm. This photo is a courtesy of Dr. Liu (personal gift).

In spite of successful cultivation of different cell cultures, Liu et al. (31) stressed the need of further characterization of these simple though efficient shaking bioreactors.

3. Theory

3.1. Conventional temperature method

The conventional temperature method was developed by Sumino et al. (14). The heat balance for a given shaking vessel can be defined by the following equation,

$$-m \cdot C_p \cdot \frac{dT_f}{dt} = UA \cdot (T_f - T_o) - P \qquad 3.1$$

where,

m Mass of the fluid (kg)

c_p Specific heat capacity (J/kg/K)

T_f Fluid temperature (K)

t Time (s)

UA Overall heat transfer coefficient (W/K)

A Heat transfer area (m^2)

T_o Temperature of the surrounding atmosphere (K)

where, $-m \cdot C_p \cdot (dT_f/dt)$, $UA \cdot (T_f - T_o)$ and P denote the cooling rate of the liquid, the heat loss to the surroundings and the heat generation rate because of dissipation of power. According to the existing theory the power consumption as well as the overall heat transfer coefficient remains constant over time at given operating conditions. Therefore, these two parameters can be estimated from the data of the liquid and room temperature profile over time, as described by Sumino et al. (14, 15).

3.2. Extended temperature method

In the extended temperature method the power consumption or heat generation rate is not taken as a constant value but treated as a variable value, which changes with respect to the temperature. The dynamic behaviour of the power consumption can be incorporated in the extended method as follows:

According to Büchs et al. (17) power consumption of shake flasks can be defined in terms of the dimensionless modified Newton number (Ne'),

$$Ne' = \frac{P}{\rho \cdot n^3 \cdot d^4 \cdot V_L^{1/3}} \quad 3.2$$

Ne' can be calculated as a function of the Reynolds number *(Re)* as follows,

$$Ne' = 70 \cdot Re^{-1} + 25 \cdot Re^{-0.6} + 1.5 \cdot Re^{-0.2} \quad 3.3$$

where,

$$Re = \frac{\rho \cdot n \cdot d^2}{\eta} \quad 3.4$$

Equation 3.2 and 3.4 show that at a given operating condition, with a fixed vessel diameter, *Re* is a function of the liquid physical properties, i.e. viscosity and density. However, in the temperature ranges encountered in the temperature method for the measurement of the power consumption other physical properties except viscosity do not vary to a great extent (variation < 12%). Therefore, the effect of change of other physical properties on the determination of power consumption can be considered negligible.

Hence, from equation 3.2 and 3.4 it can be concluded that,

$$P = f(\eta) = f(T) \quad 3.5$$

In the present work two fluids, namely, water and an 80% (w/w) glycerol/water solution were used. Their viscosity can be defined over temperature as follows,

$$\eta(T) = 1.28 \cdot e^{-0.0157 \cdot T} \quad 3.6$$

for water (33) and

$$\eta(T) = 1.46 \cdot 10^8 \cdot e^{2.54 \cdot 10^8 / T^2} - 2.14 \cdot 10^{-2} \cdot T - \frac{5.43 \cdot 10^3}{T} \quad 3.7$$

for an 80% glycerol/water solution (34), where,

η Dynamic viscosity of fluid (Pa·s)

T Fluid temperature (K)

Analogous to the description of the power consumption in shake flasks, a model for disposable shaking bioreactors can be derived as follows. Under the assumption that transitional flow and turbulent flow prevails in large disposable shaking bioreactors,

only the second and third term of equation 3.3 is taken into account, hence, *Ne'* can be correlated with *Re* as,

$$Ne' = C_{fit1} \cdot Re^{-0.6} + C_{fit2} \cdot Re^{-0.2} \qquad 3.8$$

Hence, for each temperature profile obtained for a given operating condition, there are three parameters to be fitted as described in equation 3.1 and 3.8, namely, *UA, C_{fit1}* and *C_{fit2}*. It should be noted here that in the conventional temperature method, power consumption was the fitting parameter, but now they are the parameters *C_{fit1}* and *$C_{fit2,}$* which describes the hydrodynamic behaviour of the system. Henceforth, power consumption will vary according to the relationship given in equation 3.5 with temperature. However, the power consumption measured with the extended temperature method can only be specified with respect to a given standard temperature. This temperature was chosen to be 30°C in this thesis.

3.3. Oxygen transfer rate measurement

3.3.1. The sulfite system

Mass transfer characteristics of solutions having water-like viscosity are readily measured by an aqueous chemical model system developed and well studied by Linek and Vacek (35). This model system comprises of a sodium sulfite solution in a specific buffer. The sulfite ions are oxidized into sulfate ions in presence of Co^{+2}, Cu^{+2}, Fe^{+2} or Mg^{+2}, acting as catalysts. The oxygen transferred from the air to the aqueous solution characterizes the mass transfer capacity of a given reactor at a given operating condition. The irreversible oxidation reaction can be written as,

$$SO_3^{-2} + \frac{1}{2} O_2 \xrightarrow{Co^{+2}} SO_4^{-2} \qquad 3.9$$

The mass transfer rate (transfer of oxygen from air to solution) as well as the reaction rate defines the oxidation reaction regime. The reaction regime can be defined as dimensionless Hatta number (*Ha*),

$$Ha = \frac{\text{reaction rate}}{\text{mass transfer rate}}$$

Depending upon the value of *Ha*, the reaction regimes can be defined as delayed reaction regime (*Ha* < 0.03), non accelerated reaction regime (0.03 < *Ha* < 0.3), transitional regime (0.3 < *Ha* < 3) and accelerated reaction regime (*Ha* > 3). The

oxidation reaction must take place in the non-accelerated reaction regime to determine the maximum oxygen transfer rate (36).

The completion of the oxidation reaction can be easily measured using a pH indicator since sulfate ions are more acidic than sulfite ions. There are a number of parameters which influence the oxidation mechanism of above mentioned reaction, such as, concentration of buffer solution, pH of the solution, ionic strength, catalyst concentration etc. All these parameters were very well studied and optimized for shaking bioreactors by Maier et al. (21) and Hermann et al. (36). Maier et al. studied the mass transfer characteristics in conical shaking bioreactors at different operating conditions using above mentioned optical sulfite oxidation method in the non accelerated reaction regime. The authors also measured and compared the progress of the oxidation reaction online using the Respiration Activity Monitoring System (RAMOS) developed by Anderlei and Büchs (37).

3.3.2. Online oxygen transfer rate measurement

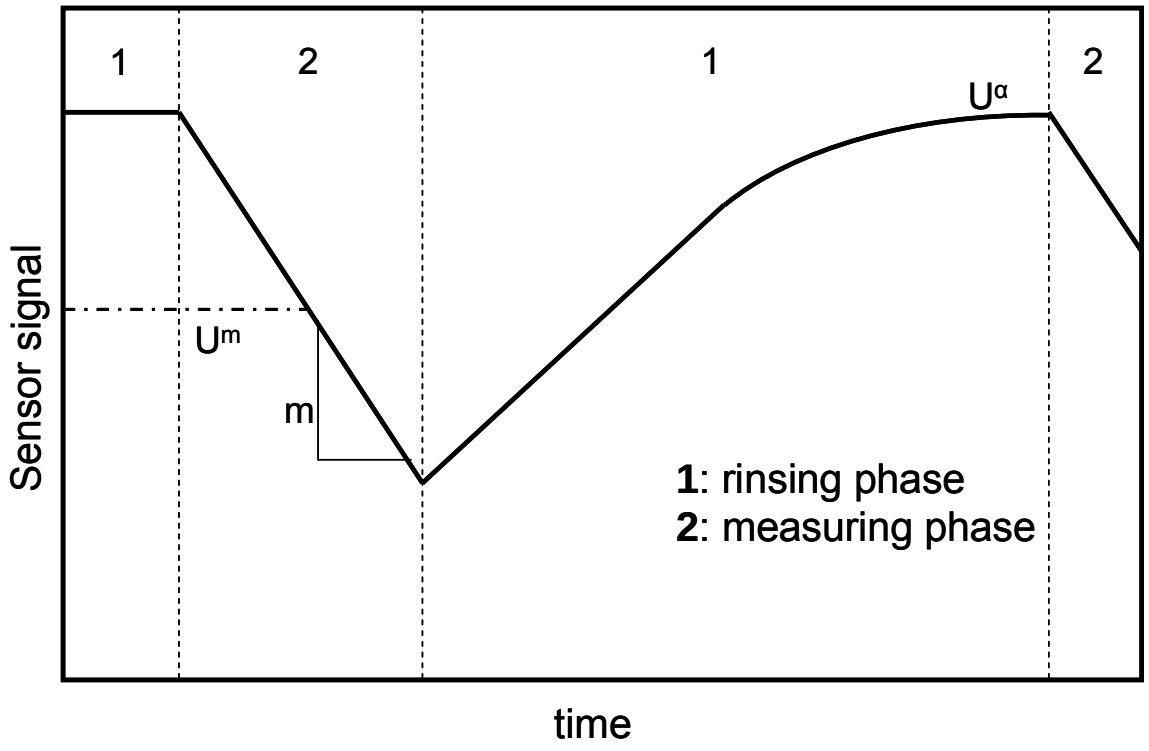

Figure 3.1: Sensor signal profile observed during the measurement of online oxygen transfer rate. U^m = sensor signal at mid point, m = slope, U^α = sensor signal at steady-state.

The RAMOS technology is based on the principle of the rate of change of the oxygen partial pressure in a closed head space of a shake flask. An oxygen sensor is mounted on the top of the shake flask which measures the change in the partial pressure of oxygen. The shake flask is aerated for a specific period of time (rinsing

phase) and then aeration is stopped for a specific period of time (measuring phase). The rate of change of the oxygen partial pressure is measured during the measuring phase using the oxygen sensor. The oxygen transfer rate is then determined using a material balance on oxygen in the head space. Diagrammatically the process is shown in Figure 3.1. As shown in Figure 3.1, during the rinsing phase, the oxygen partial pressure reaches a steady-state value which is followed by the measuring phase. The oxygen sensor measures the rate of decrease of the oxygen partial pressure from which the oxygen transfer rate is calculated. After a definite period of time the rinsing phase starts again. The oxygen transfer rate calculation steps are explained below.

3.3.3. Calibration of the oxygen sensor

There is a linear relationship between the oxygen partial pressure and the voltage of the sensor. This relationship can be written as,

$$p_{o_2} = a \cdot U + b \qquad 3.10$$

where,

a Slope of the calibration curve (bar/V)

b Intercept on the y-axis (bar)

A two point calibration is performed to avoid any sensor drifts. Voltage of the sensor is measured at 0% partial pressure of oxygen and the value is taken as the first calibration point. Air is then passed through the system and voltage of the sensor is measured till steady-state condition is reached. This value is taken as the second point of the calibration curve.

Mathematically,

let U^0 and $Po_2{}^0$ be the voltage and oxygen partial pressure at 0% oxygen,

let U^α and $Po_2{}^\alpha$ be the voltage and oxygen partial pressure at steady-state.

Then, from equation 3.10 it can be concluded that

$$\frac{dp_{o_2}}{dt} = \frac{p_{o_2}^{\alpha}}{U^{\alpha} - U^{0}} \frac{dU}{dt} \qquad 3.11$$

3.3.4. Material balance on oxygen at steady-state (in the rinsing phase)

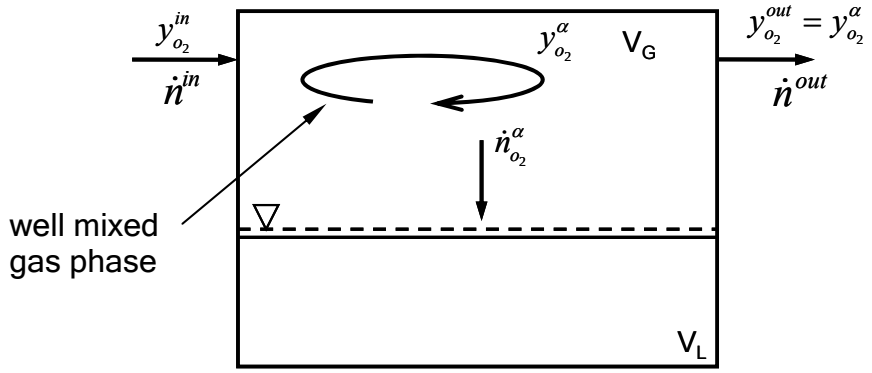

Figure 3.2: Molar flow of oxygen in and out of the system in the rinsing phase. Here, V_L represents filling volume and V_G represents head space volume in the shake flask.

Since, the gas phase is well mixed,

$y_{o_2}^{out} = y_{o_2}^{\alpha}$, therefore,

molar oxygen balance at steady-state can be written as,

$$y_{o_2}^{in} \cdot \dot{n}^{in} = y_{o_2}^{out} \cdot \dot{n}^{out} + \dot{n}_{o_2}^{\alpha} \qquad 3.12$$

where,

$y_{o_2}^{in}$ Mole fraction of oxygen in the gas phase entering the system (-)

$\dot{n}^{in}$ Molar flow rate of air entering the system (mol/s)

$y_{o_2}^{out} = y_{o_2}^{\alpha}$ Mole fraction of oxygen in the gas at the end of the rinsing phase (-)

$\dot{n}^{out}$ Molar flow rate going out of the system (mol/s)

$\dot{n}_{o_2}^{\alpha}$ Molar flow rate of oxygen transferred from the gas to the liquid phase (mol/s).

Material balance based on the total molar flow rates can be written as,

$$\dot{n}^{in} = \dot{n}^{out} - \dot{n}_{o_2}^{\alpha} \qquad 3.13$$

From equation 3.12 and 3.13 it can be written as,

$$y_o^{\alpha} = \frac{y_{o_2}^{in} \cdot \dot{n}^{in} - \dot{n}_{o_2}^{\alpha}}{\dot{n}^{in} - \dot{n}_{o_2}^{\alpha}} \qquad 3.14$$

Molar volume of a gas can be written as,

$$V_m = \frac{R \cdot T^N}{p^N} \quad 3.15$$

where,

V_m Molar volume of gas at normal temperature and pressure (L/mol)

R Ideal gas constant ($8.314 \cdot 10^{-2}$ bar·L/mol/K)

T^N Normal temperature (273.15 K)

p^N Normal pressure (1.013 bar)

Oxygen transfer rate can be defined as,

$$\dot{n}_{o_2}^{\alpha} = OTR_{\alpha} \cdot V_L \quad 3.16$$

where,

OTR_{α} Steady-state oxygen transfer rate at the end of rinsing phase (mol/L/s)

According to ideal gas law,

$$\dot{n} = \dot{V} \cdot \frac{p}{R \cdot T} \quad 3.17$$

where,

$\dot{n}$ Molar flow rate (mol/s)

$\dot{V}$ Flow rate of a gas (L/s)

p Pressure (bar)

T Temperature (K)

Since, $y_i = p_i/p$, equation 3.14 can be rearranged as

$$p_{o_2}^{\alpha} = p \cdot \frac{\frac{p_{o_2}^{in}}{p} \cdot \frac{\dot{V}^{in}}{V_L} - V_m \cdot OTR_{\alpha}}{\frac{\dot{V}^{in}}{V_L} - V_m \cdot OTR_{\alpha}} \quad 3.18$$

where,

y_i Mole fraction of component i (-)

p_i Partial pressure of component i (bar)

$\dot{V}^{in}$ Total volumetric flow rate entering the system (L/s)

The unknown parameter OTR_α in equation 3.18 can be calculated from the mass balance of oxygen in the measuring phase.

3.3.5. Material balance in measuring phase

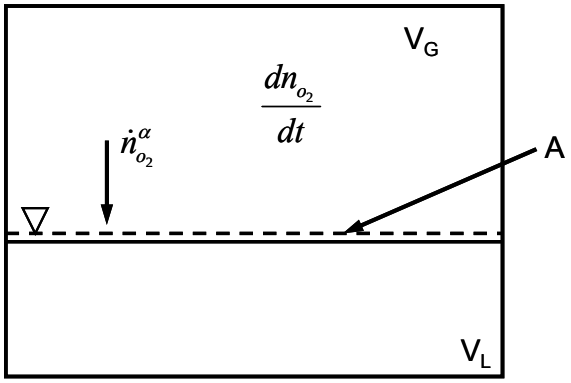

Figure 3.3: Molar flow of oxygen during measuring phase. Here, V_L represents filling volume and V_G represents head space volume in the shake flask.

Oxygen in the head space is transferred into liquid during the measuring phase, therefore,

$$\frac{dn_{o_2}}{dt} = -\dot{n}_{o_2} \qquad 3.19$$

The oxygen transfer rate *(OTR)* can be defined as,

$$OTR = \frac{\dot{n}_{o_2}}{V_L} \Rightarrow \frac{1}{V_L} \cdot \frac{dn_{o_2}}{dt} = -OTR \qquad 3.20$$

Using the ideal gas law relationship, above equation can be written as,

$$OTR = -\frac{V_G}{V_L} \cdot \frac{1}{R \cdot T} \cdot \frac{dp_{o_2}}{dt} \qquad 3.21$$

where,

V_G Volume of gas in the head space (L)

Combining equation 3.11 and 3.21 results in

$$OTR = -\frac{V_G}{V_L} \cdot \frac{1}{R \cdot T} \cdot \frac{p^{\alpha}_{o_2}}{U^{\alpha} - U^{\circ}} \cdot \frac{dU}{dt} \qquad 3.22$$

In the measuring phase oxygen partial pressure decreases and hence oxygen transfer rate also decreases which may result in non-liner decrease in the voltage of the sensor. However, the duration of the measuring phase is always very short and hence, during this short duration, the decrease in oxygen partial pressure can be taken as negligible. Therefore, the decrease in the sensor signal can be taken as linear. Hence,

$$\frac{dU}{dt} = m = constant \qquad 3.23$$

where,

m Slope of the decreasing voltage signal of the oxygen sensor (V/s)

Therefore, the oxygen transfer rate using the slope m can be calculated as,

$$OTR_m = -\frac{V_G}{V_L} \cdot \frac{1}{R \cdot T} \cdot \frac{p_{o_2}^{\alpha}}{U^{\alpha} - U^{\circ}} \cdot m \qquad 3.24$$

where,

OTR_m Oxygen transfer rate corresponding to slope m (mol/L/s)

However, this oxygen transfer rate corresponds to the mid point of the sensor signal U^m and not U^{α}. The actual oxygen transfer rate can be calculated as follows.

Oxygen transfer rate can be defined as,

$$OTR = k_L a \cdot \left(c_{o_2}^{*} - c_{o_2} \right) \qquad 3.25$$

where,

c^*_{O2} Oxygen concentration at the gas-liquid interface (mol/L)

c_{O2} Oxygen concentration in the bulk liquid (mol/L)

The reaction regime of the sulphite system being used is in the non-accelerated reaction regime, where 0.03 < Ha <0.3. In this reaction regime, the chemical reaction is of first order in terms of sulfite concentration. Therefore, the concentration of oxygen in the liquid phase can be calculated from the first order reaction constant as follows,

$$c_{o_2} = \frac{OTR}{k_1} \qquad 3.26$$

where,

k_1 First order reaction constant of sulfite oxidation (0.6625 1/s,accoding to Hermann et al. (36))

The oxygen solubility in the liquid phase is very low, therefore, according to Henry's law,

$$He \cdot c^*_{o_2} = p_{o_2} \tag{3.27}$$

where,

He Henry's law constant for oxygen in sulphite system (bar·L/mol)

From equation 3.10, 3.26 and 3.27, it can be written as,

$$OTR \propto \left(c^*_{o_2}\right) \propto \left(p_{o_2}\right) \propto \left(U\right) \tag{3.28}$$

Hence, from equation 3.18, 3.24 and 3.28, the oxygen transfer rate can be calculated as

$$OTR_m = \frac{A - \sqrt{A^2 - 4 \cdot m \cdot p \cdot \dot{V}^{in} \cdot V_G \cdot V_m \cdot \left(U^{\alpha} - U^{\circ}\right) \cdot T \cdot R}}{2 \cdot V_m \cdot V_L \cdot \left(U^{\alpha} - U^{\circ}\right) \cdot T \cdot R} \tag{3.29}$$

Where,

$$A = \dot{V}^{in} \cdot \left(U^{\alpha} - U^{\circ}\right) \cdot T \cdot R + V_m \cdot V_G \cdot m \cdot p \tag{3.30}$$

Since $U^0 << U^{\alpha}$,

$$OTR = OTR_m = \frac{A - \sqrt{A^2 - 4 \cdot m \cdot p \cdot \dot{V}^{in} \cdot y^{in}_{o_2} \cdot V_G \cdot V_m \cdot U^{\alpha} \cdot T \cdot R}}{2 \cdot V_m \cdot V_L \cdot U^{\alpha} \cdot T \cdot R} \tag{3.31}$$

Where,

$$A = \dot{V}^{in} \cdot U^{\alpha} \cdot T \cdot R + V_m \cdot V_G \cdot m \cdot p \tag{3.32}$$

From equation 3.26 and 3.31, the maximum oxygen transfer rate can be calculated as follows,

$$OTR_{\max} = OTR \cdot \left(\frac{c^*_{O_2}}{c^*_{O_2} - c_{O_2}} \right) \tag{3.33}$$

where,

OTR_{max} Maximum oxygen transfer rate (mol/L/s)

3.4. Ventilation in shake flasks

The shake flasks are closed with sterile closures in biotechnology laboratories. The ventilation of air from the surrounding atmosphere into the head space of the flask depends on the geometry of the neck of the flask and type of sterile closure (28, 38).

According to Mrotzek et al. (28), the oxygen transfer rate because of the ventilation through the sterile closure can be defined as,

$$OTR_{plug} = k_{plug} \cdot \frac{1}{V_L \cdot p_{abs}} \cdot \left(p_{O_2 out} - p_{O_2} \right) \qquad 3.34$$

where,

OTR_{plug} Oxygen transfer rate through the flask closure (mol/L/s)

K_{plug} Gas transfer coefficient (mol/s)

V_L Flask filling volume (L)

p_{abs} Absolute pressure (bar)

p_{o2out} Partial pressure of oxygen in the surrounding atmosphere (bar)

p_{o2} Partial pressure of oxygen in the head space of the shake flask (bar)

The oxygen transferred through the aeration of shake flask can be given as,

$$OTR_{flow} = \frac{q_{in}}{p_{abs} \cdot V_m} \cdot \left(p_{O_2 out} - p_{O_2} \right) \qquad 3.35$$

where,

OTR_{flow} Oxygen transfer rate because of aeration of flask (mol/L/s)

V_m Molar volume of air (L/mol)

q_{in} Specific aeration rate in the flask (L/L/s)

Equating equation 3.34 and 3.35, results in a aeration value which is equivalent to the ventilation through the sterile closure, mathematically,

$$q_{in} = \frac{V_m}{V_L} \cdot k_{plug} \qquad 3.36$$

The gas transfer coefficient can be obtained by the neck geometry of the flask and the diffusion coefficient of oxygen through the flask closure (28). The value of gas transfer coefficient and oxygen transfer rate through flask closure can be calculated by the combination of the model developed by Henzler and Schedel (23), Mrotzek et al. (28) and unsteady-state model developed by Amoabediny et al. (39). From the gas transfer coefficient, the aeration values can be calculated by the model developed by Amoabediny et al. (40). Detailed description of these models is beyond the scope of this thesis. Therefore, readers are requested to read the cited references for thorough understanding of the ventilation in shake flasks.

4. Materials and methods

For all the experiments 2L polycarbonate (PC) bottles and 20L and 50L polypropylene (PP) bottles (Nalgene, USA) were used. A table-top shaker (LS-W, Kuehner AG, Switzerland) was used to impart shake mixing in 2L bioreactors and a commercially available pilot scale shaker RC-6 (Kuehner AG, Switzerland) was used to impart shake mixing in 20L and 50L bioreactors. All the experiments were performed at 5 cm shaking diameter. All the chemicals were obtained from ROTH, Germany, unless otherwise stated.

4.1. Hydrophilic shake flasks

Shake flasks of size 5L were washed with deionized water. Later ca. 1L of a 65% (v/v) nitric acid solution was poured into the shake flasks. Following this, the shake flasks were heated on a heating plate in an exhaust chamber and the solution was brought to boil. They were kept under this condition for 5 min. Then, the shake flasks were removed from the heating plate and cooled down to room temperature. Subsequently these flasks were thoroughly washed with deionized water and dried in a drying oven at 50°C for 24 h.

4.2. Hydrophobic shake flasks

The inner surface of the 5L shake flasks were made hydrophilic as described above. Then the inner surface of the shake flask was made hydrophobic by silanisation. A 5% (w/v) Dichlorodimethylsilan (Sigma) solution was prepared in toluene (Sigma) and about 1L of it was poured into each flask. Subsequently, the flasks were vigorously shaken under the hood for 15 min in such a way that the liquid made a uniform film all over the inner surface. The remaining solution was discarded from the shake flasks. The flasks were kept in an exhaust chamber at room temperature for 24 h to evaporate remaining Dichlorodimethylsilan solution.

4.3. Mixing performance

Mixing performance of the disposable shaking reactors was measured by an electrical conductivity method (20). The vessel was filled with deionized water. At given operating condition, the tracer, 0.5 mL of 1M sodium chloride, was added instantaneously into the vessel at steady state. As shown in Figure 4.1, the electrical

conductivity of the liquid was measured by a conductivity meter after addition of the tracer. The mixing time is defined as the time required for 99% of the total change in concentration resulting from the addition of the tracer.

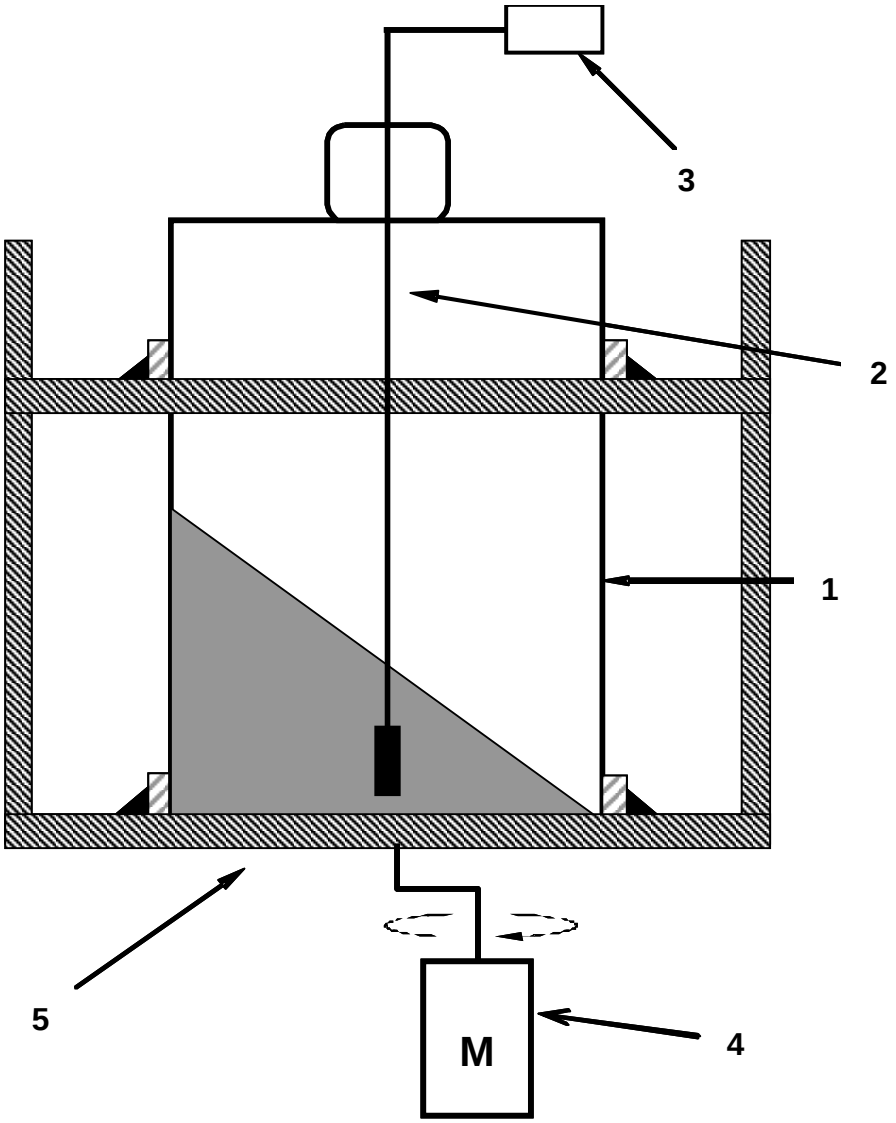

Figure 4.1: Experimental setup for electrical conductivity measurement in 20L and 50L vessel. 1) Cylindrical vessel, 2) Electrode, 3) Electrical conductivity meter, 4) Shaking machine motor, 5) Mechanical support.

4.4. Measurement of power consumption

4.4.1. Torque method

Power consumption in 2L and 20L disposable reactors mounted on a shaker table was measured by the method developed by Büchs et al. (41). The method is based on the measurement of the torque developed by the liquid which rotates around the axis of the vessel. The torque is generated on the axis of the motor. Mechanical friction losses and wind resistance of the vessel are compensated by measuring the torque

generated by a dead weight which should be the same as that of the rotating liquid and the vessel.

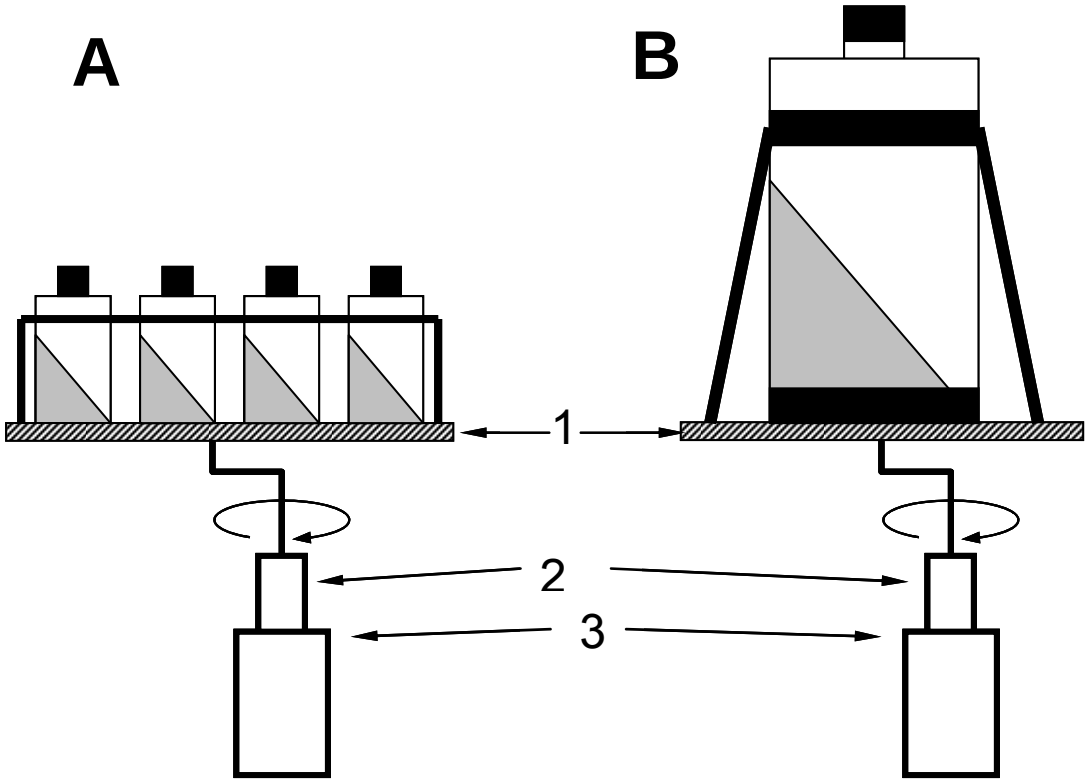

Figure 4.2: Experimental setup for the determination of the power consumption by the torque method in A) 2L cylindrical vessels and B) 20L vessel. 1) Shaker table, 2) Torque sensor, 3) Shaker motor.

The power consumption can be calculated by following equation,

$$\frac{P}{V_L} = \frac{(M_1 - M_2) \cdot 2 \cdot \pi \cdot n}{Z_K \cdot V_L} \qquad 4.1$$

where,

M_1 Torque developed by rotating liquid (N·m)

M_2 Torque developed by the dead weight (N·m)

Z_K Number of shake flasks mounted on the shaker table (-)

Figure 4.2A and B show the arrangements used for torque measurement for 2L and 20L vessels, respectively. As shown in Figure 4.2A, four 2L PC bottles instead of one were mounted on the shaker table to maximise the accuracy in the torque measurements. The shaker was rotated by the external motor which had an integrated torque sensor (ViskoPakt, HiTech-Zang, Germany). The control of this motor was automated by a LabView software (National Instruments, Germany) which also recorded the data from the torque sensor. Figure 4.2B shows the same

arrangement for a 20L PP vessel. To keep the torque produced within the limits of the torque sensor (0 to 1 Nm), only one 20L vessel was used. Measurements were performed at different shaking frequencies as well as different filling volumes.

4.4.2. Conventional temperature method

Power consumption in disposable bioreactors was measured by the method developed by Sumino et al. (14). The method is described in section 3.1. Figure 4.3A and B shows the arrangements used to measure power consumption for 2L, 20L and 50L vessels, respectively. An insulated 2L vessel was used. Polyurethane foam was used to make insulated vessel from a non-insulated vessel of the same size. The insulation was done by Mr. H. Pütz at “Institute für Werkstoffe der Elktrotechnik”, RWTH Aachen. The diameter and height of the 2L vessel was 12.5 cm and 20 cm respectively. Thickness of the polyurethane foam insulation was 3 cm. It was proved in preliminary experiments that the insulation was necessary to prevent rapid heat losses to the surrounding. Temperature of the liquid inside the 20L and 50L vessel was measured as shown in Figure 4.3.

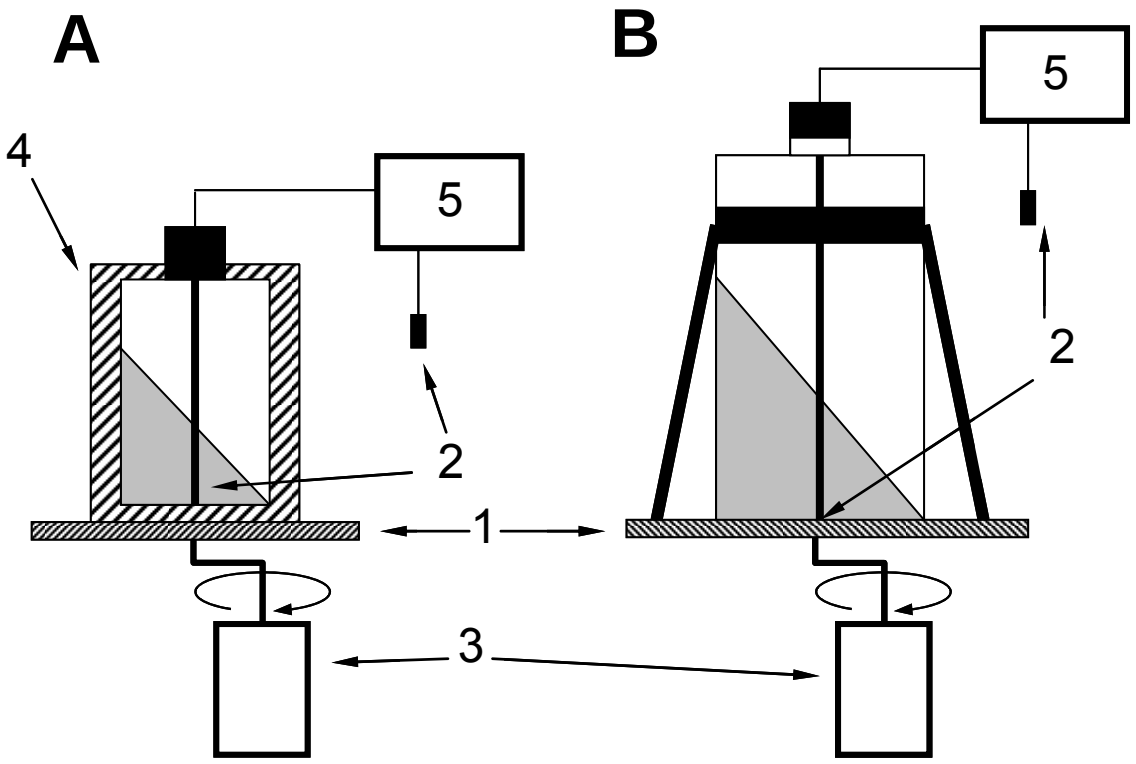

Figure 4.3: Measurement of power consumption using the temperature method in (A) insulated 2L cylindrical shaking vessel, (B) insulated 20L and non-insulated 20L and 50L cylindrical shaking vessel. 1) Shaking table, 2) temperature sensor, 3) shaking machine motor, 4) heat insulation, 5) digital multimeter

Since power consumption in a 20L and 50L vessel is higher than that obtained in 2L vessel, insulation of the 20L and 50L vessel was not required. The height, diameter and wall thickness of 20L vessel were 40 cm, 27 cm and 4 mm, respectively. The height, diameter and thickness of 50L vessel were 50 cm, 38 cm, and 15 mm, respectively. The entire surface of the 20L cylindrical vessel except its opening was covered with 5 cm thick polyurethane foam to make insulated vessel. The insulation was done by Mr. H. Pütz at "Institute für Werkstoffe der Elktrotechnik", RWTH Aachen. A PT100 (Conrad, Germany) temperature sensor was mounted at the centre of the vessel using a thin stainless steel rod to measure the liquid temperature. The rod did not result in significant additional disturbance of the shake mixing because of its central location (42). The temperature of the surrounding air was simultaneously measured by another PT100 sensor. Both sensors were connected to digital multimeters (GMC-instruments, Germany) to record the temperature over time. The fluid filling volumes in the range of 20% to 75% were employed. The shaking frequency was varied from 100 to 300 rpm. The fluid at room temperature was poured into the non insulated 20L and 50L vessels and then heated to ca. 5°C higher than the desired initial temperature by immersion heater (Karl Roth GmbH, Germany). This difference was accounted for initial adjustments such as closing the vessel lid, setting up desired shaking frequency etc. When using 2L insulated vessel, previously heated fluid to about 50°C was poured. However, for 20L insulated vessel, fluid was poured at room temperature. The vessel was closed air-tight at the top and operated at given operating conditions. Due to the power consumption induced by shaking, the given fluid was heated up in the 20L insulated vessel, whereas it was cooled down in the 20L and 50L non-insulated vessels and 2L insulated vessel until a steady state temperature difference between the fluid and surrounding air was reached. The temperature profile of the fluid in non-insulated and insulated vessels were monitored over time using above mentioned Pt100 temperature sensors. This data of temperature profile of fluid being heated up or cooling down was used to determine the parameters P and UA in equation 3.1. For this purpose, a mathematical model was developed in the differential equation solver software ModelMaker (Cherwell Scientific, UK), fitting the simulation to the measured data by optimising the parameters P and UA.

4.4.3. Extended temperature method

The experimental setup for the extended temperature method remained the same as in the case of the conventional method. The liquid and room temperature profiles were measured in a similar way as described in the conventional temperature method. However, the analysis of the experimental data differed from that of the conventional method. A model was developed as described in section 3.2 in the differential equation solver software ModelMaker (Cherwell Scientific, UK), fitting the simulation to the measured data for each operating condition by optimising the parameters *UA*, C_{fit1} and C_{fit2}. Consistency of the model parameters was validated by implementing the same model in the gPROMS (PSE Ltd, UK) process simulation software. Dynamic parameter estimation was performed using all the experimental data sets simultaneously.

4.5. Determination of overall heat transfer coefficient *(UA)*

4.5.1. Characterization without lateral air flow

An 80% (w/w) glycerol-water mixture and water were used as fluids. Figure 4.3B represents the experimental set up used for measurement of liquid and room temperature profile. The procedure for determination of *UA* remained the same as described in section 4.4.3.

4.5.2. Characterization with lateral air flow

The experimental set up used for determination of *UA* with lateral air flow is represented in Figure 4.4. Water was used as a fluid in 20L and 50L non insulated vessel with 50% and 40% filling volumes, respectively. The shaking frequencies from 150 to 250 rpm were employed. The experimental procedure to determine the fluid temperature profile remained the same as described in section 4.4.2. However, producing and measuring the lateral air flow was different. The lateral air flow was produced by two revolving fans (HV-181E, Honeywell, Germany) placed opposite to each other on either side of the shaker. The fans were placed in such a way that the air current produced by them would break the swirl of the air produced because of the shaking motion of the vessel and thus enhance turbulence in air current around the vessel. The distance of the fan with respect to the axis of the shaking vessel is given in Figure 4.4B. The distance of 80 cm was the nearest from the shaking machine. The

farthest distance of the fans from the centre of the vessel was ca. 100 cm because of the lack of the space in the shaking machine room.

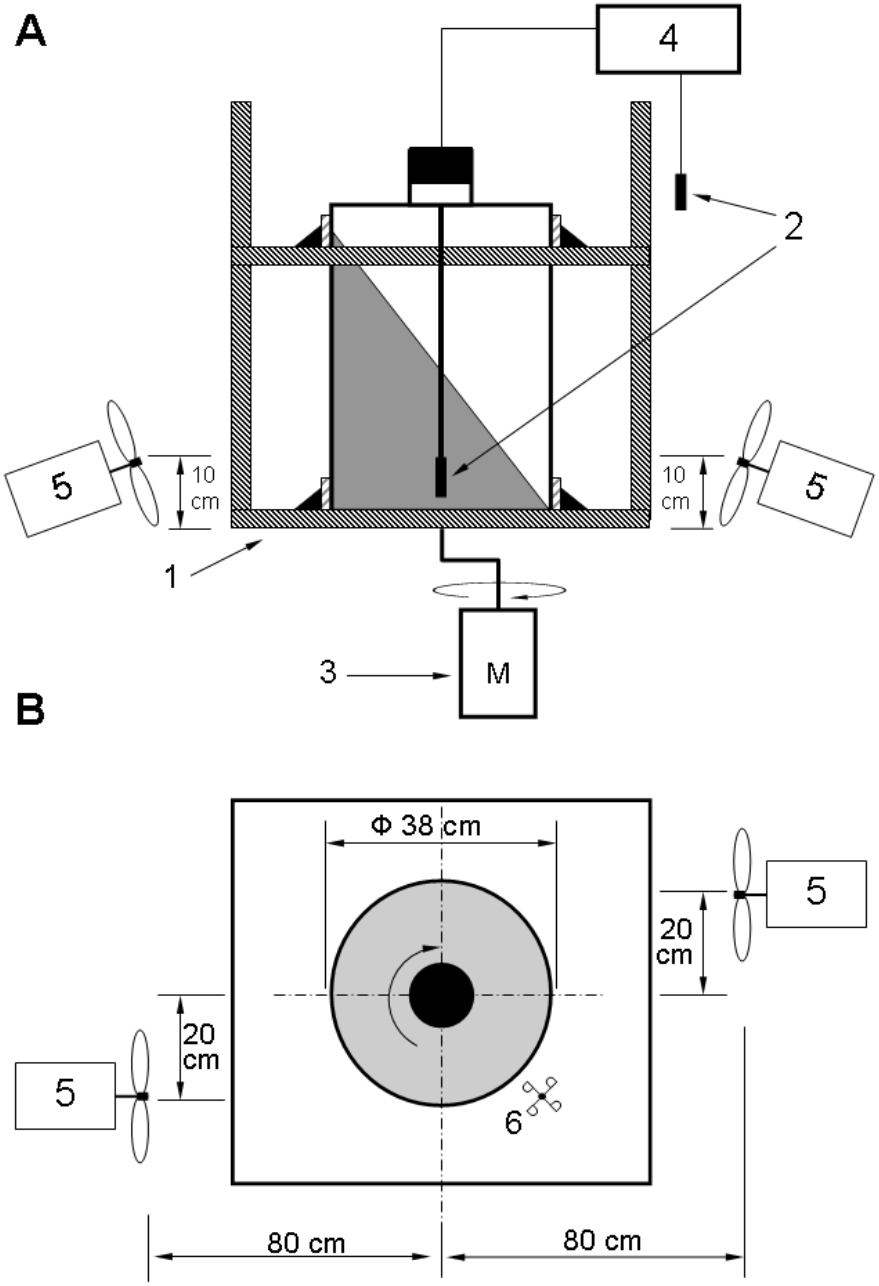

Figure 4.4: Experimental setup for determination of overall heat transfer coefficient with lateral air flow. 1) shaker table, 2) temperature sensor, 3) motor, 4) digital multimeter, 5) fan, 6) anemometer

The air flow was controlled by a 4-stage fan speed regulator. The fans produced maximum local air velocity of 9 m/s. However, the air velocities shown in this thesis are average air velocities. The average air velocity was measured by an anemometer (Windmaster 2, Conrad, Germany) over the entire surface of the vessel. The

anemometer calculated and showed the average air velocity along with the maximum and minimum local air velocity. The fan position was tilted manually about the horizontal axis whenever required to minimize the difference between the maximum and minimum local air velocities and thus minimize cavities along the surface of the vessel. The maximum average air velocity of 6.5 m/s was encountered using two fans. The deviation of ±0.2 to ±0.5 m/s was encountered for average air velocities up to 4.5 m/s. This deviation increased from ±0.8 to ±1.5 m/s for average air velocities from 4.5 to 6.5 m/s. The mathematical procedure remained the same for determination of *UA* without lateral air flow and its value was calculated as described in section 4.4.3.

4.5.3. Measurement of heat transfer area

For simplicity, it was assumed that the shaking vessel is a perfect cylinder. Water was used as a fluid. Bromothymol Blue was added to give blue color to water and enhance visibility of the siquel formed inside the vessel. The disposable bioreactor was filled with different filling volumes in the range of 25% to 75%. The shaking frequencies used were in the range of 100 rpm to 300 rpm. A measuring scale was marked from the bottom to the top of the bioreactor with increments of 1 cm. The bioreactor was operated at a given operating condition. The liquid height was measured by taking photograph of the bioreactor and comparing the liquid height to the scale marked on the bioreactor. The heat transfer area comprised of the surface area touched by the rotating fluid i.e. surface area of the vessel bottom and the cylindrical surface over the vessel wall. Therefore, the heat transfer area was calculated as the summation of the surface area of a cylinder with height equivalent to liquid height and diameter equivalent to vessel diameter and the surface area of a circle whose diameter was equivalent to vessel diameter.

4.6. Determination of oxygen transfer rate (*OTR*)

The oxygen transfer rate was measured by sulfite oxidation method (36). Shaking bioreactors of size 20L and 50L were employed with filling volumes in the range of 25% to 75%. Since large filling volumes were employed, the *OTR* was determined by the method based on the RAMOS technology (37) to save experimental time and chemicals. Sodium sulfite (98% purity, Roth, Karlsruhe, Germany), cobalt sulfate (Fluka, Neu-Ulm, Germany) and sodium phosphate buffer (Merck, Darmstadt, Germany) were used without further purification. All experiments were carried out with a 0.5 M sulfite solution including 10^{-7} M $CoSO_4$, 0.012 M phosphate buffer and a

$2.4 \cdot 10^{-5}$ M bromothymol blue (Merck, Darmstadt, Germany) at pH 8 (36). Before and during the preparation of the sodium sulfite solution, the deionized water was gassed with nitrogen to avoid a prior oxidation of sulfite. The sulfite solution was poured into the vessel. Figure 4.5 shows the experimental set up for *OTR* measurement.

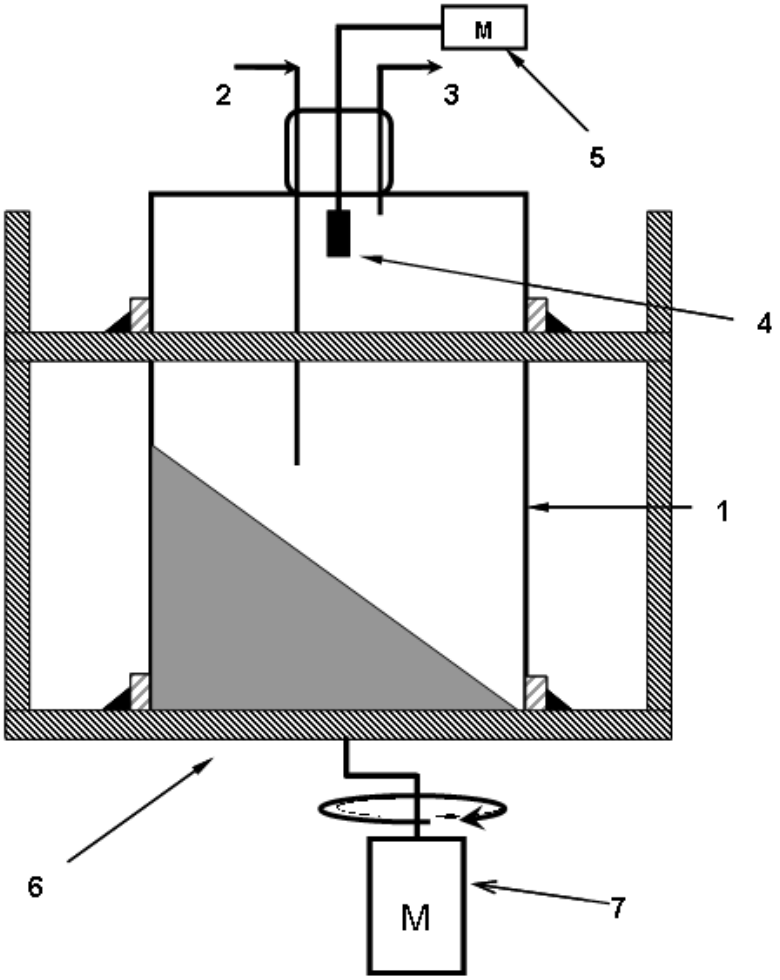

Figure 4.5: Experimental setup for determination of online oxygen transfer rate measurement in 20L and 50L vessels. 1) vessel, 2)air inlet, 3) air outlet, 4) oxygen sensor, 5) digital multimeter, 6) mechanical support, 7) motor.

The vessel was closed air tight and air was passed in the head space during the rinsing phase. After a definite period of time, the measuring phase started. The air inlet was closed first and then the outlet valve was closed to avoid increase in the head space pressure. The decrease in the oxygen partial pressure in the head space was monitored by an oxygen sensor mounted on top of vessel as shown in the Figure 4.5. After the measuring phase, the air inlet and outlet valves were opened again and the rinsing phase started. The operating condition was changed either by changing shaking frequency or by changing filling volume and the same rinsing phase and measuring phase repeated again to measure the *OTR* at this new operating condition. The surrounding atmosphere was ventilated to avoid any temperature increase of fluid

in the vessel due to mixing; especially at shaking frequencies more than 200 rpm. The change in the pH of the sulfite solution was observed by a pH indicator, bromothymol blue. The optimal pH for sulfite oxidation method in non-accelerated reaction regime is 8. This pH decreases to 6.2 at the end of the oxidation reaction when all the sulfite is converted into more acidic sulfate. The bromothymol blue solution changes from dark blue at pH 8 to yellow at pH 6.2. However, there is a transition phase when the sulfite solution has pH of ca. 7 and at this pH the solution containing bromothymol blue is green colored. This condition may lead to non-accelerated reaction regime because of high absorption rate of oxygen in the solution (36). Since, large filling volumes in the range of 25% to 75% were employed, this non-accelerated reaction regime may prevail for longer time and give higher *OTR* values as compared to that measured in non-accelerated reaction regime. To avoid such conditions, whenever, the sulfite solution in the disposable bioreactor changed to green color, it was replaced by a freshly made solution.

4.7. Determination of the ventilation through aluminum foil in shake flasks

The purpose of the determination of ventilation in small shake flasks was to find an equivalent value of aeration for large disposable shaking bioreactors. Dr. Amoabediny developed a scale-up strategy from laboratory shake flasks to standard stirred tank fermentors based on aeration (40). In this strategy, an equivalent value of aeration for standard stirred tank fermentor is obtained from the ventilation through the shake flask closure.

It is usual in Institute of Molecular Biotechnology to use aluminum foil as shake flask closures. The plant cell cultures are covered with aluminum foil in 250 mL wide neck shake flasks with 20% filling volume. Therefore, it was necessary to measure the mass transfer resistance of aluminum foil for ventilation of shake flask. Dr. Amoabediny developed a scale-up strategy to calculate the aeration for standard stirred tank fermentors using the mass transfer resistance of the flask closure (40). This aeration value is equivalent to the ventilation found in a normal ventilated shake flask covered with a closure. The mass transfer resistance of aluminum foil as a flask closure was determined by two flask method mentioned by Mrotzek et al (28) and Anderlei et al (38). Water was used as a fluid in one flask and other flask was filled with a saturated, aqueous sodium chloride salt solution. Since, tightness of aluminium foil covered on flask can vary from person to person, four persons were chosen for the experiment. Each person covered aluminum foil on four wide neck flasks (three flasks

filled with water and fourth flask filled with saturated sodium chloride solution) of same size (250 mL) with same filling volume (60%) and incubated at 25°C. The shaking frequency and shaking diameter were 180 rpm and 5 cm, respectively. Weight of each flask was measured at the start of incubation and again after 8 days at the end of the experiment. Decrease in flask weight indicated water loss at given operating condition. The water evaporation rate was calculated from the water loss. This water evaporation rate was incorporated in mathematical model developed by Anderlei et al. to calculate the oxygen transfer coefficient mentioned in section 3.4 through flask closure (38), which was further used in a model developed by Amoabediny et al. (39, 40) to obtain aeration values equivalent to the ventilation in shake flasks as described in section 3.4.

4.8. Biological experiments

4.8.1. Maintenance of plant cell suspension culture in shake flask

The suspension culture was sub cultured every seven days into 250 mL shake flasks with 20% filling volume of fresh nutrient medium containing Murashige and Skoog (MS) medium (43) + Kinetin (Kn) (0.2 mg/L) + 2, 4, dichlorophenoxy acetic acid (2, 4 – D) (0.2 mg/L). For sub culturing, 10% inoculum was used. The cultures were incubated on orbital shaker (Kühner AG, Switzerland) at 180 rpm and 5 cm shaking diameter at 25°C. The pH of the media was adjusted to 5.8 before autoclaving.

4.8.2. Cultivation of *N. tabacum* suspension culture at large-scale

The cell suspension culture of *N. tabacum* was scaled-up in a 10L (7L filling volume) standard stirred tank fermentor and in disposable shaking bioreactors of size 2L (1L filling volume), 20L (10L filling volume) and 50L (35L filling volume). The aeration was kept at 0.1 vvm. Preliminary experiments at the Institute of Molecular Biotechnology, RWTH Aachen revealed that the Gamborg's B5 medium was optimal for cell growth and human serum albumin production. Therefore, the cells were cultured in Gamborg's B5 medium (44) + Kn (0.2 mg/L) + 2,4-D (0.2 mg/L). The pH and pO_2 of the suspension culture was measured by the fiber-optic sensor spots whose luminescence was measured by Fibox (PreSens GmBH, Regensburg, Germany). Following is the diagram which shows experimental set up for plant cell culture cultivation.

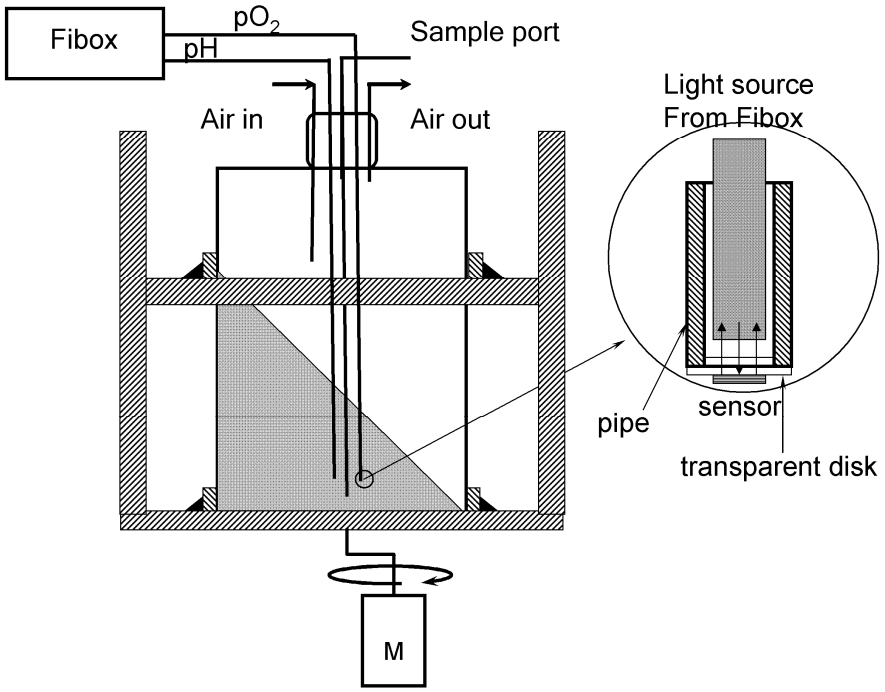

Figure 4.6: Experimental setup for plant cell cultivation in 20L and 50L bioreactor, 5 cm shaking diameter. The zoomed figure shows the oxygen sensor glued to a transparent polycarbonate disk. The disk is fitted into a pipe. A light source is inserted into the pipe.

The sensor spots were mounted on the transparent polycarbonate disk. The disk was fixed onto a thin stainless still pipe. A light source coming from Fibox was inserted into the pipe up to the point where sensor was mounted on disk.

4.8.3. Hybridoma cell culture cultivation

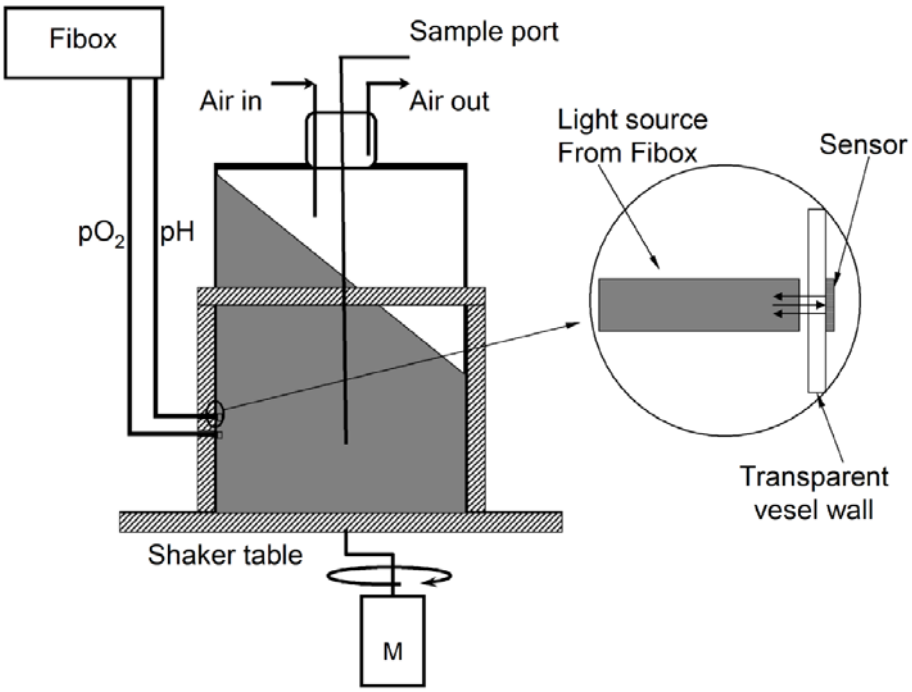

Figure 4.7: Experimental set up for hybridoma cell culture in 2L polycarbonate bioreactor with 1L filling volume, 95 rpm and 5 cm shaking diameter.

The experimental setup for the cmyc-hybridoma cell cultivation is shown in Figure 4.7. The sensor was glued on the transparent vessel wall. The pH and pO_2 of the culture medium was measured by Fibox (PreSens GmBH, Regensburg, Germany). The cells were cultivated in a 2L PC disposable shaking bioreactor with 50% filing volume. A shaking diameter of 5 cm and a shaking frequency of 95 rpm were employed. The cell culture was aerated with sterile air enriched with 5% CO_2 when the pO_2 level decreased below 19% saturation or the pH decreased below 7. The cell culture and medium composition were taken from the institute of molecular biotechnology. All media components were obtained from Sigma-Aldrich, USA. Typical medium formulation was,

Roswell Park Memorial Institute (RPMI) medium containing glutamine (0.3 g/L) (45)

5% Fetal Calf Serum (FCS)

ß- mercaptoethanol (1ml/L)

penicilin/steptomycine (100 ug/ml)

Glucose (2 g/L)

Cell-culture tested glutamine solution 200 mM (0.2 g/L)

The above medium was inoculated with $1 \cdot 10^5$ cells/mL at 37°C. The cells were counted using the haemocytometer. The haemocytometer consisted of two chambers each of which was divided into nine 1 mm^2. A cover glass was supported 0.1 mm over these squares, thus total volume over each cell was 0.1 mm^3. A 0.4% trypan blue solution (Sigma Aldrich, USA) was used as a color indicator to differentiate between live and dead cells. A 0.2 mL of 0.4% trypan blue solution was added in 0.8 mL of balanced salt solution (Sigma Aldrich, USA). This diluted trypan blue solution was added (0.1 mL) to a well mixed 0.5 mL sample solution. After 5 minutes, the sample solution was placed on the top of haemocytometer with the help of a micropipette. The cells were counted under a microscope. The dead cells took the trypan blue stain and were blue in color which differentiated them from the live cells. The cells per mL were counted as follows,

Cells/mL = average count per square $\cdot 10^4$

The count was repeated thrice to check reproducibility. The error should be in the range of ±15%.

4.9. Analytical methods

4.9.1. Determination of fresh weight and dry weight of plant cell culture

The plant cell suspension was centrifuged at 3000 rpm for 20 min. Cell pellets were collected in pre-weighed aluminum trays. The difference in weight indicated fresh weight (FW) of the cells. The fresh cells were then dried in an oven at 60°C until final weight became constant. The final weight was taken as the dry weight (DW) of cells.

4.9.2. Determination of extracellular sugar concentration in plant cell culture

The plant cell suspension was centrifuged at 3000 rpm for 20 min. Residual sucrose, glucose and fructose concentrations in the supernatant were determined using an HPLC system (Dionex with Chromeleon Software, 232 XL Sampling Injector (Abimed/Gilson), UVD 170S (Dionex, Idstein, Germany), Shodex RI71 (Dionex), P 580 Pump (Dionex), 1mM sulphuric acid, flow 0.6 ml/min, organic acid resin column (RP8, CC125/4 sperisorb 50-5 C8, CS-Chromatographie, Langerwehe, Germany).

4.9.3. Determination of phosphate concentration in plant cell culture

Phosphate concentration in the supernatant was estimated using a colorimetric assay based on the formation of a blue colour complex with molybdate ions. Molybdate reagent was prepared by mixing 2.6 g Ammonium Molybdate tetrahydrate [$(NH_4)Mo_7O_{24} \cdot 4H_2O$)], 20 mL deionized water, 0.07 g potassium antimony oxide tartrate hemi hydrate [$K(SbO)C_4H_4O_6 \cdot 0.5H_2O$], 60 ml sulphuric acid and 100 mL deionized water. 100 µL of sample was taken in a 10 mL vial. To this 9 mL of deionized water was added, followed by 200 µL of ascorbic acid solution (0.1 g/mL) and 400 µL of the molybdate reagent. The volume was made up with deionized water to 10 mL. The absorbance was measured at 680 nm, 15 min after addition of the molybdate reagent. To obtain the standard curve of concentration vs. absorbance, different concentrations of KH_2PO_4 in the range of 0.061 mg/L to 2.45 mg/L were used instead of unknown sample.

4.9.4. Determination of Human Serum Albumin (HSA) produced by plant cell cultures of *N. tabacum*

HSA was determined by enzyme linked immunosorbent assay (ELISA). The protocol was developed and standardised at the institute of molecular biotechnology, RWTH Aachen. Goat-anti HSA antibody (stock solution 1mg/ml) (Bachem) was diluted 1:1000 in TBS buffer (pH 8, Tris-HCl, pH 8: 0.05M; NaCl: 0.138 M; KCl: 2.7 mM).

Each well of a 96-well microtiterplate was coated with 200 µL of above mentioned goat-anti HSA solution. The sample application scheme is shown below

	2 Blanks	3	4	5	6	7	8	9 HSA Standard	10 HSA standard	11 HSA standard
B	TBS buffer	S	S	S	S	S	S	100 ng/mL	100 ng/mL	100 ng/mL
C	TBS buffer	S	S	S	S	S	S	50 ng/mL	50 ng/mL	50 ng/mL
D	TBS buffer	S	S	S	S	S	S	25 ng/mL	25 ng/mL	25 ng/mL
E	TBS buffer	S	S	S	S	S	S	20 ng/mL	20 ng/mL	20 ng/mL
F	TBS buffer	S	S	S	S	S	S	10 ng/mL	10 ng/mL	10 ng/mL
G	TBS buffer	S	S	S	S	S	S	5 ng/mL	5 ng/mL	5 ng/mL

Figure 4.8: A figure of the sample application on a 96 well microtiterplate. Here, S represents sample.

The plate was covered with parafilm and kept overnight at 4°C. After incubation with antibody, the plate was brought to room temperature and washed thrice with washing buffer (pH 8; TBS Buffer; Tween-20: 0.05%). This was followed by blocking with 200 µL of blocking buffer (pH 8; TBS Buffer; 5% skimmed milk solution in double distilled water) for 30 min at room temperature. After blocking, microtiterplate was washed thrice with washing buffer (pH: 8, TBS Buffer, Tween-20: 0.05%). This was followed by the addition of HSA standard solution in the range of 5 to 100 ng/mL and the diluted samples (in case of supernantant, in range of the 1:10, 1:20 and 1:50; in case of cell extract in range of 1:50, 1:100: 1:200) to the ELISA plate according to sample application scheme shown in the Figure 4.8. The plate was incubated for 24 h at 4°C. After incubation, the plate was washed thrice with washing buffer. A 100 µL of 1:20,000 diluted rabbit anti-HSA antibody conjugated with peroxidises (Rockland, USA) was placed into each well and incubated for 1 h at room temperature. After incubation, the plate was washed with washing buffer as described before. The bound anti-HSA antibody was detected using 2-2'-azinobis(3-ethylbenzothiazoline-6-sulfonic acid (ABTS) substrate tablets dissolved in ABTS buffer (Boehringer Mannheim, Germany). A 100 µL of this buffer was placed in each plate and incubated for 2 h. The microtiterplate was then placed in multichannel photometer and absorbance was measured at 690 nm.

5. Results and discussion

5.1. Effect of hydrophobicity on power consumption

The disposable cylindrical shaking bioreactors are made of either PP or PC material which is hydrophobic. In a previous study, Maier et al. concluded that the *OTR* is reduced substantially in hydrophobic shake flasks (21). Therefore, the effect of hydrophobicity on power consumption was examined. The torque method was used to measure power consumption in 5L shake flasks with 300 mL filling volume at 2.5 cm shaking diameter. A very interesting phenomenon called as “out-of-phase” was observed in shake flasks (16, 46). In this condition, the fluid inside the shake flask was either not mixing uniformly or just rotating along the surface of the flask wall. During “in-phase” operating conditions, power consumption increased with increase in shaking frequency. But in “out-of-phase” operating conditions, power consumption suddenly decreased to a very low value with increase in shaking frequency. Hydrophobic nature of the reactor surface may have changed the onset of “out-of-phase” condition. Since, this phenomenon was distinguishable and can be readily measured by the torque method; it was used as criterion to study the effect of the flask surface on power consumption. Water, Water+surfactant (TX-100) and a 30 mPa·s PVP solution was used as a fluid for this purpose. The results of power consumption are shown in Figure 5.1 for A) water, B) water+surfactant and C) a 30 mPa·s viscous solution. Power consumption increased with increasing shaking frequency. However, at one operating condition, the power consumption started to decrease with increase in shaking frequency and “out-of-phase” operating condition was started. Some shaking machines accelerate quickly to come to the desired shaking frequency and then decelerate till set point is reached. To incorporate this effect, this experiment was carried out with increasing and decreasing shaking frequencies.

The dashed curves in Figure 5.1 represent measurement of power consumption with increasing shaking frequency. The dotted lines represent measurement of power consumption with decreasing shaking frequency. When water was used as a fluid, the “out-of-phase” condition started at ca. 101 rpm with increasing shaking frequency, while with decreasing shaking frequency, the ”in-phase” condition started at ca. 90 rpm. The same difference of ca. 10 rpm was also observed for water+TX-100 solution. This hysteresis between “in-phase” and “out-of-phase” was also observed in rotating cylinders and shake flasks (16, 47).

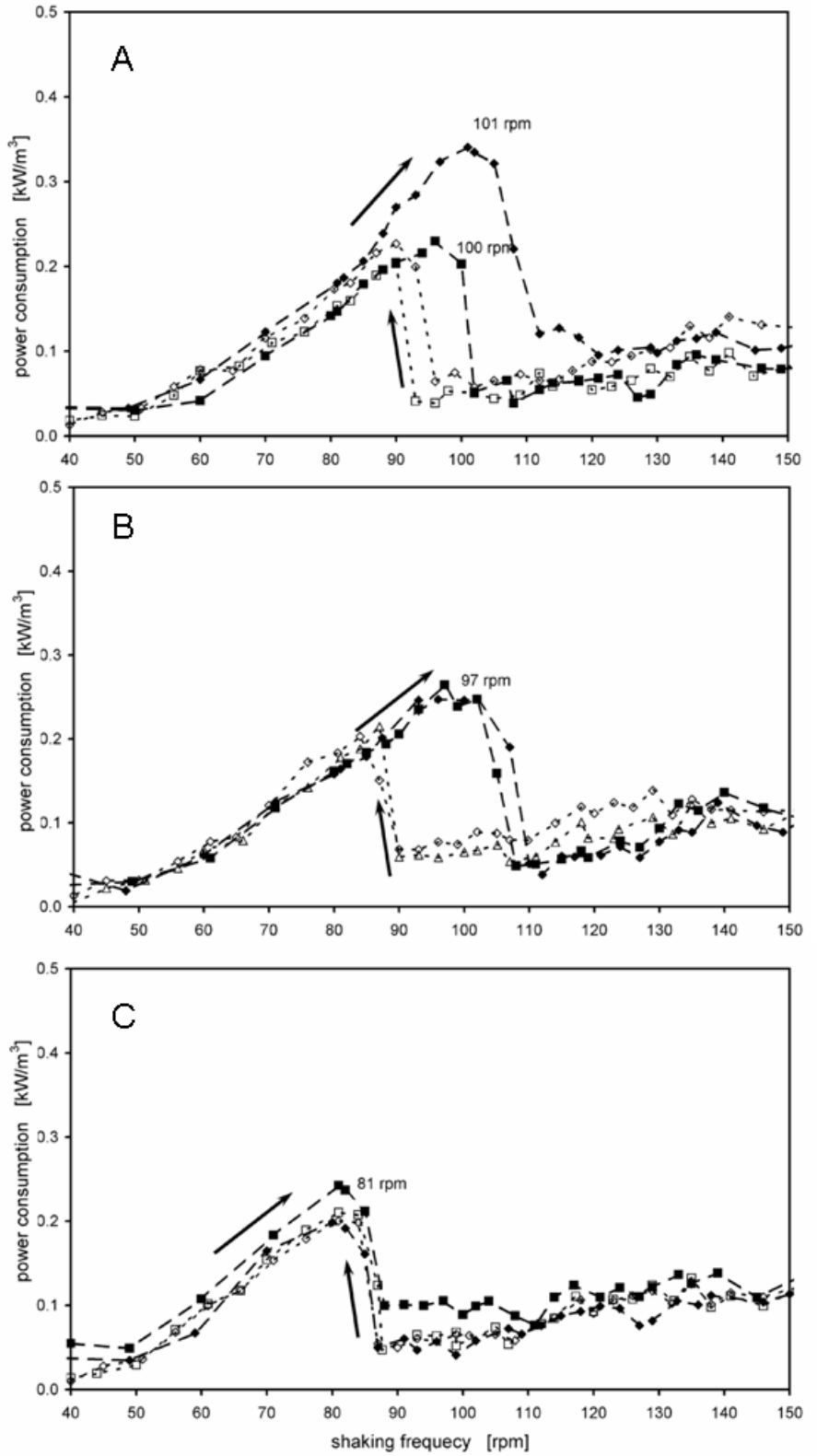

Figure 5.1: Power consumption vs shaking frequency for (A) water, (B) water+TX-100, (C) 30 mPa·s viscous solution. (■)& (□) hydrophobic shake flask, (◆) & (◇) hydrophilic shake flask. Dashed lines with filled symbols indicate increasing shaking frequency and dotted lines with open symbols indicate decrease in shaking frequency. The shake flask size, filling volume and shaking diameter were, 5L, 300 mL and 5 cm, respectively.

However, such a hysteresis was not observed for the investigated viscous solution. Moreover, the value of power consumption observed was also similar for all solutions

except water. When shaking frequency increased, a maximum difference of 50% in the value of power consumption was observed in hydrophilic and hydrophobic shake flask (water as fluid), however such a huge difference was not observed while measuring power consumption with decreasing shaking frequency. This could be because of the measuring error encountered at such a low value of power consumption. These findings indicate that the hydrophobicity does influence onset of "out-of-phase" conditions depending upon the fluid physical property. However, more investigations are required to reach any final conclusion and hence, for the present work, its effect is not taken into account.

5.2. Mixing performance and critical shaking frequency

Cell culture systems are sensitive to concentration, pH and temperature gradients. These gradients may appear because of non-homogeneous or poor mixing. Therefore, bioreactors used for animal/plant cell culture must possess good mixing characteristics and at the same time should not generate large hydro-mechanical stress (11, 31). Mixing performance of disposable shaking reactors was measured by electrical conductivity method as described in section 4.3. The mixing time was defined as the time required for 99% of the total change in concentration after addition of the tracer.

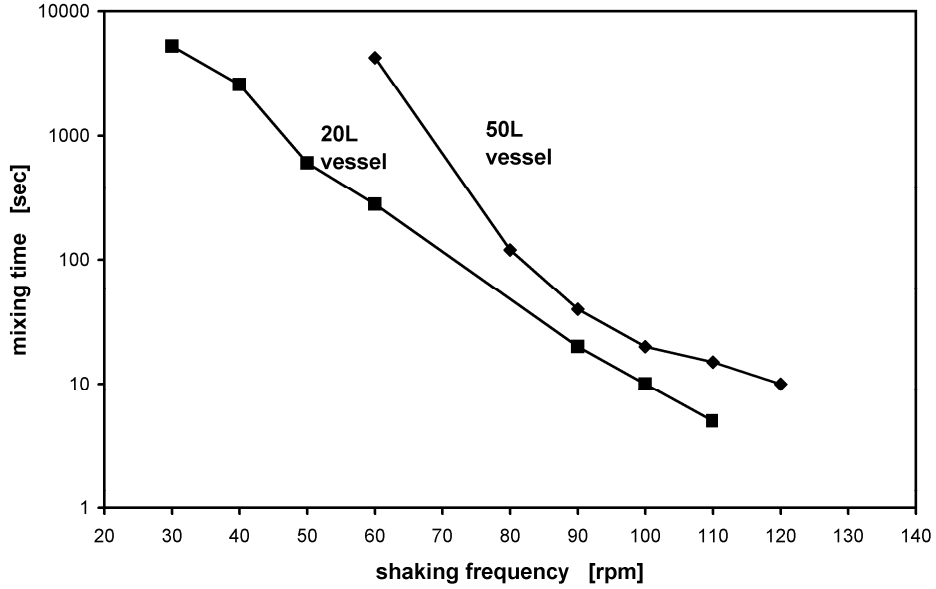

Figure 5.2: Mixing time in 20L and 50L vessel with 15L and 35L filling volume respectively at 5 cm shaking diameter.

As Figure 5.2 depicts, for shaking frequencies larger than 80 rpm, mixing occurred within a few seconds after addition of the tracer. The electrical conductivity meter had a minimum time interval of 5 seconds. Therefore, it was not possible to measure

mixing times less than 5 seconds. Although mixing occurred at frequencies lower than 80 rpm, it is not recommended to operate under these conditions as there is no regular liquid flow pattern observed. Kato et al. (20) investigated cylindrical shaking vessels of different sizes for the determination of critical shaking frequency. They defined the critical shaking frequency as the minimum shaking frequency required to achieve complete mixing. Kato et al. derived following empirical correlation for critical shaking frequency,

$$n_c = 1.137 \cdot d^{-0.46} \cdot d_0^{-0.16} \cdot \eta^{0.08} \qquad 5.1$$

Where,

n_c critical shaking frequency (1/s)

d vessel diameter (m)

d_0 shaking diameter (m)

η fluid viscosity (Pa·s)

Based on the above equation, the calculated value of critical shaking frequency for 20L and 50L vessel, at 5 cm shaking diameter is 116 rpm and 102 rpm respectively. However, the experimental findings indicate that the mixing occurs at shaking frequencies as low as 60 rpm. It should be noted that, Kato et al. investigated shaking vessels of size ranging from 8.5 to 20.6 cm, shaking diameter in the range of 1 cm to 4 cm and shaking frequencies in the range of 75 rpm to 200 rpm. Except for shaking frequency, all the other experimental conditions applied in this thesis are out of the range of the operating conditions investigated by Kato et al. This could be the reason for the deviation of the experimental values and predicted values of the critical shaking frequency.

5.3. Power consumption in disposable shaking bioreactors

5.3.1. Comparison of the temperature method and the torque method

To date it was assumed that the temperature method can be used to measure power consumption for fluids having water-like viscosities but the accuracy of this method was unknown in comparison to other validated methods like the torque method (18). Therefore, both torque and temperature methods were used for the determination of power consumption in 2L and 20L disposable shaking bioreactors to check the validity of the temperature method. Figure 5.3 shows the values of specific power

consumption obtained using the torque and the temperature method in 2L disposable shaking vessels.

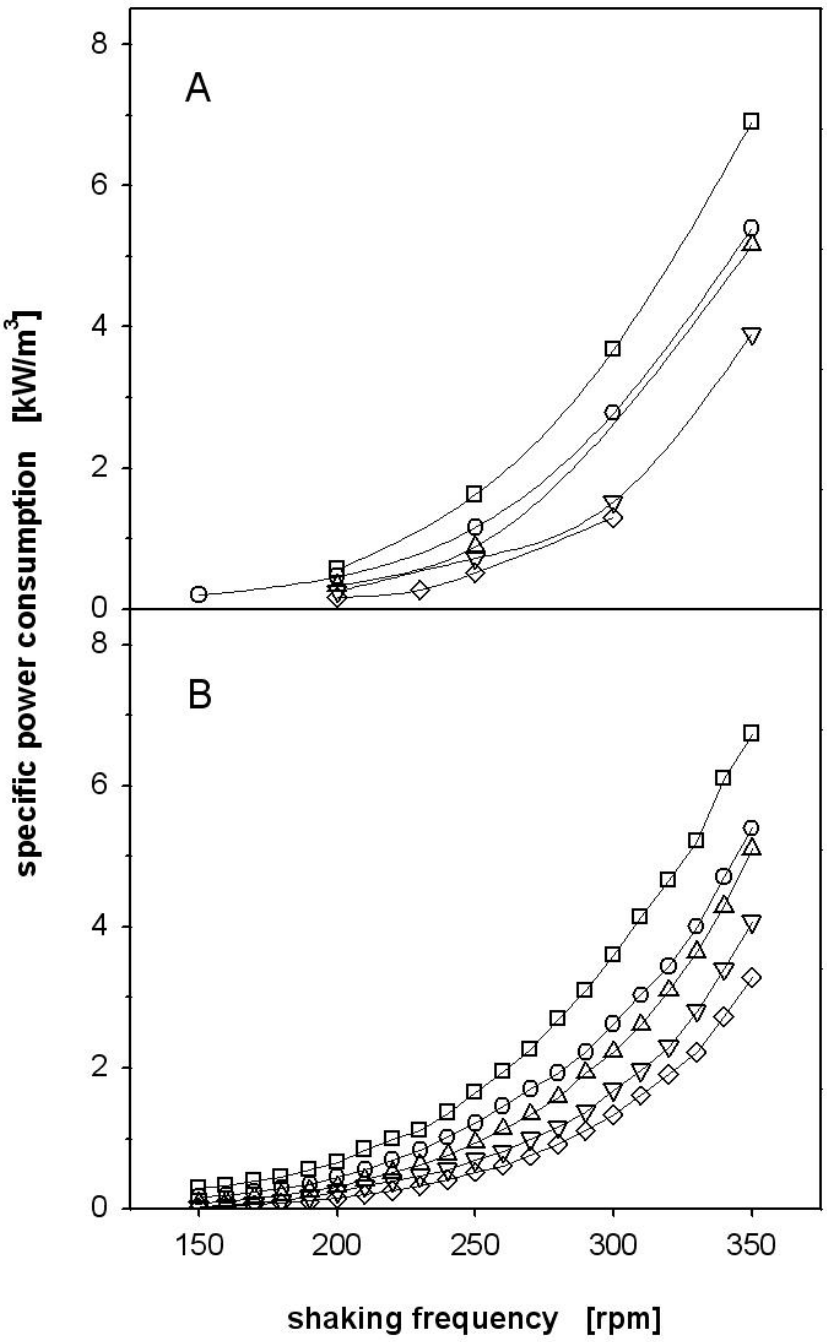

Figure 5.3: Specific power consumption measurement in 2L cylindrical vessel at different shaking frequencies (A) using the temperature method and (B) the torque method with (□) 0.25L, (○) 0.5L, (△) 0.75L, (▽) 1L, (◇) 1.5L filling volumes. Shaking diameter 5 cm.

As shown in Figure 5.3, the tendency and magnitude of the specific power consumption was almost identical with both methods. The power consumption increased with increasing shaking frequency. This general tendency was also found in other cylindrical shaking vessels where power consumption was measured by an electrical method (20). Kato et al. used different vessel sizes but kept a constant ratio

of liquid height to vessel diameter. Moreover, the shaking frequencies used were in the range of 100 to 200 rpm and shaking diameter was kept in the range of 1 cm to 4 cm. In this work wide ranges of shaking frequency were used (100 to 350 rpm). However, the shaking diameter was kept constant at 5 cm. In the work of Büchs et al. on shake flasks the same tendency and same order of magnitude of power consumption was found (18). As the filling volume increased, the specific power consumption decreased due to a decrease of the surface (friction) area to volume ratio. Here filling volumes were changed from 12.5 to 75% of the total vessel volume. Büchs et al. observed similar tendency in conical shake flasks by changing the filling volumes from 4 to 20% of the total flask volume (18).

The specific power consumption in 20L shaking vessels was also measured by the temperature method over a wide range of filling volumes (5L to 15L) and shaking frequencies (100 to 300 rpm) (48). Since the applied integrated torque sensor has a maximum limit of 1 N·m, it was not possible to measure the power consumption by torque method for all the operating conditions. Therefore, a filling volume of 5L was chosen. Power consumption was measured for shaking frequencies from 110 rpm to 160 rpm. It was not possible to measure the power consumption beyond 160 rpm.

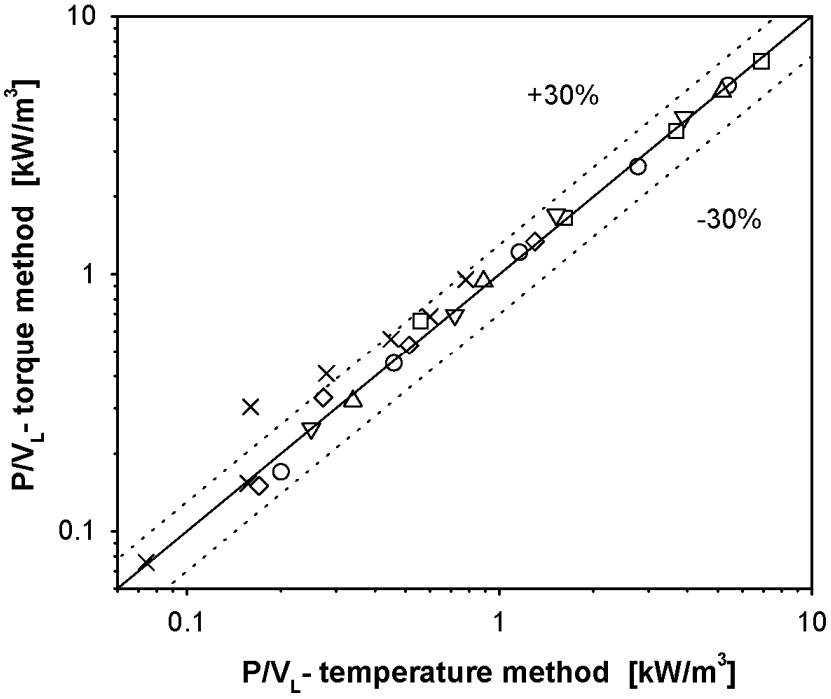

Figure 5.4: A parity plot of values of specific power consumption measured by the torque method and the temperature method in 2L and 20L cylindrical shaking bioreactors at different operating conditions. Water was used as a fluid, 5 cm shaking diameter. The filling volumes in the 2L vessel were (□) 0.25L, (○) 0.5L, (△) 0.75L, (▽) 1L, (◇) 1.5L and in the 20L vessel (X) 10L.

The available data of specific power consumption for 2L and 20L vessels are plotted in a logarithmic parity plot in Figure 5.4. Almost all the data points lie within the tolerance of ±30%. This proves that the temperature method is also a reasonably accurate method.

5.3.2. Extended temperature method

To date, the conventional temperature method was used to determine the power consumption in disposable shaking bioreactors (48). Kato et al. used insulated and non-insulated 20L shaking vessels. In most of the experiments conducted with non-insulated vessel, they used initial fluid temperatures of ca. 40°C (48).

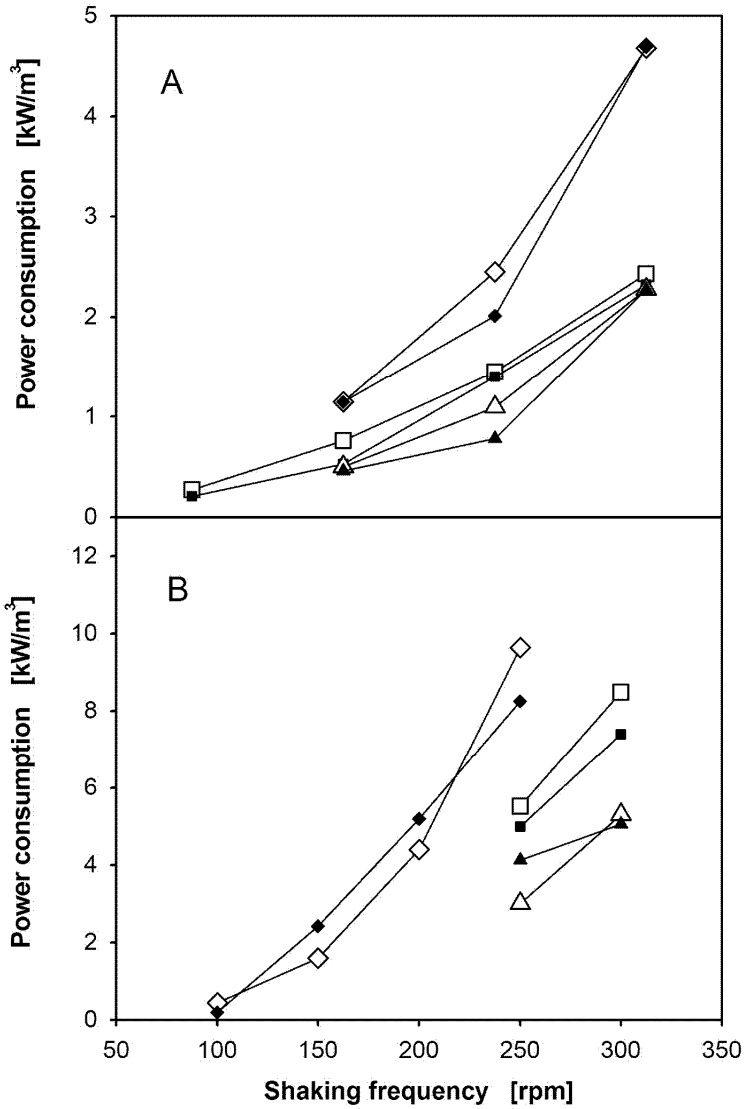

Figure 5.5: Comparison of values of power consumption during heating up and cooling down of a liquid in 20L vessel. Shaking diameter 5 cm. (A) water was heated up for (◇) 25%, (□) 50% and (△) 75% filling volume in insulated vessel and cooled down for (◆) 25%, (■) 50% and (▲) 75% filling volume in non-insulated vessel. (B) 80% glycerol/water mixture was heated up from room temperature for (◇) 25% filling volume in insulated vessel and for (□) 50%, (△) 75% filling volume in non-insulated vessel and was cooled down from ca. 60°C for (◆) 25%, (■) 50% and (▲) 75% filling volume in the non-insulated vessel

Based on all experimental results obtained from both types of the vessels Kato et al. concluded that the maximum deviation was 11%. Henceforth, they used non-insulated shaking vessels for further investigation (48). Figure 5.5A and B compares the values of power consumption obtained in insulated and non-insulated vessels at different operating conditions for water and for 80% glycerol water mixtures, respectively. At these operating conditions, initial fluid temperatures larger than 40°C were used. Figure 5.5A indicates that there are many operating conditions at which the values of power consumption obtained differ from each other, though, maximum difference encountered was 22%. The differences encountered were cross-checked for consistency by repeating the experiments. Results revealed good reproducibility with maximum percentage deviation in the range of ±5 % for both types of vessels used. However, differences in the value of power consumption obtained from insulated and non-insulated vessel still remained. The other conspicuous behaviour was in the values of power consumption obtained in insulated cylindrical vessel which remained always higher than the values obtained by the non-insulated vessel.

A comparison of the power consumption values for the 80% glycerol water mixture is shown in Figure 5.5B. Insulated vessel was used to conduct experiments only with 25% filling volume. The rate of heat generation was relatively higher in the viscous system as compared to that of water. Therefore, for higher filling volumes the insulated vessel was not required to heat up the liquid at operating conditions shown in Figure 5.5B. Hence, experiments of heating up as well as cooling down of liquid were conducted in the non-insulated vessels only.

When power consumption was evaluated by the conventional temperature method, the results did not show a clear trend at different operating conditions. For 25% filling volume, the values of power consumption obtained were similar at 100 rpm, but at 150 and 200 rpm the values obtained from the non-insulated vessel were 40% and 18% higher than that obtained from the insulated vessel, respectively. At 250 rpm the trend reversed and power consumption obtained from the insulated vessel was higher than that obtained from the non-insulated vessel. Similar inconsistent results were encountered for higher filling volumes. The minimum and maximum difference encountered in the value of power consumption for all the operating conditions were 10 and 50% respectively. The unclear trend observed for the 80% glycerol/water system can be explained by the change of fluid physical properties especially, viscosity with temperature.

The change in viscosity of an 80% glycerol/water mixture is more profound with temperature than that for water. For example, at 25° and 40°C the viscosity of an 80% glycerol solution are ca. 45 mPa·s and 20 mPa·s respectively. However, the viscosity of water changes only from ca. 0.9 mPa·s to 0.7 mPa·s between 25° and 40°C. The change in viscosity of water was not as large as for the 80% glycerol/water mixture.

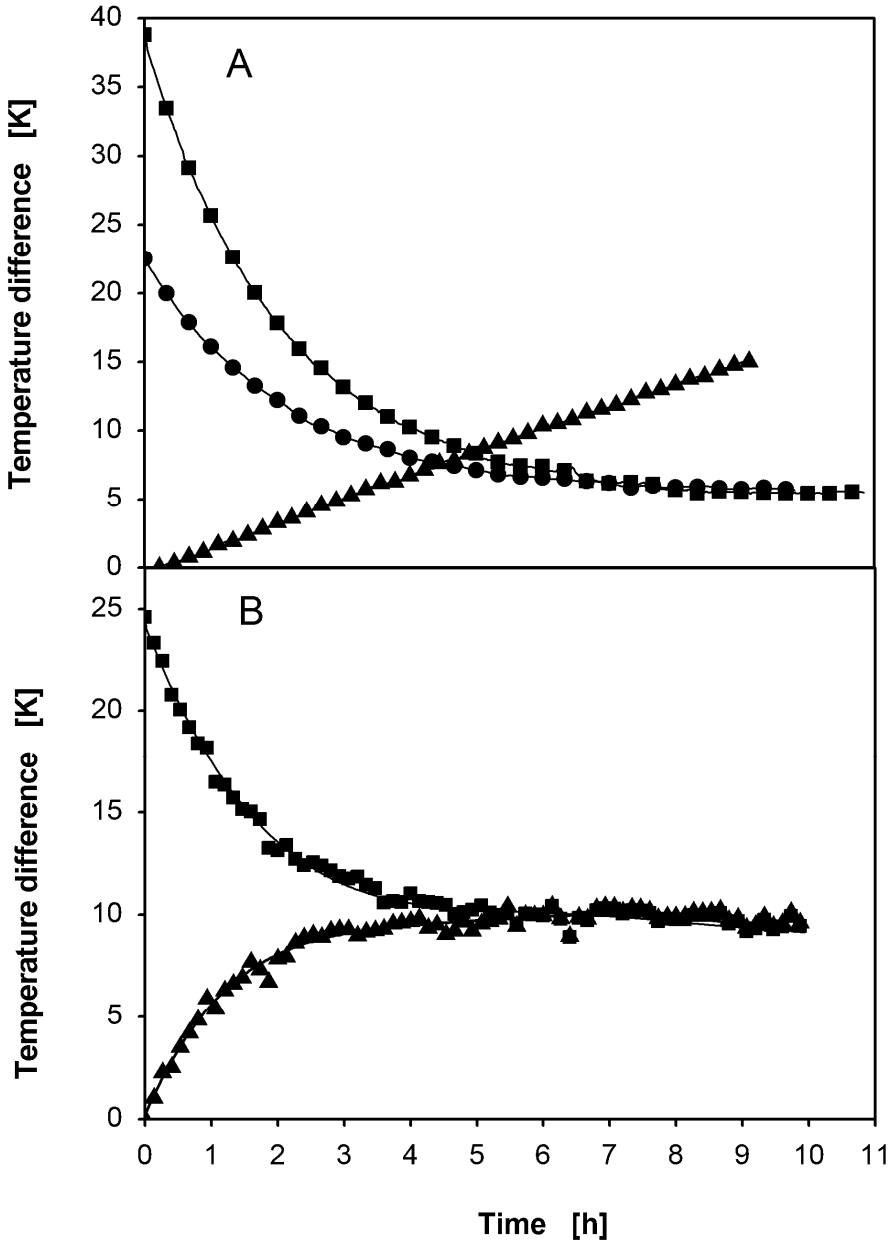

Figure 5.6: Fluid temperature profile over time for 20L cylindrical shaking vessel, 50% filling volume, 250 rpm, 5 cm shaking diameter. (A) water as a fluid at following initial temperatures; (●) 64°C, (C_{fit1}=15.9, C_{fit2}= 3.89, UA = 6.85 W/K), (■) 45°C, (C_{fit1}= 15.2, C_{fit2} = 4.0, UA = 6.85 W/K) in non-insulated vessel, (▲) 20°C, (C_{fit1}= 15, C_{fit2} = 3.95, UA = 0.7 W/K) in insulated vessel and (B) 75% filling volume, 300 rpm, 80% (w/w) Glycerol/water mixture as a fluid at following initial temperatures; (▼) 60°C, (C_{fit1}= 16.2, C_{fit2} = 4.1, UA = 8.7 W/K) and (◆) 27°C, (C_{fit1}=15.5, C_{fit2} = 3.96, UA = 8.7 W/K) in non-insulated vessel. Values in brackets indicate the fitting parameter (C_{fit1}, C_{fit2}) and overall heat transfer coefficient (UA) of equation 3.1 and 3.8, respectively. The solid lines represent simulation generated using these parameters and actual room temperature profile.

Therefore, experiments were performed at different initial temperatures for water where viscosity changes more than 50%, to verify the consistency of the basic model used. All the other operating conditions were kept constant. The measured temperature differences between the fluid inside the vessel and surrounding atmosphere for above mentioned experiments are shown in Figure 5.6. Water was used as fluid in Figure 5.6A with initial temperatures of 64°, 45° and 20°C, respectively. A non-insulated vessel was used for measurement of power consumption at initial temperatures of 64° and 45°C whereas an insulated vessel was used to obtain power consumption with initial temperature of 20°C. Since steady-state temperature differences shown in Figure 5.6 are identical for experiments with different initial fluid temperature, the value of power consumption obtained should remain same. However, at a given operating condition, with water as a fluid, the conventional temperature method predicted values of power consumption of 1.8, 2.32 and 2.43 kW/m^3 at initial temperatures of 64°, 45° and 20°C, respectively. Thus, the difference observed (water as fluid) for initial temperatures of 20° and 45°C was just less than 5%, which is relatively small. However, for an initial temperature of 64°C, a marked difference of 20% from that of the value obtained at 45°C was observed. The significant change in viscosity of water from 1 mPa·s to 0.4 mPa·s at 20° and 64°C, respectively influences the hydrodynamics of the system due to which a marked difference was observed.

The distinct influence of change in the hydrodynamic behaviour of the system on power consumption was readily seen in the 80% glycerol/water system. The temperature profiles observed for two initial temperatures, namely, 60° and 27°C for the 80% glycerol/water mixture (75% filling volume) are shown in Figure 5.6B. The power consumption obtained using the conventional temperature method was 5.13 and 8.33 kW/m^3 for initial temperatures of 60° and 27°C, respectively. In the conventional temperature method, the power consumption or heat generation rate is assumed constant over the entire temperature profile. This assumption however, can not be satisfied when liquid viscosity changes drastically over temperature. The above experiment validated that the effect of changing viscosity must be incorporated into the conventional temperature method. As described in the theory part of the extended temperature method, the dependency of power consumption on viscosity was included in the evaluation method and the assumption of a constant heat generation rate was omitted. An example of parameter estimation by the extended temperature method is shown as solid lines in Figure 5.6. Since filling volume and the shaking

frequency do not change, the parameter *UA* remains constant for the non-insulated vessel (48). However, C_{fit1} and C_{fit2} of equation 3.8 did change in all the three experiments although the percent deviation was less than 2% in Figure 5.6A and 1.7% in Figure 5.6B.

The significance of the new approach is graphically visualized in Figure 5.7. The case when water was cooled down from an initial temperature of 64°C (Figure 5.6A) is shown in Figure 5.7A.

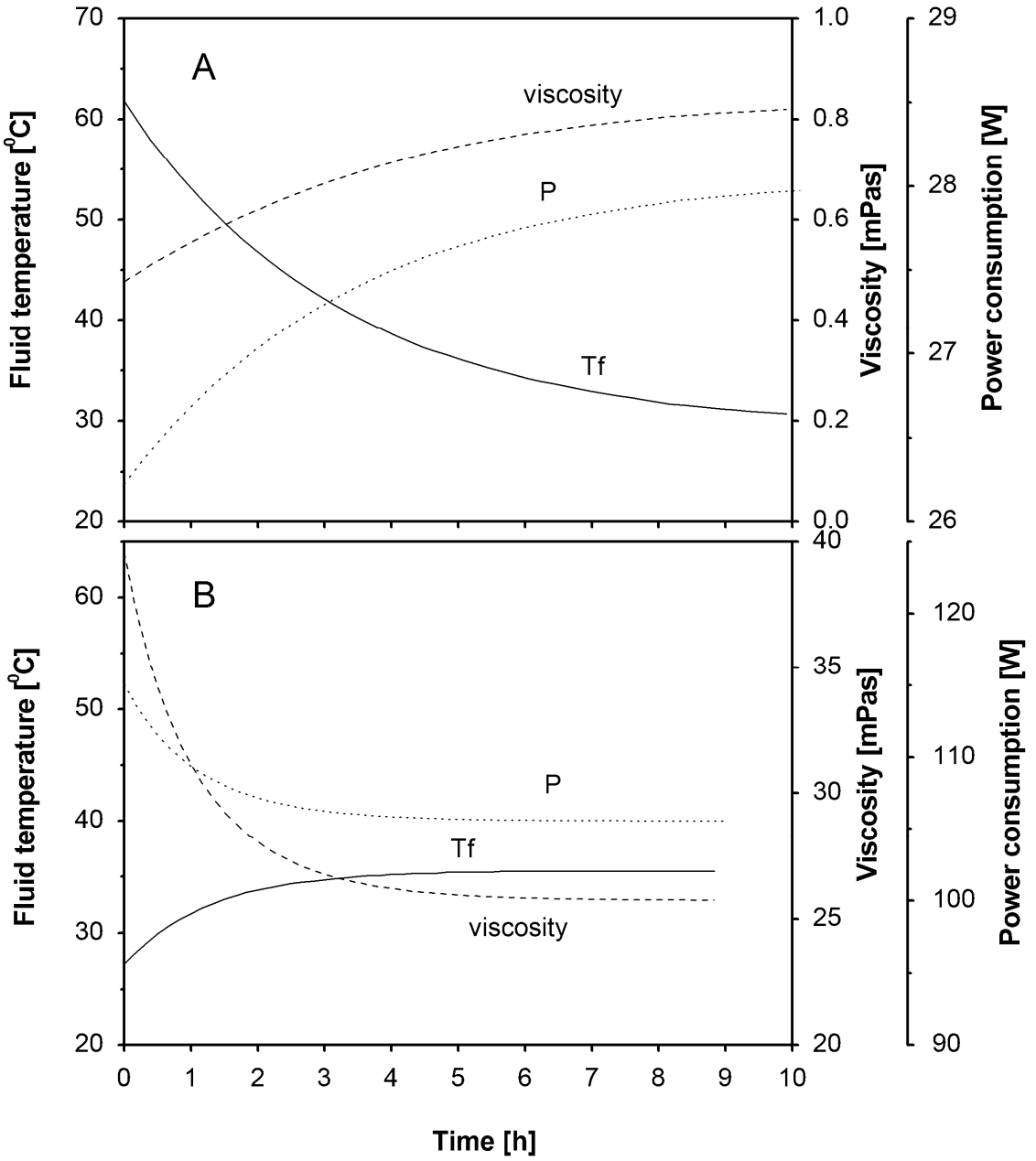

Figure 5.7: Effect of temperature on viscosity as well as on power consumption calculated by extended method in 20L cylindrical shaking vessel, 50% filling volume, 250 rpm, 5 cm shaking diameter. (A) for water (C_{fit1}=15.9, C_{fit2} = 3.89 and *UA* = 6.85 W/K), (B) for 80% (w/w) glycerol/water mixture, 75% filling volume, 300 rpm (C_{fit1}=15.5, C_{fit2} = 3.96, *UA* = 8.7 W/K). The temperature profile shown for explanation in Figure 5.7A is from Figure 5.6A at a starting temperature of 64°C and in Figure 5.7B is from Figure 5.6B at initial temperature of 27°C.

As seen in the Figure 5.7A, the viscosity of water changed from ca. 0.4 mPa·s to 0.85 mPa·s as the water cooled down. This change was taken into account in equation 3.8 and the total power consumption for water changed from 26 W at 64°C to 28 W at 30°C. The case of the 80% glycerol/water mixture when it is heated up from 27°C (Figure 5.6B) is represented in Figure 5.7B. The effect of change of the viscosity on power consumption for the glycerol/water mixture was much larger than that of water and it changed from 114 W at 27°C to 105 W at 35°C.

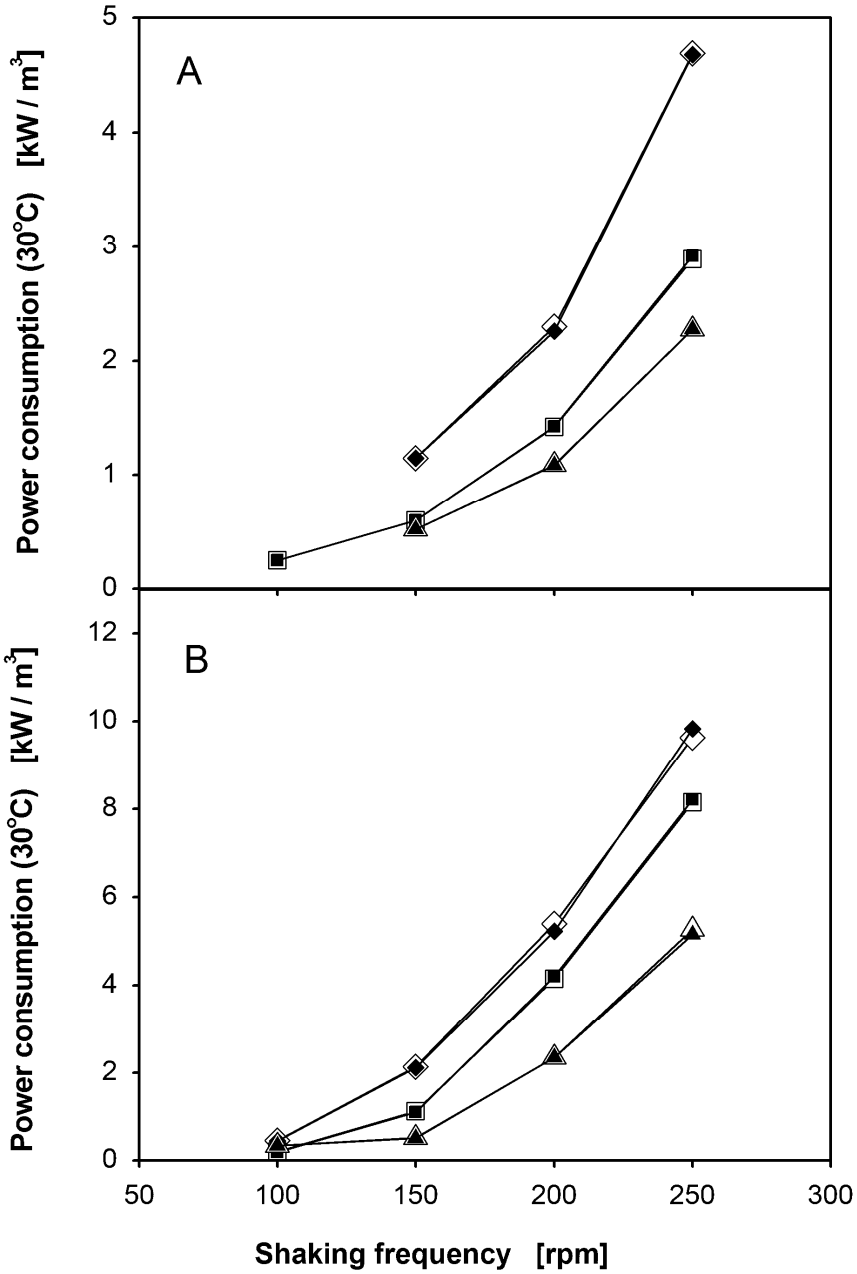

Figure 5.8: Comparison of values of power consumption at 30°C, obtained by the extended temperature method during heating up or cooling down of a fluid in 20L insulated and non-insulated shaking vessel. (A) Water was heated up for (◇) 25%, (□) 50% and (△) 75% filling volume in insulated vessel and cooled down for (◆) 25%, (■) 50% and (▲) 75% filling volume in non-insulated vessel. (B) 80% glycerol/water mixture was heated up from room temperature for (◇) 25% filling volume in insulated vessel and for (□) 50%, (△) 75% filling volume in non-insulated vessel and was cooled down from ca. 60°C for (◆) 25%, (■) 50% and (▲) 75% filling volume in the non-insulated vessel

Thus, it was proved that the change of viscosity must be taken into account for quantification of the power consumption of a fluid whose viscosity changes drastically over temperature. The extended temperature method was applied to measure the power consumption at all operating conditions shown in Figure 5.5. The power consumption obtained from insulated and non-insulated vessel was compared at 30°C. The results are represented in Figure 5.8A and B for water and for the 80% glycerol/water mixture, respectively. The results indicate that the differences between the values of power consumption are reduced to a great extent with the maximum percent deviation of ±3%. However, it should be noticed that the parameters *UA,* C_{fit1} and C_{fit2} were evaluated for each operating conditions separately. That means that each data point had unique values of parameters C_{fit1} and C_{fit2}. These parameters did change with change in operating conditions. Therefore it was necessary to check the statistical significance of parameters C_{fit1} and C_{fit2}. Parameters C_{fit1} and C_{fit2}. were evaluated by simultaneous parameter estimation using all the data sets of temperature profiles obtained for insulated and non-insulated vessels by the gPROMS software as described in the materials and methods part. Results of the simultaneous parameter optimisation were compared with estimated values of parameters for each experiment. Results indicated good agreement with 80% of data points lying in the maximum percent deviation of ±15% and the rest 20% lying in the maximum percent deviation of ±30%. The final values of parameters C_{fit1} and C_{fit2} were 15 and 3.5, respectively.

5.4. Non-dimensional description of power consumption

The extended method was then used to measure power consumption for the 80% glycerol/water solution for different operating conditions. Figure 5.9 shows the power consumption obtained for water and for an 80% glycerol/water system. As expected, the specific power consumption increased with increasing shaking frequency for different filling volumes. The specific power consumption decreased with increasing filling volume in both size of vessels. Specific power consumption increased with increasing fluid viscosity. Büchs et al. found a similar behaviour in conical shake flasks but the maximum filling volume investigated was 20% (18). The trend of specific power consumption tends to decrease at two operating conditions for the 80% glycerol/water mixture, namely, 50% filling volume, 300 rpm in 20L vessel and 75% filling volume, 275 rpm for 50L vessel. Unfortunately, it was not possible to operate the shaking machine beyond above mentioned shaking frequency because of

mechanical instability of the vessel supports. The tendency of decreasing power consumption with increasing shaking frequency demonstrates onset of “out-of-phase” mixing conditions.

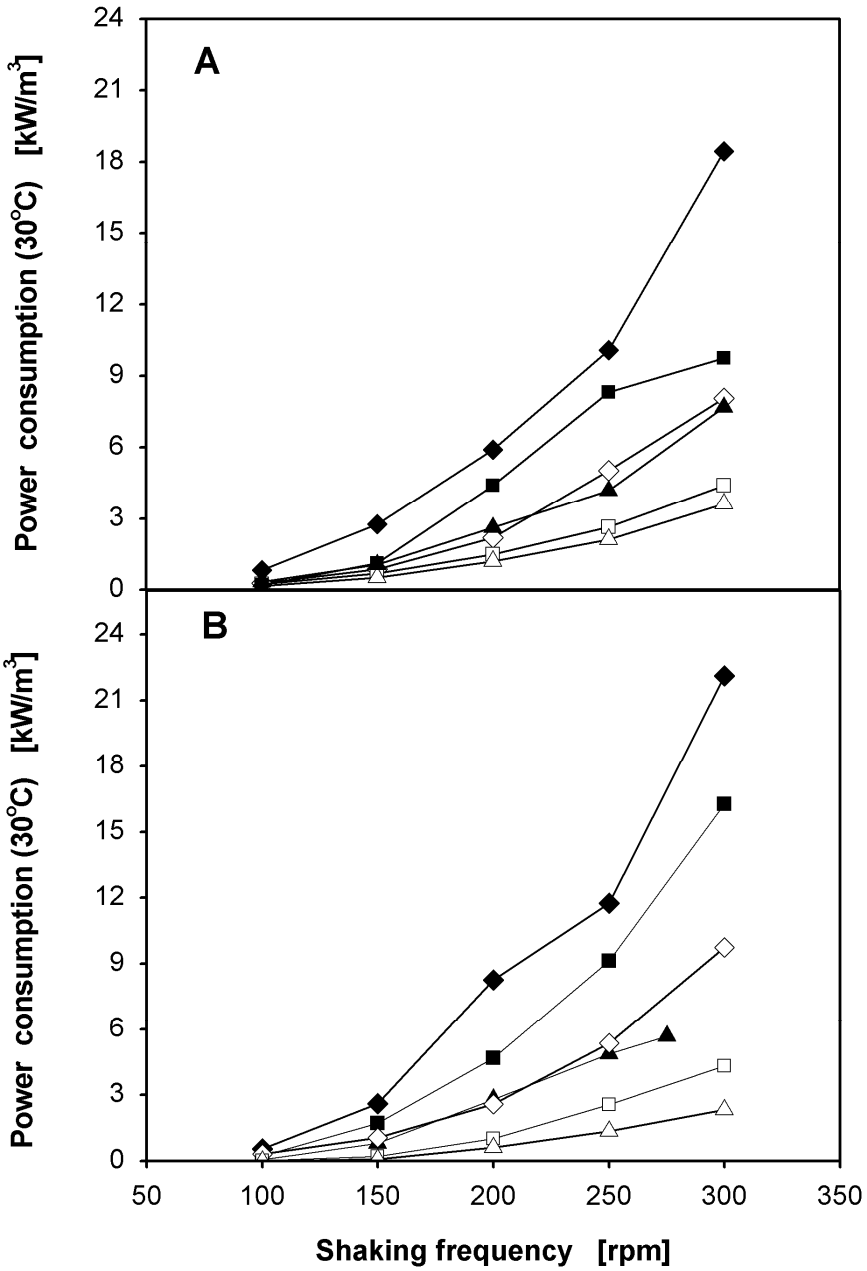

Figure 5.9: Specific power consumption obtained at a 5 cm shaking diameter for (A) 20L vessel, water as a fluid, (◇) 25%, (□) 50% and (△) 75% filling volume and 80% glycerol/water mixture as fluid, (◆) 25%, (■) 50% and (▲) 75% filling volume (B) 50L vessel, water as fluid, (◇) 25%, (□) 37.5% and (△) 75% filling volume and 80% glycerol/water mixture at (◆) 25%, (■) 40% and (▲) 75% filling volume.

Lotter et al. investigated these unfavourable “out-of-phase” operating conditions in large shake flasks (46). They developed following empirical equation for start of “out-of-phase” operating conditions for large shake flasks of sizes 1L, 2L and 5L.

$$n_{crit} = 424 \cdot \eta^{-0.037} \cdot V_L^{0.267} \cdot d_0^{0.633} \cdot V_F^{-0.41} \qquad 5.2$$

where,

n_{crit} Critical shaking frequency at which “out-of-phase” condition starts (rpm)

η Fluid viscosity (mPa·s)

V_L Filling volume (mL) (in the range of 10 to 750 mL)

d_0 Shaking diameter (cm) (1.25 and 2.5 cm)

V_F Shaking vessel volume (mL) (1000 to 5000 mL)

The calculated values of n_{crit} for the 20L (50% filing volume) and 50L (75% filing volume) vessel are 208 rpm and 203 rpm respectively, for the 80% glycerol/water mixture. The observed values of shaking frequencies for onset of the “out-of-phase” conditions for the 80% glycerol/water mixture in 20L and 50L vessel are 300 rpm and 275 rpm, respectively. The predicted values of n_{crit} differ from what was observed in large disposable shaking vessels. Therefore, the empirical equation developed by Lotter et al. could not be simply extrapolated to cylindrical shaking vessels.

Figure 5.9 is rearranged to show a fluid specific diagram (Figure 5.10A for water and Figure 5.10B for the 80% glycerol/water mixture) of specific power consumption obtained in shaking bioreactors of size 20L and 50L. At 25% filling volume, the specific power consumption obtained in 50L vessel was higher than that obtained in 20L vessel. The same trend was observed for the 80% glycerol/water mixture but 150 rpm onwards. As vessel diameter increased, the relative velocity between the vessel wall and rotating liquid increased which lead to higher power consumption in large shaking vessels than in small shaking vessels. The same trend was observed in cylindrical shaking vessels of the size up to 12L (20) and conical shaking vessels for size up to 5L (18). However, for water as a fluid (Figure 5.10A), as the filling volume increased the trend changed and the value of power consumption obtained in 50L vessel at 50% filling volume were similar to that obtained for 20L vessel. At 75% filling volume the power consumption obtained in 50L vessel was lower than that obtained in 20L vessel. The same behaviour was observed while evaluating power consumption at different operating conditions in conical shaking vessels but for viscous fluid system (16-18) which were defined as the "out-of-phase" mixing conditions where no homogeneous mixing was observed.

For an out-of-phase operating condition, as the fluid viscosity increases the power consumption becomes worse. That means that if instead of water, a viscous fluid

system is used in cylindrical shaking vessels, the differences observed in values of power consumption at different relative filling volumes shall become larger.

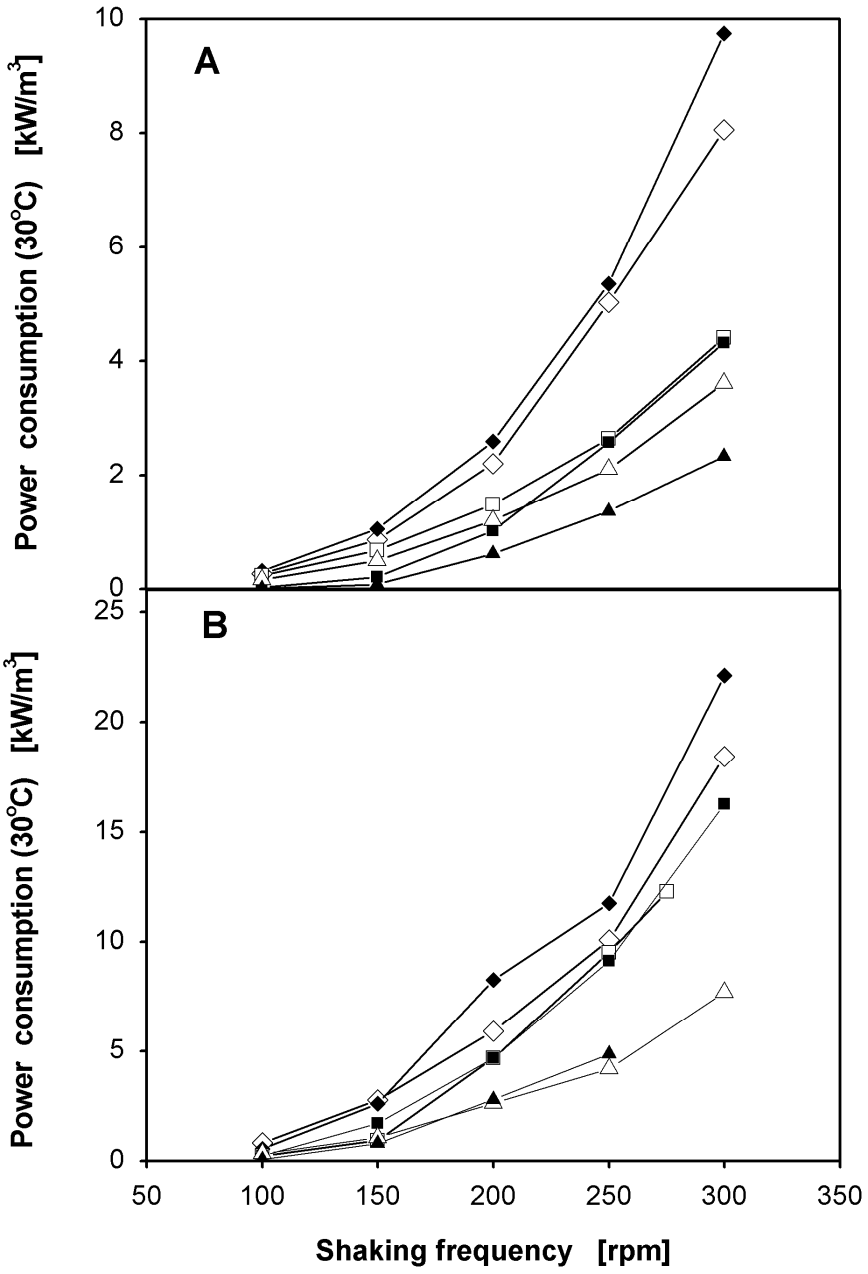

Figure 5.10: Specific power consumption obtained in 20L and 50L cylindrical vessels at 5 cm shaking diameter for (A) water as a fluid, (◇) 25%, (□) 50% and (△) 75% filling volume in 20L vessel and (◆) 25%, (■) 50% and (▲) 75% filling volume in 50L vessel and (B) 80% glycerol/water as a fluid, (◇) 25%, (□) 37.5% and (△) 75% filling volume in 20L vessel and (◆) 25%, (■) 40% and (▲) 75% filling volume in 50L vessel.

However, this phenomenon was not observed for viscous system. Figure 5.10B represents a different behaviour with increasing relative filling volumes for the glycerol/water system. The specific power consumption obtained in 20L and 50L vessels with 40 and 75% filling volume remained almost the same. These results indicate that the mixing observed at above mentioned operating conditions, especially

in the case of the 50L vessel may be in the transitional region between "in-phase" and "out-of-phase" operating conditions. The above hypothesis is explained in the Figure 5.11.

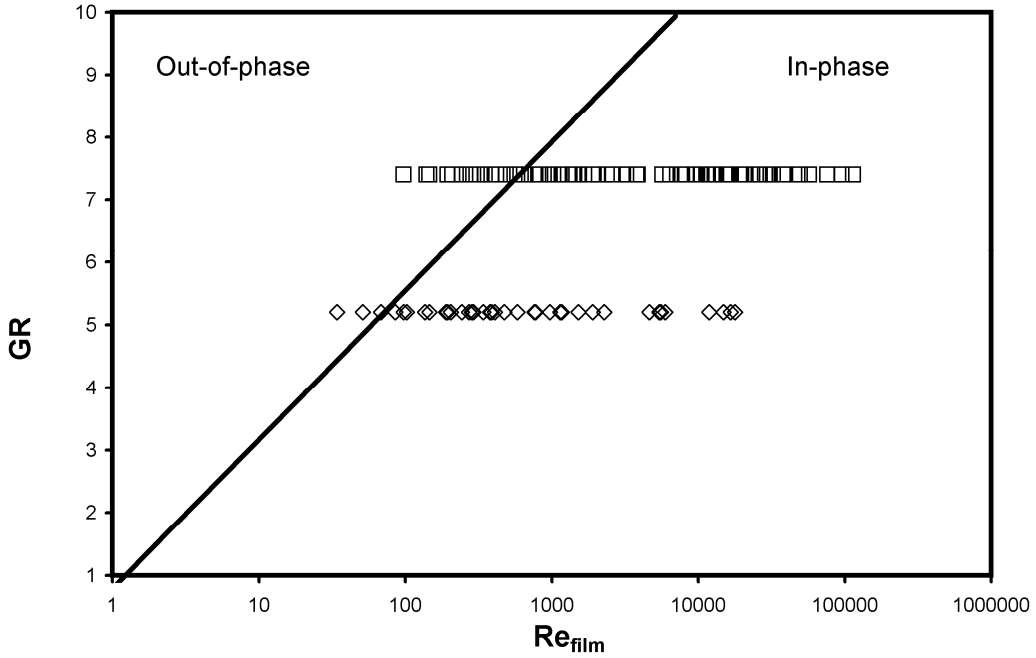

Figure 5.11: Diagram of Geometric Ratio *(GR=d_0/d)* versus film Reynolds number (*Re_{film}* for (□) 50L and (◇) 20L cylindrical shaking vessel. Solid line indicates boundary between in-phase and out-of-phase operating conditions for conical shaking bioreactors derived by Büchs et al (17).

The operating conditions of 20L and 50L vessels are plotted as a function of dimensionless Geometric Ratio *(GR)* in figure 5.11. The diagram also shows the boundary between in-phase and out-of-phase operating conditions for conical shake flasks of size up to 5L. This boundary is defined as Phase number (*Ph*) developed by Büchs et al. for conical shake flasks (17). The *Ph* describes the fluid mixing inside the shake flask and if *Ph* is less than 1.26 for a given operating condition, then there is no mixing observed and that condition is defined as out-of-phase operating condition. Mathematically,

$$Ph = \frac{d}{d_0} \cdot \left(0.41 + 4.24 \cdot \log\left(\mathrm{Re}_f\right)\right) > 1.26 \qquad 5.3$$

where,

$$\mathrm{Re}_f = \frac{\rho \cdot (2 \cdot \pi \cdot n) \cdot f^2}{\eta} \qquad 5.4$$

$$f = \frac{d}{2} \cdot \left(1 - \sqrt{1 - \frac{4}{\pi} \cdot \left(\frac{V_L^{\frac{1}{3}}}{d} \right)^2} \right) \qquad 5.5$$

Here, the solid line is shown as a reference to different hydrodynamic behaviour of the system and it can not be taken as a boundary between “in-phase” and “out-of-phase” conditions in large cylindrical shaking bioreactors. Though the hydrodynamic conditions for small shake flasks can not be applied directly to large cylindrical shaking vessels, the Figure 5.11 gives a hint of the transitional hydrodynamic behaviour for shaking bioreactors of size 50L. Almost 30% of all data points of the 50L vessel lie in “out-of-phase” region. This could be the reason of employing 10 cm shaking diameter for cylindrical vessels of size 50L by Liu et al (31, 32) (Personal communication). It also indicates that if vessel sizes larger than 50L are used at 5 cm shaking diameter, the “out-of-phase” condition can be readily observed and it may lead to unfavourable fluid flow and consequently poor mixing in the system.

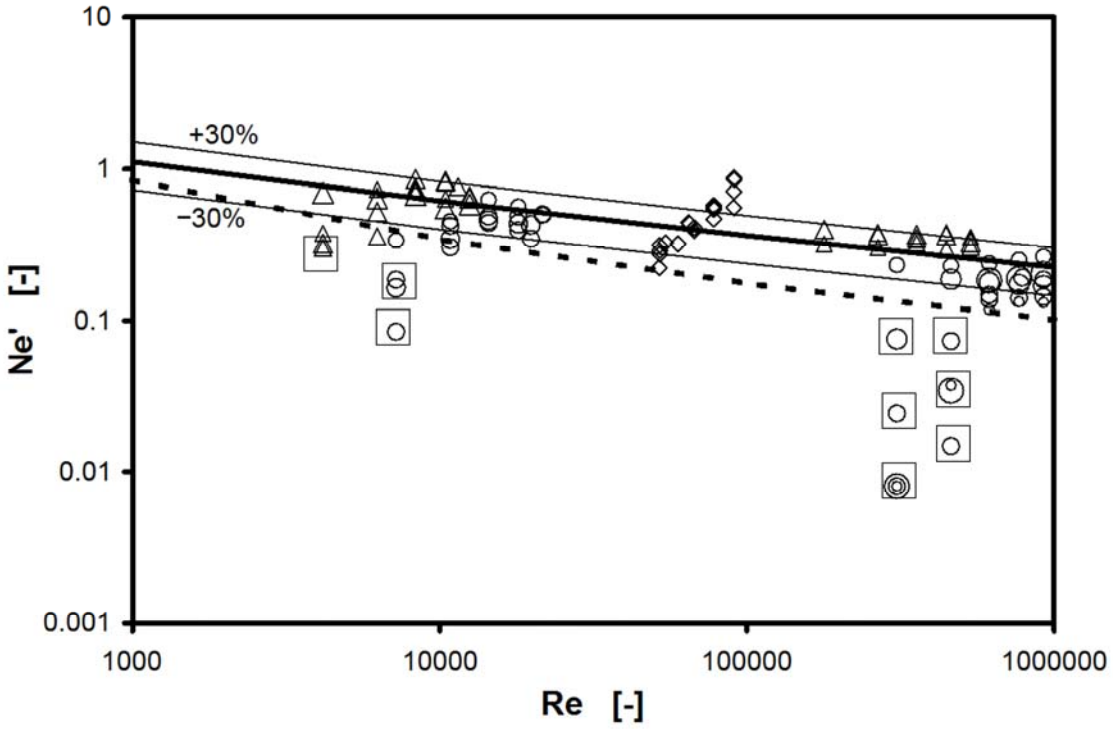

Figure 5.12: Modified Newton number versus Reynolds number diagram for (◇) 2L, (△) 20L and (○) 50L cylindrical shaking bioreactors at 5 cm shaking diameter. The bold solid line generated from equation 5.6 represents the band which comprises of all data sets lying between the two thin lines marked with +30% and -30%, respectively. The dotted line is the correlation of Ne' as a function of Re developed by Büchs et al. (17). The data points marked with open squares represent “out-of-phase” operating conditions and therefore they are not taken into account for curve fitting.

So far, only one shaking diameter (5 cm) was used for all the operating conditions shown in this thesis. A detailed investigation of the effect of the shaking diameter on

power consumption is required before reaching to any final conclusion between "in-phase" and "out-of-phase" for above mentioned operating conditions as the shaking diameter has a major influence in the shake mixing (17).

All the above mentioned data sets and the data sets of the 2L vessel were plotted in dimensionless *Ne'* vs *Re* diagram (Figure 5.12). As the Figure depicts, most of the data sets lay well on a band except a few data sets marked with the squares. The value of *Ne'* for these circle marked operating conditions was almost one to two orders lower than the other data sets. At these operating conditions, the power consumption was measured by measuring cooling rate of liquid in non-insulated vessels. The heat generation rate was much lower than the heat removal rate through vessel wall and the steady-state temperature difference between the fluid inside the vessel and the surrounding atmosphere was less than 0.8 K. This represents likelihood of “out-of-phase” conditions.

For the present “in-phase” data set an empirical model was developed by choosing all the operating conditions where the temperature difference between the fluid and surrounding atmosphere at steady state was higher than 0.8 K. The result of parameter estimation is presented as solid line in the Figure 5.12. The empirical model can be written in terms of *Ne'* vs *Re* as follows,

$$Ne' = 15 \cdot Re^{-0.6} + 3.5 \cdot Re^{-0.2} \qquad 5.6$$

The model predicted the actual data sets with the maximum deviation of ±30%. The model developed for conical shake flasks by Büchs et al. (17) is also shown as a dotted line in Figure 5.12. The model line representing the conical shake flasks lie below the model line of cylindrical shaking vessels. The reason of which can be in the different geometries of the conical and cylindrical vessels.

5.5. Heat transfer characteristics

5.5.1. Necessity to characterize the bioreactors in terms of heat transfer

The effect of power consumption on fluid heating in non-insulated vessels with no lateral air flow is elucidated in Figure 5.13.

Figure 5.13A details an experiment in which water was cooled down in a 50L vessel at 100 rpm till steady state was reached and then the shaking frequency was increased to 250 rpm to study the increase in steady-state fluid temperature. As Figure 5.13A shows, at 250 rpm the fluid temperature was almost 10 K higher than the surrounding

atmosphere at steady-state. The heat generation rate for viscous fluid was higher than that for water, as expected and therefore, the steady-state fluid temperature was also high. The heating of the 80% glycerol/water solution in the 50L non-insulated cylindrical vessel at 250 rpm without lateral air flow is shown in Figure 5.13B. The steady-state fluid temperature was almost 25 K higher than the surrounding atmosphere.

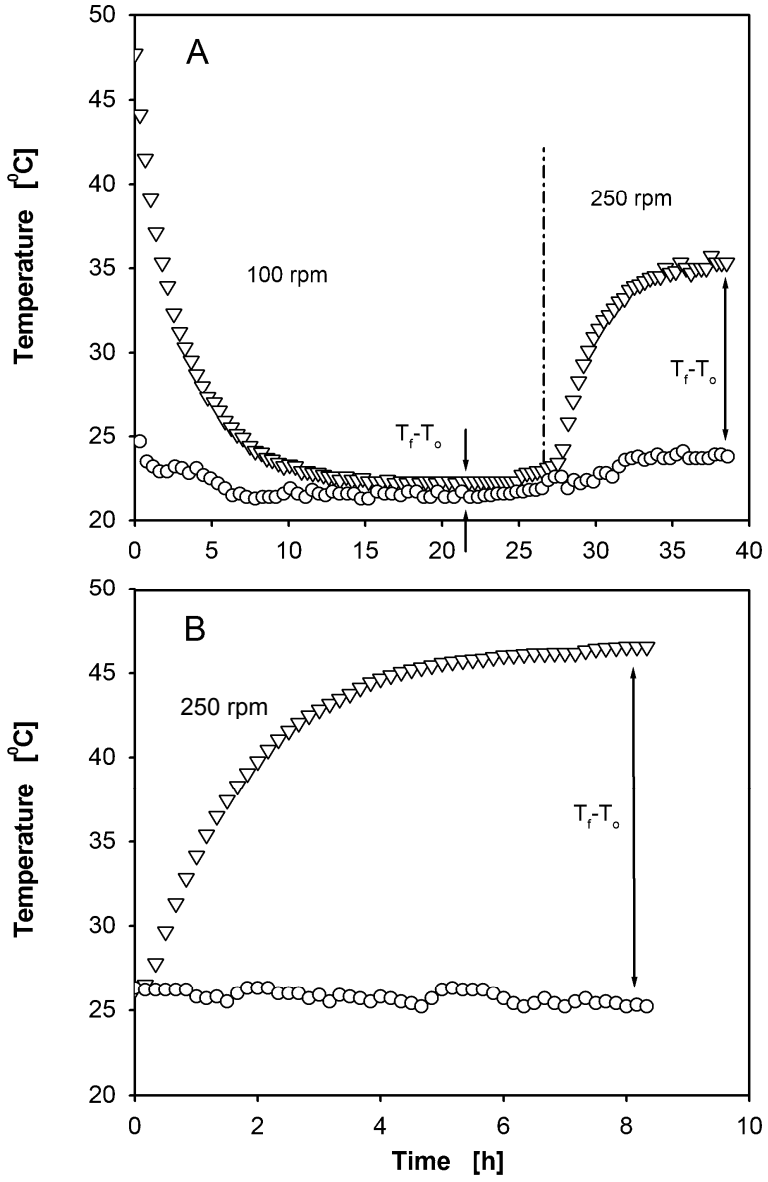

Figure 5.13: Fluid temperature profile in a 50L cylindrical vessel with 25% filling volume for (A) water and (B) an 80% glycerol/water mixture; at 5 cm shaking diameter. The symbol (▽) shows fluid temperature profile *(T_f)* and (○) shows room temperature profile *(T_o)* over time.

5.5.2. Characterization of *UA* without lateral air flow

Steady-state temperature difference between the fluid and the surrounding atmosphere for 20L and 50L disposable shaking bioreactors at different filling volumes is represented in Figure 5.14.

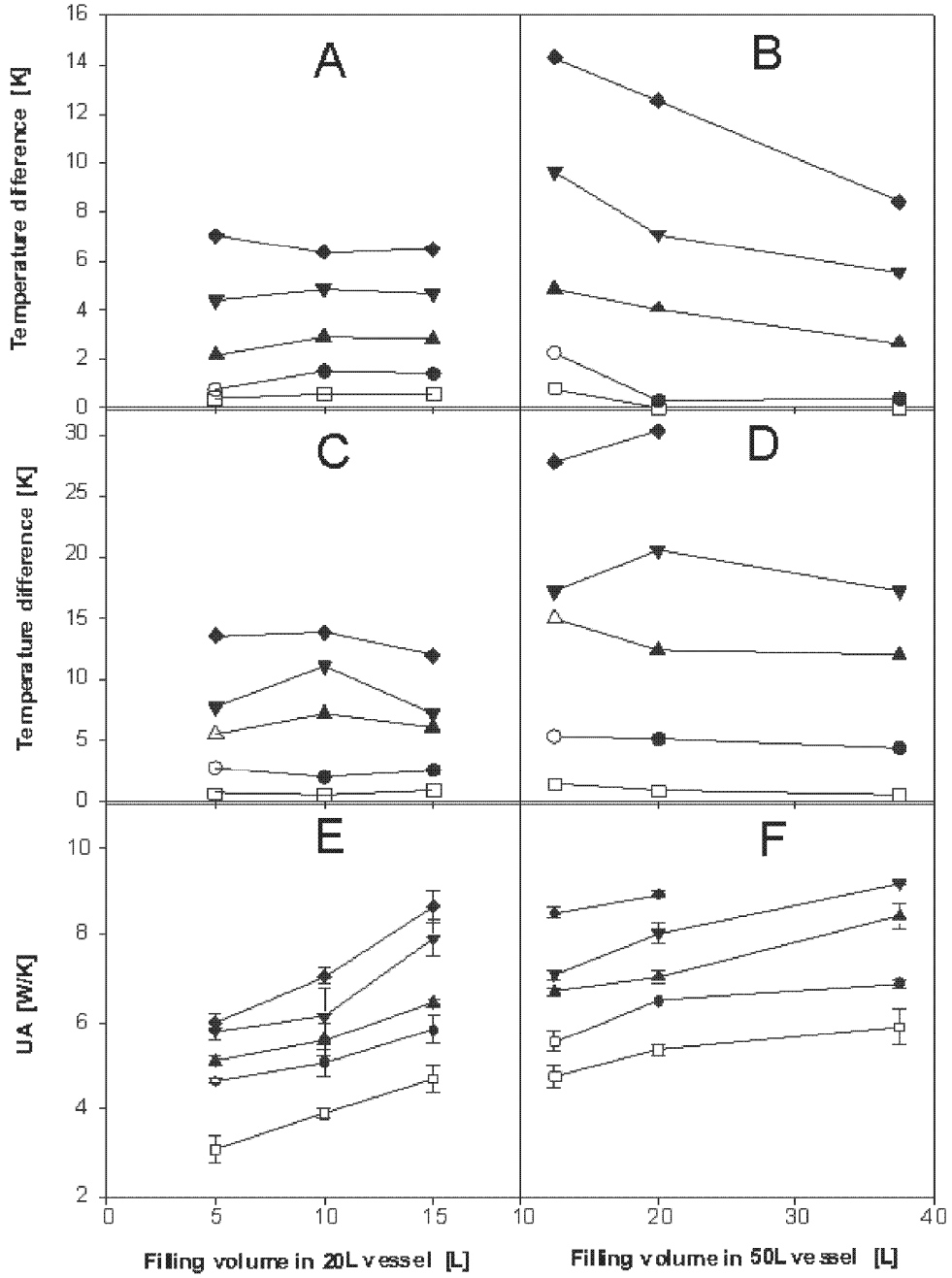

Figure 5.14: Figure shows temperature difference between fluid inside the vessel and surrounding atmosphere for (A, B) water; (C, D) 80% glycerol/water mixture. Figure (E, F) shows average values of overall heat transfer coefficient obtained with water and an 80% glycerol/water mixture in the 20L (E) and 50L (F) cylindrical bioreactors at different operating conditions. The shaking frequencies used were (□) 100 rpm, (○) 150 rpm, (△) 200 rpm, (▽) 250 rpm and (◇) 300 rpm. Solid symbols indicate operating conditions at which fluid touched vessel top. All experiments were carried out at 5 cm shaking diameter.

The data points at a specific filling volume represent values of steady-state temperature difference obtained with an increase in shaking frequency from 100 to 300 rpm with increment of 50 rpm. Figure 5.14A and B shows the steady state temperature differences obtained with water as a fluid at different operating conditions for 20L and 50L vessels, respectively. In the case of 20L and 50L vessel the maximum steady state temperature differences of 7 K (Fig. 5.14A) and 15 K (Fig.

5.14B) were observed, respectively. No difference in the steady state temperature difference was observed for 20L vessel as the filling volume increased. Whereas a sharp decrease in the steady state temperature difference with increase in filling volume was observed for 50L vessel. As described in equation 3.1, the steady state temperature difference is dependent on the heat generated due to shake mixing as well as heat removal from the vessel to the surrounding atmosphere. For the 50L vessel, with increase in the filling volume, there was no increase in rate of heat generation in proportion to the heat removal which could have resulted in lower steady state temperature differences. Moreover, at 100 rpm the steady state temperature difference was almost 0 K with increasing filling volume in 50L vessel, which proves that the heat removal rate was much higher than the heat generation rate. Figure 5.14C and D shows the steady state temperature differences obtained for an 80% glycerol/water mixture. The maximum temperature difference obtained in 20L and 50L vessel was almost two times higher than that obtained for water as a fluid. As the fluid viscosity increased, the heat generation rate or power consumption increased. Therefore, as shown in Figure 5.14D, the sharp decrease of steady state temperature difference with increasing filling volume in 50L vessel was not observed for the 80% glycerol/water mixture.

The overall heat transfer coefficient is the summation of the liquid side heat transfer coefficient, the ratio of wall thick to thermal conductivity of vessel wall and gas side heat transfer coefficient. Mathematically,

$$\frac{1}{U} = \frac{1}{h_L} + \frac{l}{k} + \frac{1}{h_g} \qquad 5.7$$

where,

U Overall heat transfer coefficient (W/m^2/K)

h_L Liquid side heat transfer coefficient (W/m^2/K)

l Thickness of the vessel wall (m)

k Thermal conductivity of vessel material (W/m/K)

h_g Gas side heat transfer coefficient (W/m^2/K)

For cylindrical vessel, the liquid side heat transfer coefficient can be correlated with power consumption as follows (49),

$$\frac{h_L}{\rho \cdot c_p} = 0.13 \cdot \left(\frac{P_V \cdot \rho}{\eta^2} \right)^{\frac{1}{4}} \cdot P_r^{-2/3} \qquad 5.8$$

where,

$$P_r = \frac{c_p \cdot \eta}{k}$$

If power consumption is assumed to be ca. 1 kW/m^3, then according to the above equation the value of liquid side heat transfer coefficient is in the range of 3000 W/m^2/K (for water) to 610 W/m^2/K at the maximum viscosity encountered for 80% glycerol/water mixture (P_v = 1 kW/m^3, 45 mPa·s at 25˚C). The thickness of the 20L and 50L polypropylene vessel wall was 0.4 cm and 1.5 cm, respectively and its thermal conductivity was 0.4 W/m/K which results in a wall heat transfer coefficient of about 100 W/m^2/K for 20L vessel wall and 26.5 W/m^2/K for 50L vessel wall. As Figure 5.14E and 5.14F shows, the value of overall heat transfer coefficient (UA) is in the range of 3 to 9 W/K. Considering the liquid height of ca. 20 cm in 20L vessel and 40 cm in 50L vessel, the heat transfer area between the fluid inside the vessel and the surrounding can be assumed to be ca. 3000 cm^2 for 20L and 5000 cm^2 for 50L vessel including the bottom surface of the vessel. This yields to an overall heat transfer coefficient in the range of 10 W/m^2/K to 30 W/m^2/K for 20L vessel and 6.6 W/m^2/K to 17 W/m^2/K for 50L vessel. If the values of overall heat transfer coefficient (ca. 10 W/m^2/K) are compared with the liquid side heat transfer coefficient (from 3000 to ca. 610 W/m^2/K) and wall resistance (ca. 100 W/m^2/K for 20L, ca. 30 W/m^2/K for 50L), then the outside heat transfer coefficient should have values near to the overall heat transfer coefficient. Therefore, under the normal operating conditions without lateral air flow, the outside heat transfer coefficient is the limiting step for overall heat transfer from the liquid inside the vessel to the surrounding atmosphere, irrespective of the fluid viscosity inside the vessel. This fact is justified in Figure 5.14E and F which shows the averaged values of experimentally found UA for water and viscous system for different operating conditions. The error bars represents the differences obtained in the UA for water and an 80% glycerol/water viscous system. There was no dramatic difference observed between the estimated UA for water and an 80% glycerol/water viscous system. As the filling volume increased, the UA increased because of the large surface area available for heat removal from the vessel to the surrounding. In Figure 5.14, the close symbols indicate the fluid touching at the top of the shaking vessel. Although the fluid touched at the top of the vessel at lower filling volumes, the

UA increased with increase in the filling volume. The contact area between the surrounding atmosphere and fluid inside the vessel varied with varying shaking frequency and filling volume. The example of which is shown in Figure 5.15.

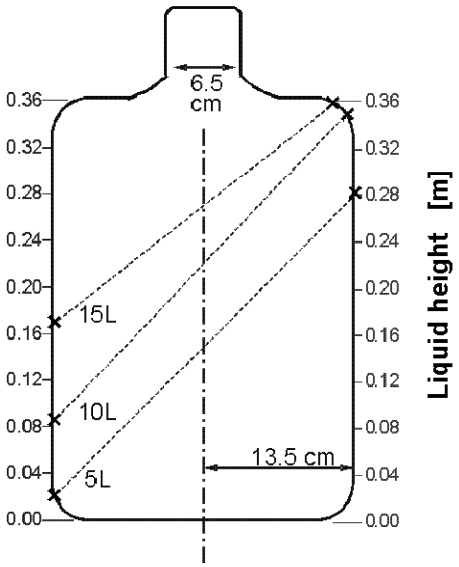

Figure 5.15: Actual liquid height in a 20L cylindrical vessel at 150 rpm, 5L, 10L and 15L filling volumes and 5 cm shaking diameter. Water was used as a fluid.

The Figure indicates the actual liquid height inside a 20L cylindrical vessel at 150 rpm. The liquid height observed at the two sides of a vessel is connected with a solid line. Liquid inside the vessel followed a paraboloid pattern because of the centrifugal forces acting on it. The contact area between the water inside the vessel and the surrounding atmosphere increased with increasing filing volume at a specific shaking frequency and hence, overall heat transfer coefficient also increased. In a previous publication, Kato et al. also observed increase in *UA* with increase in filling volume and shaking frequency (48).

5.5.3. Characterization of *UA* with lateral air flow

UA increased with increasing shaking frequencies because the surface area of the vessel wall in contact with the hot fluid increased and the relative air velocity around the shaking vessel increased which reduced the heat transfer barrier from vessel wall to surrounding. Therefore, this barrier to heat transfer was further reduced by thorough ventilation by lateral air flow. The resultant effect on *UA* was characterised. As shown in Figure 5.16A the steady-state temperature difference decreased with increase in lateral air flow. Although the steady-state temperature difference reduced to less than 1.2 K for the 20L vessel, its value obtained in the 50L vessel at maximum attainable lateral air velocity was 3.2 K. This can be justified from Figure 5.16B which

shows that *UA* did not increase linearly for the 50L vessel at lateral average air velocity higher than 5 m/s. The thickness of the 50L polypropylene vessel wall was 1.5 cm and its thermal conductivity was 0.4 W/m/K which results in a wall heat transfer coefficient of about 26 W/m^2/K. Considering the liquid height of 50 cm and vessel diameter of 38 cm, the heat transfer area can be estimated to be ca. 6000 cm^2.

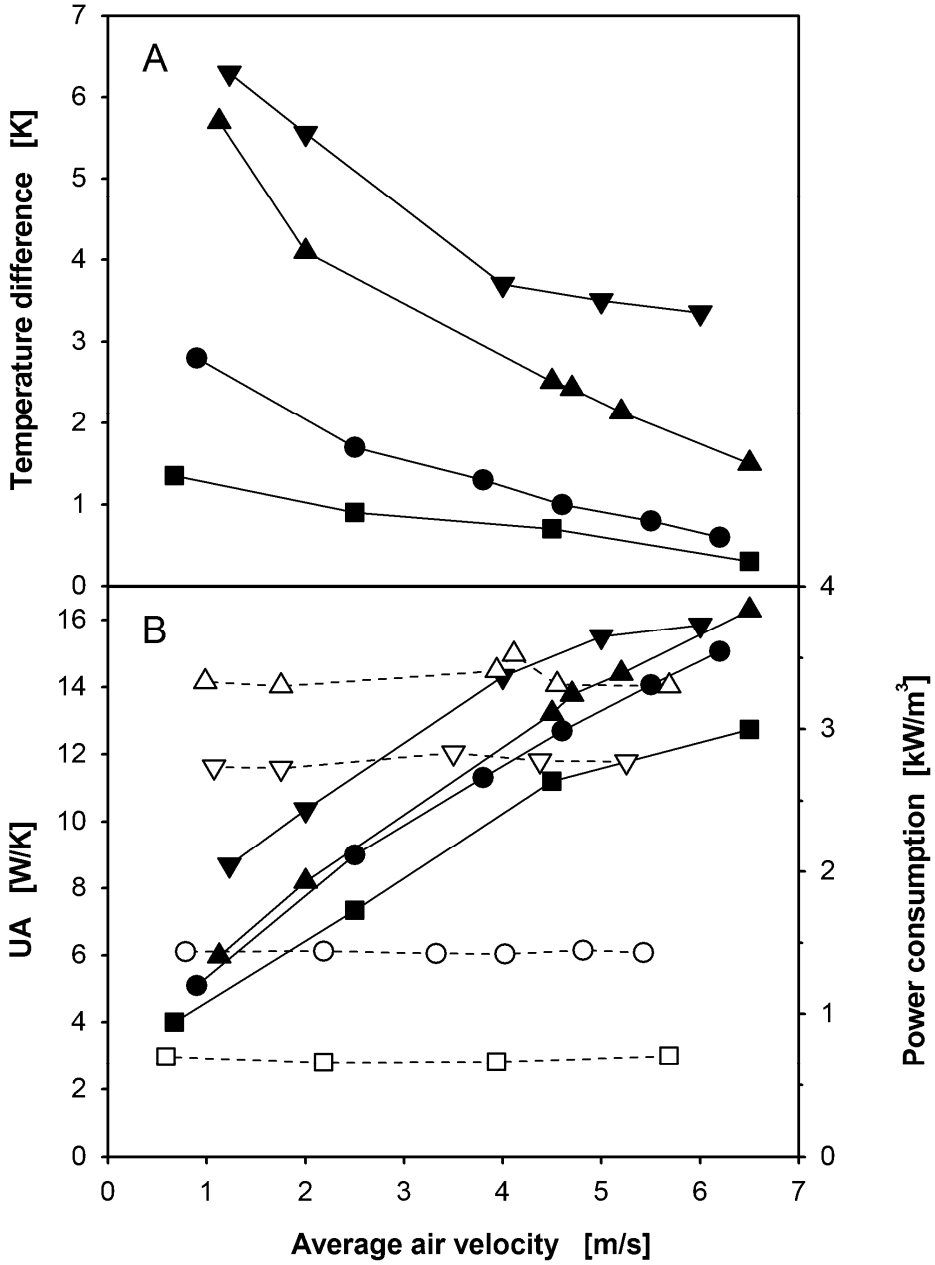

Figure 5.16: (A) Temperature difference between the fluid (water) inside the vessel and surrounding atmosphere for the 20L vessel, 10L filling volume at (■) 150 rpm, (●) 200 rpm, (▲) 250 rpm; 50L vessel, 20L filling volume at (▼) 200 rpm. The solid lines in Figure (B) shows the values of *UA* and dashed lines shows values of power consumption obtained for above mentioned operating conditions at different lateral air velocities.

At a lateral velocity of 5 m/s, the value of UA was approximately 15 W/K. Therefore, the overall heat transfer coefficient can be estimated to approximately 25 W/m^2/K. A

comparison of the overall heat transfer coefficient and the wall heat transfer coefficient indicates that the wall resistance can become limiting for higher lateral air flow rates. It should be noted here that the values of power consumption remained almost constant at different air flow rates as shown in Figure 5.16B which shows the reliability of the temperature method.

As explained above, the heat transfer from the vessel was solely dependent on the surrounding atmosphere. The relative air velocity and contact area between the liquid and surrounding atmosphere determined the heat transfer rate from vessel to the surrounding. Therefore, *UA* (W/K) can be correlated with the shaking frequency, filling volume and the lateral air velocity as follows,

$$UA = 0.18 \cdot n^{0.55} \cdot V_L^{0.25} \cdot v_{air}^{0.5} \qquad 5.9$$

where,

UA Overall heat transfer coefficient (W/K)

n Shaking frequency (rpm)

V_L Filling volume (L)

v_{air} Lateral air velocity (m/s)

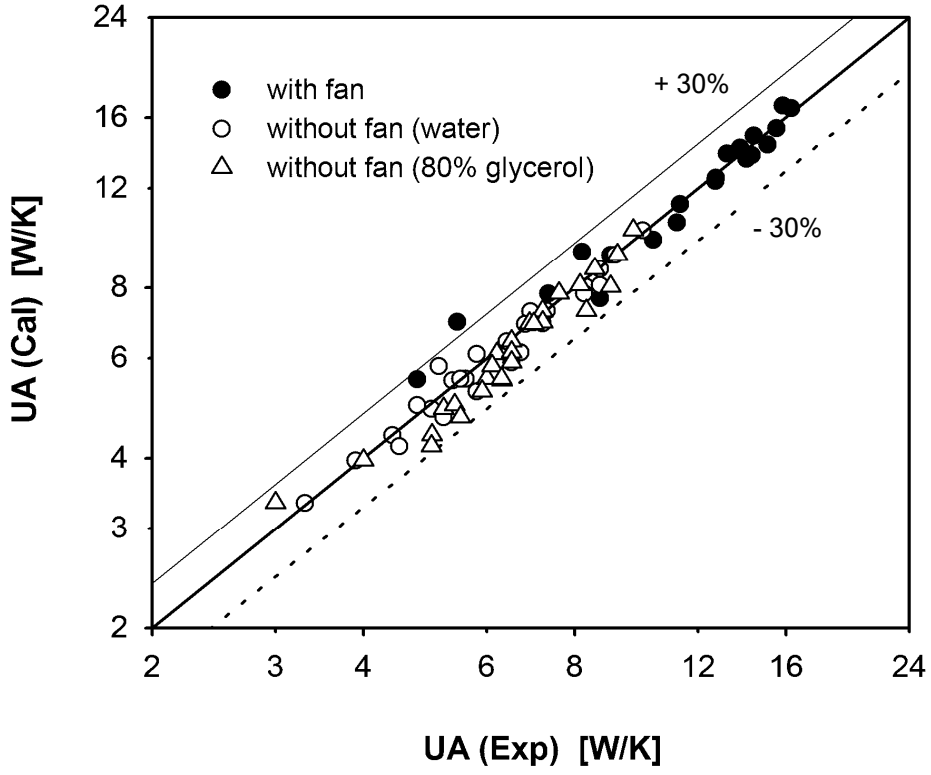

Figure 5.17: Parity plot of *UA* obtained experimentally and calculated based on the empirical equation.

The exponents of shaking frequency (0.55) and average air velocity (0.5) are much higher than that obtained in small shake flasks (0.19 and 0.2, respectively) (15). The turbulent air flow around the large shaking vessels and large surface area available for heat transfer may be responsible for the differences in the exponents. The parity plot of the *UA* values determined experimentally as well as the *UA* values determined according to above equation has been detailed in Figure 5.17. A good agreement between experimental and correlated values is obtained and the correlation can be applied while designing a biological experiment with large disposable shaking bioreactors. It also suggests that outside heat transfer coefficient is limiting factor and liquid side heat transfer is clearly not limiting step in overall heat transfer process because equation 5.9 holds good without incorporating the effect of fluid viscosity.

5.5.4. Estimation of outside heat transfer coefficient

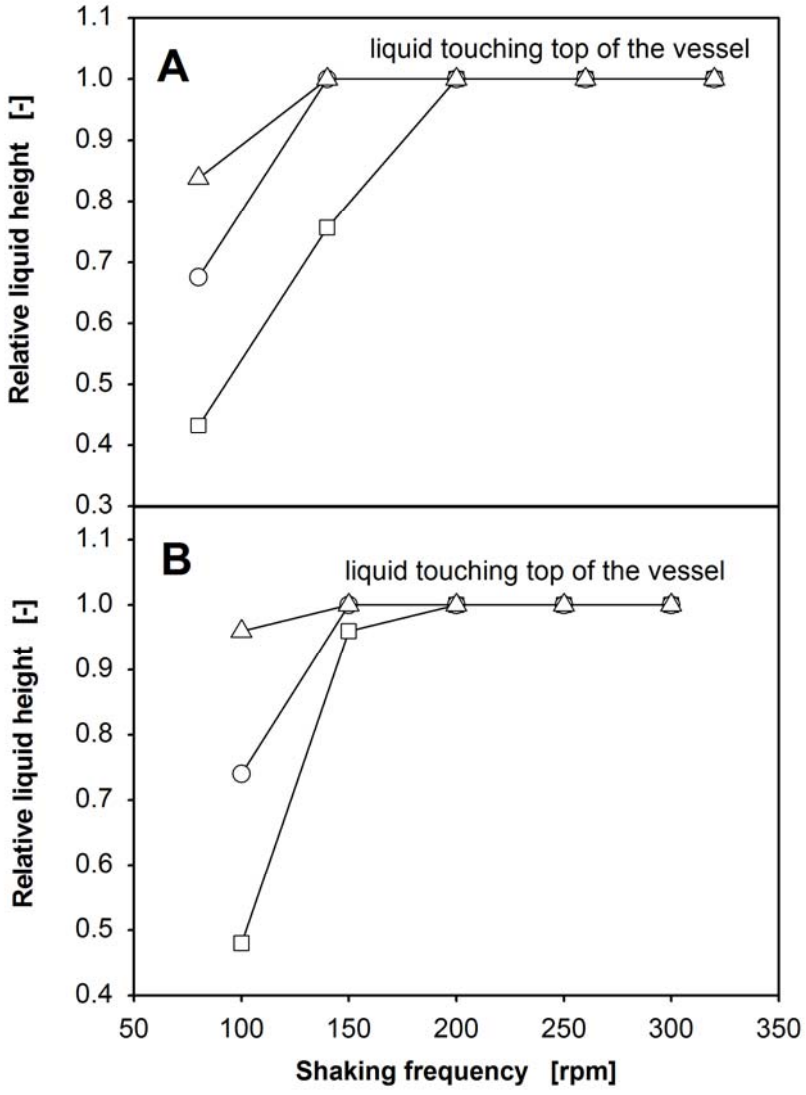

Figure 5.18: Relative liquid height in (A) 20L and (B) 50L vessel at different shaking frequencies and (□) 25%, (○) 50% and (△) 75% filling volumes. The water was used as a fluid and shaking diameter was 5 cm.

As described in section 5.5.2 and section 5.5.3, the outside heat transfer was limiting in overall heat transfer process from the fluid inside the vessel to the surrounding atmosphere. Therefore, from the values of overall heat transfer coefficient (*UA*), the heat transfer coefficient was measured by dividing the *UA* with the heat transfer area (*A*). The heat transfer area was calculated as described in section 4.5.3. Figure 5.18 shows the measured liquid (water as fluid) height in 20L and 50L vessel at different filing volumes. As the Figure 5.18 depicts, the liquid touched the vessel top at shaking frequencies higher than 150 rpm for all filling volumes.

The calculated heat transfer coefficient was converted into dimensionless form in terms of Nusselt number *(Nu)* and was correlated with the Reynolds number *(Re)* and Prandtl number *(Pr)* as follows,

$$Nu = 0.87 \cdot Re^{0.54} \cdot P_r^{0.35} \qquad 5.10$$

where,

$$Nu = \frac{h_g \cdot d}{k},\ Re = \frac{\rho \cdot v \cdot d}{\eta} \text{ and } P_r = \frac{c_p \cdot \eta}{k}$$

where,

h_g Outside heat transfer coefficient (W/m^2/K)

d Vessel diameter (m)

$\underline{K}$ Thermal conductivity of outside air (0.024 W/m/K) at 25°C

ρ Density of air (1.18 kg/m^3) at 25°C

υ Air velocity (m/s)

η Viscosiy of air ($1.85 \cdot 10^{-5}$ Pa·s) at 25°C

c_p Specifc heat capacity of air (1005 J/kg/K) at 25°C

A parity plot of correlated values and experimental values are shown in Figure 5.19. As shown in Fgiure 5.19, the correlation holds well with the accuracy of ±30%. Mizushina and Ogino (50) found the exponents of 0.6 and 0.3 for *Re* and P_r, respectively, while characterizing heat transfer from a long cylinder to a lateral air flow. The exponents of *Re* (0.54) and P_r (0.35) found in this study are within the reasonable limits of the exponents found by Mizushina and Ogino.

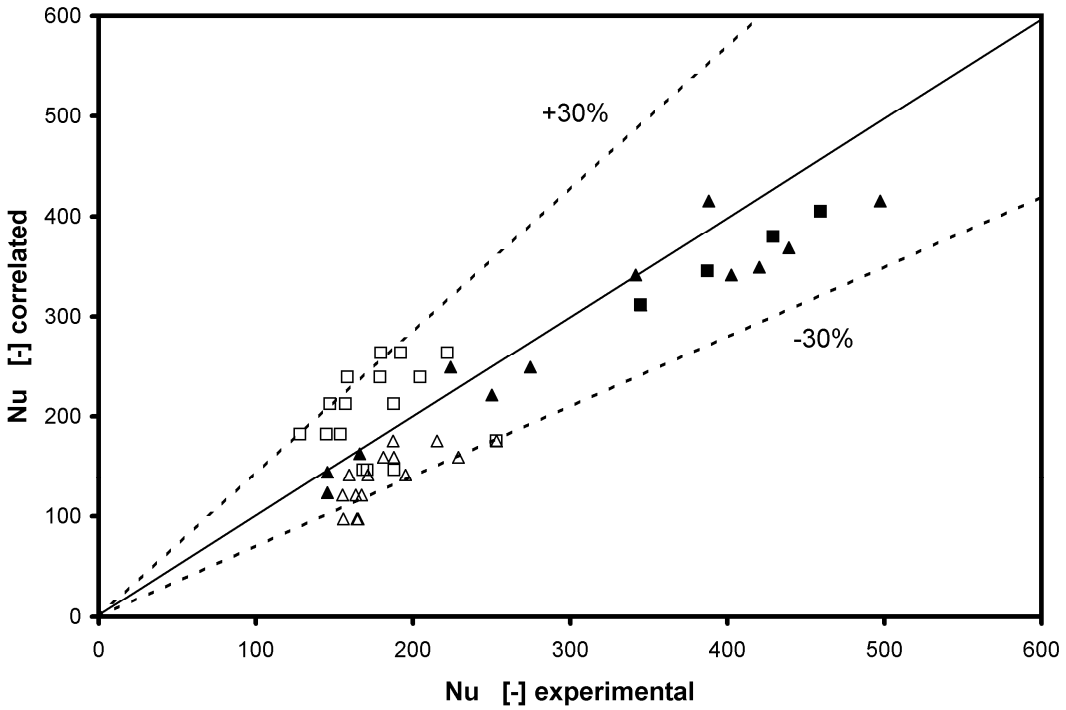

Figure 5.19: Parity plot of the experimental values of Nusselt number correlated with equation 5.10. The open symbols indicate values obtained in (△) 20L vessel, (□) 50L vessel without lateral air flow and filled symbols indicate values of Nusselt number for (▲) 20L vessel and (■) 50L vessel with lateral air flow.

5.6. Mass transfer characteristics of disposable shaking bioreactors

5.6.1. Oxygen transfer rate

The maximum oxygen transfer rate (OTR_{max}) in disposable shaking bioreactors was measured as described in section 4.6. Typical values of OTR_{max} are shown in Figure 5.20 measured at different filling volumes for disposable shaking bioreactors of size 20L and 50L. All the measurements were done in duplicates with an error of ±10% except the ones which are shown with error bars where margin of error was ±30%. The measurements shown with error bars were done in triplicates.

The OTR_{max} obtained in the 20L bioreactor was slightly higher than that for the 50L bioreactor for all operating conditions. However, the difference in values of OTR_{max} obtained in the 20L and the 50L bioreactor was not as large as it was found in small shake flasks where as the flask size increased there was a noticeable decrease in OTR_{max} for the same relative filling volumes (21). The filling volumes used for shake flasks were in the range of 4 to 16% of the total flask volume and the flask surface was hydrophilic. Therefore, for small shake flasks, at lower filling volumes, the mass transfer occurred mainly in a thin film of liquid formed on the surface of the flask wall. This caused much higher values of OTR_{max} obtained in small shake flasks as

compared to large shake flasks. Whereas here, much higher filling volumes in the range of 25 to 75% were used in a cylindrical bioreactor whose surface was hydrophobic in nature.

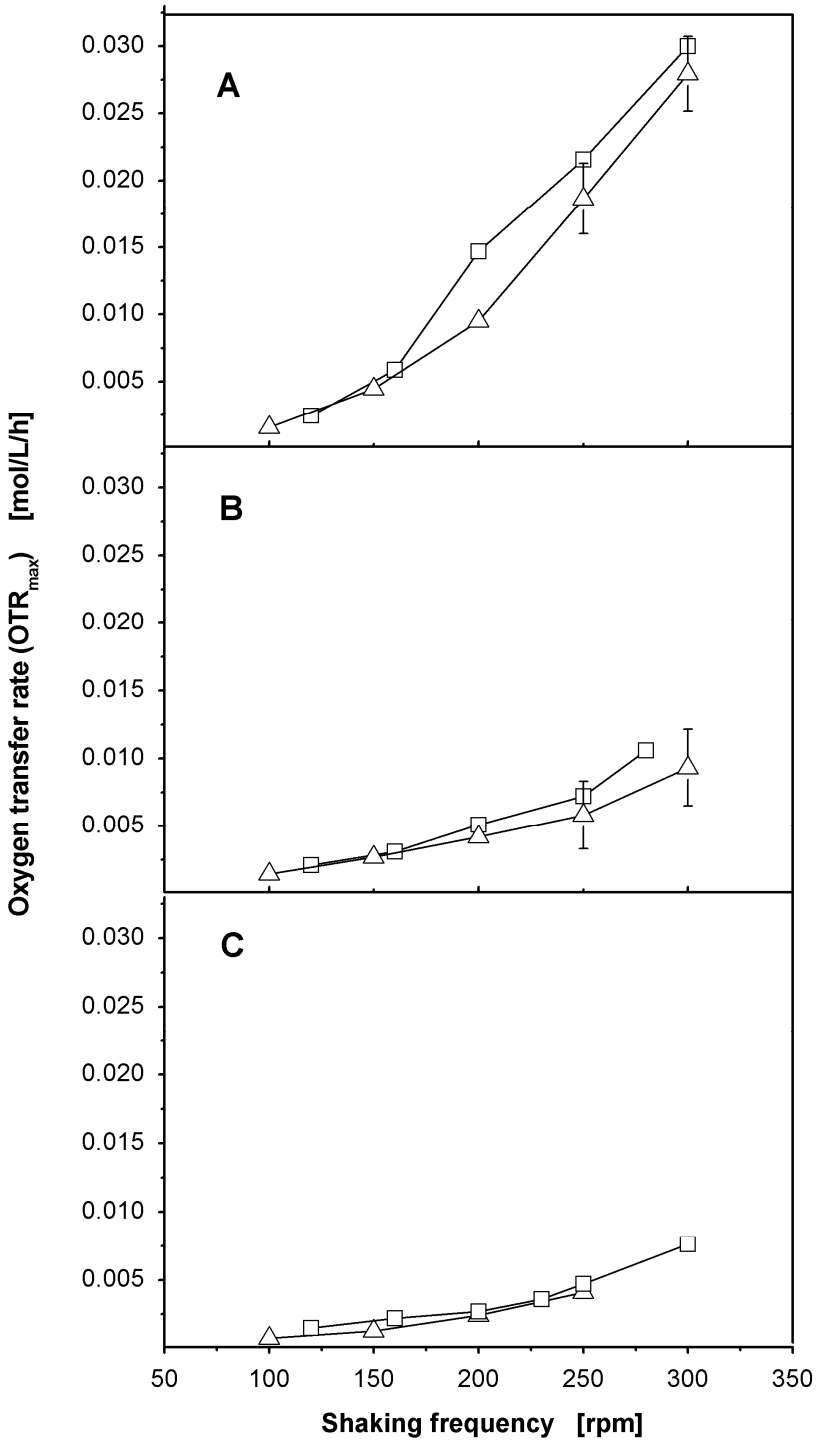

Figure 5.20: Maximum oxygen transfer rate obtained in (□) 20L and (△) 50L bioreactor at (A) 25%, (B) 50% and (C) 75% filing volume, respectively , 5 cm shaking diameter.

Therefore, the surface area to volume ration was inferior in large disposable shaking bioreactors in comparison to the small conical shake flasks. This could be the reason of the small differences obtained in the values of OTR_{max}. Kato et al. (27) also found

the similar results of small differences while working with large cylindrical vessels. Kato et al. employed 12 cm and 15 cm cylindrical shaking vessels. The shaking diameter was varied from 1 to 4 cm and shaking frequencies were varied from 75 to 200 rpm. Different filling volumes were used and the filling volume was characterized by the ratio of liquid height to vessel diameter (H/d). The H/d ratios of 0.5, 1 and 1.5 were investigated at different operating conditions. The maximum difference obtained in OTR_{max} values in 12 cm and 15 cm cylindrical vessel was 0.0018 mol/L/h at an H/d ratio of 0.5, a shaking diameter of 4 cm and 200 rpm shaking frequency.

The maximum and the minimum values of OTR_{max} investigated in this study were 0.032 mol/L/h (20L bioreactor, 25% filling volume, 300 rpm) and 0.00075 mol/L/h (50L bioreactor, 75% filling volume, 100 rpm), respectively. Animal and insect cell cultures have a typical oxygen demand of 0.0001 mol/h per 10^6 cells (11, 31). One of the fastest growing plant cell cultures, *Nicotiana tabacum* has a maximum oxygen demand of 0.008 mol/L/h (unpublished results). The actual OTR_{max} in an average biological medium is almost twice the value of OTR_{max} obtained using the sulfite oxidation method (51). Therefore, the OTR_{max} obtained in large shaking bioreactors is much higher than the oxygen demand of above mentioned plant, animal and insect cells and hence these cells can be easily cultivated at relatively “mild” operating conditions.

5.6.2. Correlation for volumetric mass transfer coefficient

Since oxygen transfer was mainly on the surface of the bulk liquid, power consumption was considered a measure to characterize the mass transfer from gas phase to liquid phase. Figure 5.21 presents the value of volumetric mass transfer coefficient (k_La) obtained with power consumption. As filling volume increased k_La decreased drastically in 20L and 50L bioreactors. The slope of the line reduced dramatically when filling volume was increased from 25 to 50% in both sizes of bioreactors. The solid symbols in the Figure 5.21 shows the operating conditions where the steady-state temperature difference between the fluid and surrounding atmosphere was less than 0.8 K. Correlations of k_La with power consumption are usually prepared for bubble columns and agitated stirred tanks (52-56). Kato et al. found such dependency of k_La in cylindrical shaking vessels (27). A typical correlation between k_La and power consumption can be written as follows,

$$k_L a = a \cdot P_V^{\ b} \cdot u_g^{c} \qquad 5.11$$

Where,

k_La Volumetric mass transfer coefficient (s)

a, b, c Constants,

P_v Volumetric power consumption (W/m^3)

u_g Superficial gas velocity. (m/s)

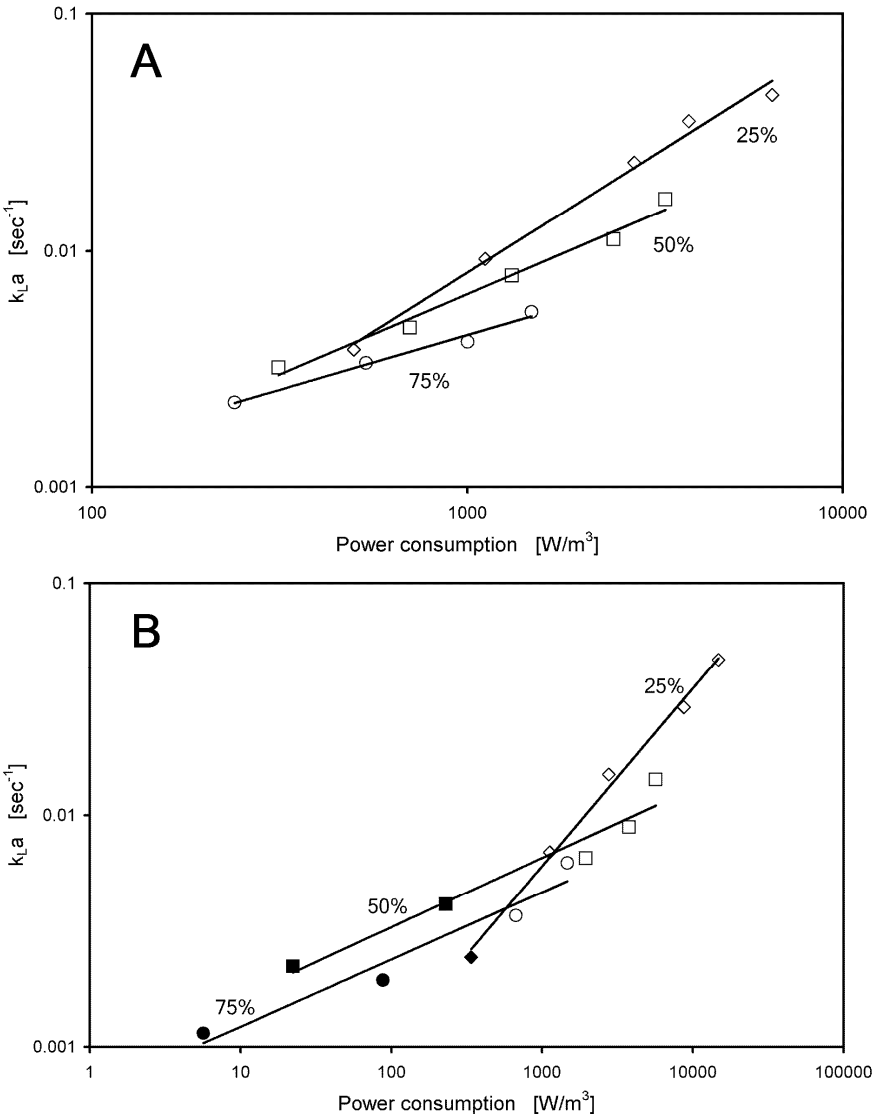

Figure 5.21: A plot of volumetric mass transfer coefficient versus volumetric power consumption for (A) 20L and (B) 50L vessel at different filling volumes (25, 50 and 75%) at 5 cm shaking diameter. Solid symbols represent operating conditions where steady-state temperature difference between fluid and surrounding atmosphere was less than 0.8 K.

In shaking bioreactors, the air was supplied on the surface of liquid and was not bubbled through the liquid. Therefore, the effect of the superficial gas velocity was not considered in the correlation. However, vessel diameter and filling volume affected the mass transfer characteristics; hence their effects were incorporated and data

points were correlated within the above equation to give a final equation of following form

$$k_L a = 1.5 \cdot 10^{-6} \cdot P_V^{1.01} \cdot d^{1.55} \cdot V_L^{-0.73} \qquad 5.12$$

where,

$k_L a$ Volumetric mass transfer coefficient (1/s)

P_V Volumetric power consumption (W/m^3)

d Vessel diameter (m)

V_L filling volume (m^3)

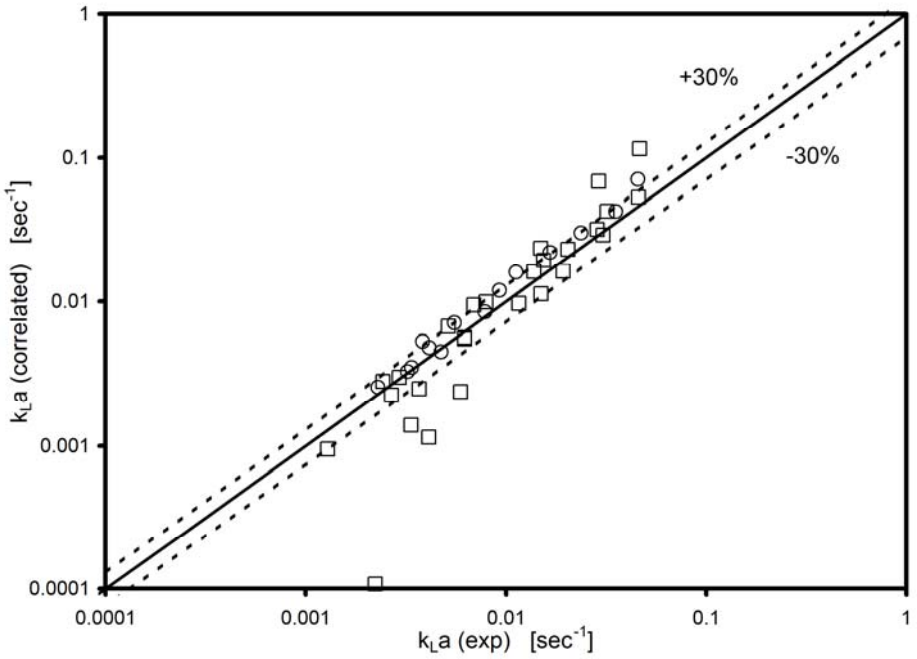

Figure 5.22: Parity plot for volumetric mass transfer coefficient obtained in (○) 20L and (□) 50L cylindrical shaking vessel at filling volumes in the range of 25% to 75% with 5 cm shaking diameter. The correlation is based on the equation 5.12.

As Figure 5.22 depicts, the correlation fits well with measured volumetric mass transfer coefficients. There are a few data points on the lower region of the graph which lie outside the range of 30%. These data points represent the operating conditions observed in 50L vessel, marked with solid symbols in Figure 5.21 where power consumption measured was much lower than expected thus giving large deviation in the correlated values of $k_L a$. Interestingly, there are a few data points at the upper region of the parity plot which lie outside the 30% margin. These data points represent shaking frequencies higher than 240 rpm. Careful investigation of Figure 5.21 reveals that $k_L a$ values found in 20L and 50L vessel, for filling volumes greater

than 25%, jumps up for P_V > 1000 W/m^3. The assumption of mass transfer occurring mainly in the fluid sequel may not be accurate for these operating conditions. The fluid inside the vessel may distribute over the entire surface of the cylindrical vessel; thus producing a mass transfer area larger than expected. This in turn may cause k_La values to shoot up. Interestingly, in the dissertation of Dr. Ulrike Maier (57), similar increasing trend of k_La values while working with hydrophobic shake flasks of size 250 mL is found. Following photo is taken from dissertation of Dr. Ulrike Maier which shows above mentioned effect.

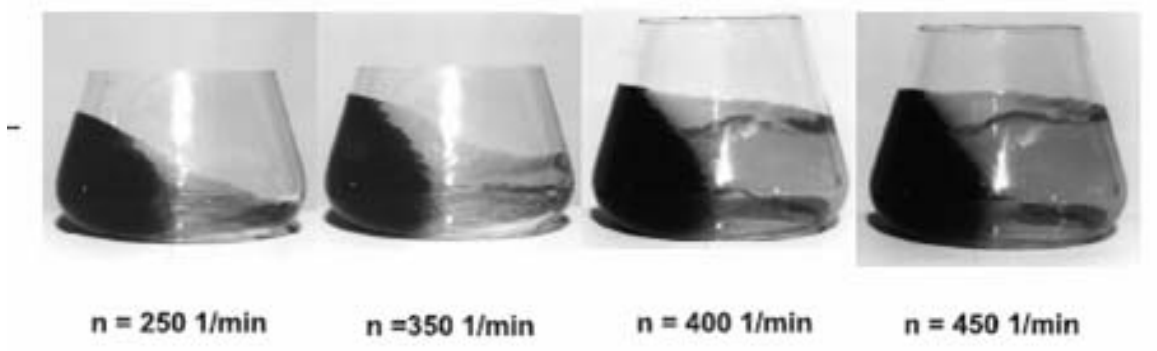

Figure 5.23: Film formation in a 250 mL hydrophobic shake flask, 10% filling volume, 5 cm shaking diameter. This photo is a courtesy of Dr. Ulrike Maier.

Dr. Ulrike Maier found that at a specific shaking frequency, the liquid inside the flask tend to distribute itself over the entire perimeter of flask thus causing a thin film of the fluid of a specific height along with the fluid sequel.

Kato et al derived following equation for characterization of mass transfer in cylindrical vessels (27)

$$k_La = 6 \cdot 10^{-5} \cdot P_V^{0.4} \cdot d^{-0.25} \cdot H^{-0.6} \qquad 5.13$$

where,

H Height of the liquid in vessel (m)

The exponent of P_v investigated in this research work is higher than that observed by Kato et al (27). Higher dependency of k_La on P_v can be explained by the fact that, in this study, a shaking diameter of 5 cm and shaking frequencies in the range of 100 to 300 rpm were employed. The values of P_v encountered were in the range of 5 to 13400 W/m^3. Whereas, Kato et al. varied shaking diameter and shaking frequency in the range of 1 to 4 cm and 72 to 200 rpm, respectively. The values of P_v encountered were in the range of 5 to 600 W/m^3. In addition, above equation can be rearranged by substituting equation 1 for power consumption and V_L to give following equation,

$$k_L a \sim N^{2.3} \cdot d^{0.95} \cdot d_0^{0.4} \cdot V_L^{-0.6} \qquad 5.14$$

Thus, the exponents of d (1.55) and V_L (-0.73) found in 20L and 50L cylindrical vessels are of the same order of that found by Kato et al (27). Interestingly, Maier et al. (21) also found similar dependency of $k_L a$ on flask diameter ($k_L a \sim d^{1.92}$) and filling volume ($k_L a \sim V_L^{-0.83}$) while working with conical shake flasks of size ranging from 50 mL to 2L. Equation 5.12 can be rearranged to give following equation,

$$k_L a = 1.5 \cdot 10^{-6} \cdot P_V^{1.01} \cdot \left(\frac{d^3}{V_L}\right)^{0.73} \cdot \frac{1}{d^{0.64}} \qquad 5.15$$

Thus, for same relative filling volumes, $k_L a$ is proportional to $d^{0.64}$. This proportionality is similar to that observed in conical shake flasks by Maier et al ($k_L a \sim d^{0.57}$) (21) and Henzler et al ($k_L a \sim d^{0.64}$) (23).

5.7. Application

5.7.1. Scale- up of plant cell culture process

A therapeutic protein production process based on the transgenic *Nicotiana tabacum* plant cell cultures was employed for scale-up studies. The transgenic plant cell cultures of *N. tabacum* producing human serum albumin (HSA) were obtained from the Institute of Molecular Biotechnology, RWTH Aachen. The oxygen transfer rate was used as a scale-up criterion since, these plant cells are not that sensitive to hydro-mechanical stress generated in a bioreactor (unpublished results). The plant cell culture growth is slow relative to microbial growth. Nevertheless, the maximum oxygen uptake rate of one of the fastest growing plant cells, *Nicotiana tabacum* is 0.008 mol/L/h in a standard MS medium. However, the production of therapeutic protein HSA is more in Gamborg's B5 medium than MS medium (unpublished results, information provided by Institute of Molecular Biotechnology, RWTH Aachen). The Gamoborg's B5 medium is less nutrient rich than MS medium (43, 44). Therefore, the maxium oxygen uptake rate of cells grown in Gamborg's B5 medium is ca. 0.0045 mol/L/h.

The sulfite system used for determination of OTR_{max} has a high concentration of ions which reduces the solubility of oxygen. Hence, the OTR_{max} obtained in a growth medium is almost double than that found using the sulfite system (51, 58). Comparison of OTR_{max} obtained in large disposable shaking bioreactors and maximum oxygen uptake rate of *N. tabacum* reveal that plant cell cultures can be

easily cultivated in large disposable bioreactors at relatively mild operating conditions (shaking frequencies less than 200 rpm).

The step by step scale-up process is described as followed.

5.7.1.1. Ventilation in shake flasks

At the Institute of Molecular Biotechnology, the suspension cultures are maintained in different size of wide neck conical shake flasks covered with aluminium foil. The flask closures have a considerable impact on diffusion of air in and out of the flask. A two flask method developed by Mrotzek et al. was used to find resistance for air diffusion in shake flasks covered with aluminum foil (28). Mrotzek et al. thoroughly investigated resistance of sterile closures to air diffusion in different sizes of shake flasks covered with different flask closures, namely, cotton plugs with different packing densities, silicon cap, aluminum cap etc. However, aluminum foil as a flask closure was not investigated. Since, tightness of aluminum foil covered on flask can vary from person to person, four persons were chosen for the experiment. Each person covered four wide neck shake flasks of the same size with the same filling volume. The resistance to air diffusion through the aluminum foil was then measured as described in materials and method section. From that, the aeration equivalent to the ventilation through the aluminum foil was measured by the model developed by Amoabediny et al. (39).

The preliminary experiments at the Institute of Molecular Biotechnology, RWTH Aachen suggested that a 250 mL wide neck conical shake flask with 150 filling volume produced maximum HSA in cell cultures of *N. tabacum*. Therefore, ventilation of shake flasks covered with aluminum foil was characterized and equivalent aeration was calculated with 60% filling volume. Figure 5.24 shows the aeration values equivalent to the actual ventilation through the aluminum foil obtained in four shake flasks covered with aluminum foil by four different persons. Very large variation in equivalent aeration was found. The minimum and maximum equivalent aeration were 0.02 and 0.1 vvm, respectively.

The error margin per person was also high. An error margin as large as 100% was obtained in an experiment (Person A). Minimum error margin of 15% was obtained in the flask covered by person D, where maximum ventilation was observed. The person who covered this shake flask was the most experienced of all the persons dealing with maintenance of plant cell culture. These results indicate highly unsuitable yet widely observed use of aluminum foil as shake flask closures. Moreover, aluminum foil does

not help at all in filtering the air passing through the gaps between glass wall and itself thus the probability of contamination is increased.

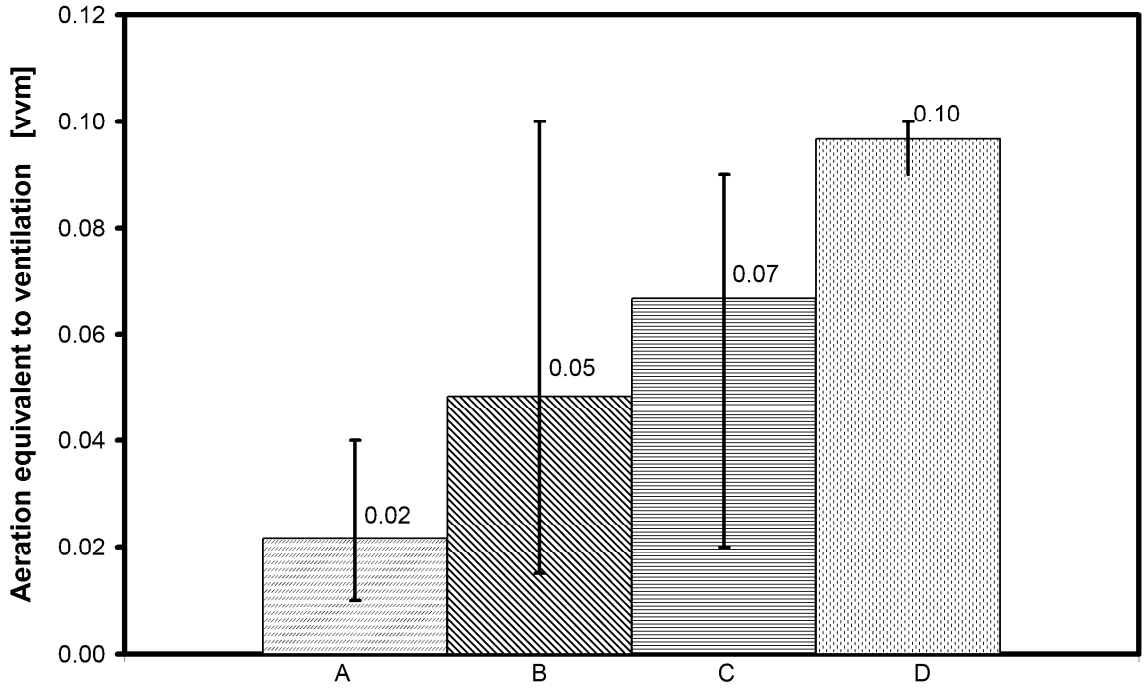

Figure 5.24: Equivalent aeration determined with aluminium foil as flask closure by model developed by Amoabediny et al. (39, 40). Four different persons (A, B, C, D) covered wide neck shake flasks of size 250 mL with 150 mL filling volume. The shaking frequency and shaking diameter were 180 rpm and 5 cm, respectively. Experiment was carried out in triplicates. Error bars shows maximum and minimum aeration obtained for each person.

Effect of flask closure on cell growth and HSA production is shown in Figure 5.25. Aluminum foil and cotton plugs were used as flask closure. The experiment was carried out in duplicate. Person D covered aluminum foil on each wide neck shake flask used for the experiment. Since an equivalent aeration of 0.1 vvm was achieved in flasks covered with aluminum foil by person D, the bulk density of cotton plugs (0.25 gm/cm^3) was chosen in such a way that the ventilation equivalent to an aeration of 0.1 vvm is achieved in each normal shake flask covered with cotton plug. A mathematical model developed by Anderlei et al. was used to calculate bulk density of cotton plug (28, 38). Cell growth was identical in flasks covered with cotton plug. The flasks covered with aluminum foil did not show reproducible results. The maximum relative error found was 20%. Moreover, maximum cell growth was attained in the shaken cultures covered with cotton plug. Figure 5.25 B shows HSA production in suspension cultures. There was no significant difference observed in specific HSA production in cell cultures covered with aluminum foil and cotton plug.

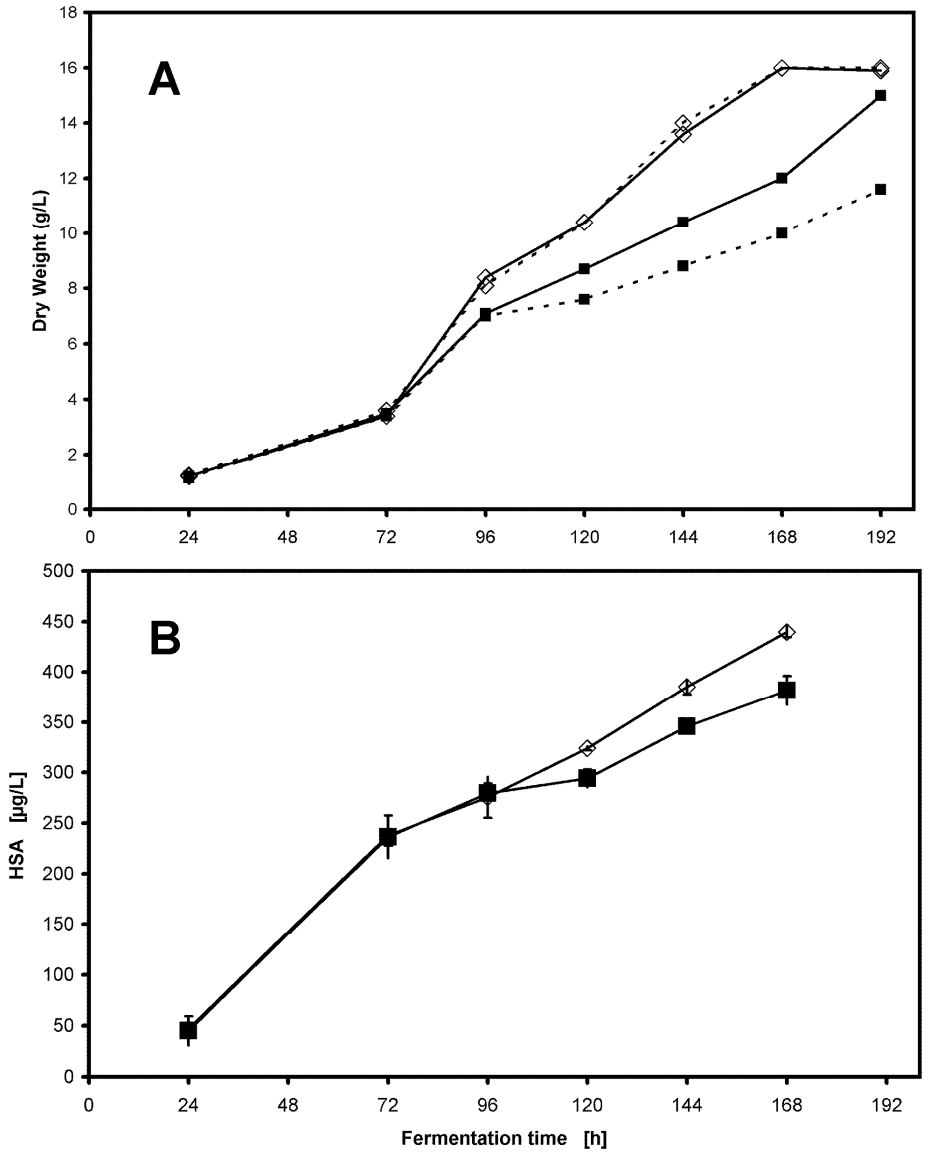

Figure 5.25: Effect of flask closure on (A) cell growth and (B) HSA production. Wide neck shake flasks were coved with (■) aluminium foil and (◇) normal neck flasks with cotton plug. Experiments were carried out in 250 mL shake flasks with 150 mL filling volume of Gamborg's B5 medium (44) at 180 rpm and 5 cm shaking diameter. Experiments were carried out in duplicates. Solid and dashed lines in Figure (A) represent cell growth in experiment 1 and 2, respectively. For simplicity, average values of HSA production obtained in duplicate experiments is shown in Figure (B) with error bars showing percentage error.

These findings indicated that cotton plugs are a better option for shake flask closures than aluminum foil. Here, self made cotton plugs and not commercially available paper plugs were used to achieve same ventilation as it was found in flasks covered with aluminum foil. Commercially available paper plugs also have good filtering properties and give reproducible results. Aluminum foils do not filter air at all and may loosen up with time when used as the flask closure. Therefore, it is recommended not to use aluminum foil as flask closures.

5.7.1.2. Cultivation of *N tabacum* cell culture in different bioreactors

5.7.1.2.1. Comparison between shake flask and 20L shaking bioreactor

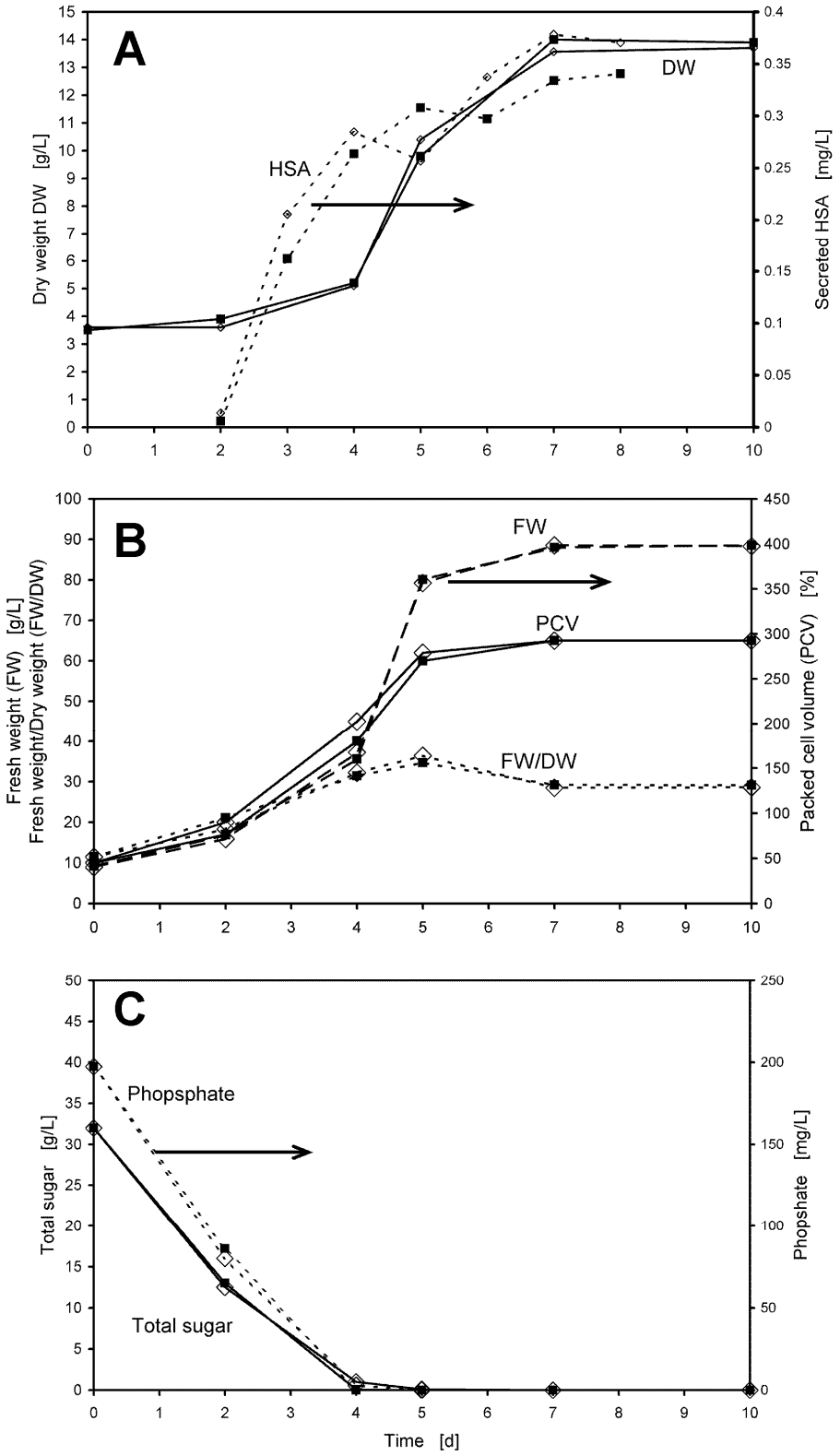

Figure 5.26: Growth and production profile of *N. tabacum* suspension cell cultures in a 250 mL shake flask with 50 mL filling volume (180 rpm) and a 20L disposable bioreactor with 10L filling volume (180 rpm), 5 cm shaking diameter. Figure 5.26 (A) indicates cell growth and HSA production, (B) indicates fresh weight, packed cell volume and fresh weight to dry weight ratio and (C) indicates concentration profiles of total sugar (sucrose+glucose+fructose) and phosphate.

Figure 5.26A shows the growth and production profile in cultures grown in a shake flask and a 20L bioreactor with 10L filing volume. The aeration rate in 20L disposable bioreactor was kept at 0.1 vvm. The suspension culture was not oxygen limited and dissolved oxygen level was above 10% saturation for the large disposable shaking bioreactors. Therefore, for simplicity, the DO profile is not shown. Figure 5.26 shows the growth and HSA production profile of *N. tabacum* cells. Growth and HSA production profile was almost identical in the shake flask and 20L bioreactor. The dry weight (DW), fresh weight (FW) and packed cell volume (PCV) increased over the fermentation period and then remained constant. The maximum packed cell volume of ca. 65% was observed. Almost 90% of a typical plant cell volume is filled with water and nutrients in a space called vacuole. The size of the vacuole increases the FW/DW ratio and PCV of plant cells more as compared to that of microbial and animal cells.

Figure 5.26C shows total sugar (sucrose + glucose + fructose) and phosphate uptake of the cells in both bioreactors. Total sugar was depleted from the medium in four to five days. Plant cell cultures initially uptake all the nutrient from the medium and grow in size. This can be seen in an increase of the FW/DW ratio. The FW/DW ratio increased up to day 5 and then decreased. The uptake of nutrients from the medium was similar to that observed by other authors in different plant suspension cultures (59-67). Since, there was no significant difference observed in nutrient uptake, FW/DW ratio and PCV by the plant cells in different sizes of bioreactors, only the dry cell mass and HSA production profiles are shown in all other experiments.

5.7.1.2.2. Comparison between disposable shaking bioreactor and standard stirred tank fermentor.

The *N. tabacum* cell culture growth and HSA production profile were also compared with a 10L standard stirred tank fermentor with 7L filling volume. The cell culture was cultivated at the same time in both types of bioreactors. Data of cell growth and production profile in the fermentor were provided by the group of contract manufacturing unit, Institute of Molecular Biotechnology, RWTH Aachen. There was no significant difference observed in maximum biomass level as well as HSA production profile in both kinds of bioreactors (Figure 5.27). However, cell growth was better than that in the fermentor as can be observed in the values of FW/DW ratio (Figure 5.27B). The maximum FW/DW ratio for the shaking bioreactor was 35 whereas maximum the FW/DW ratio observed for the stirred tank fermentor was 20.

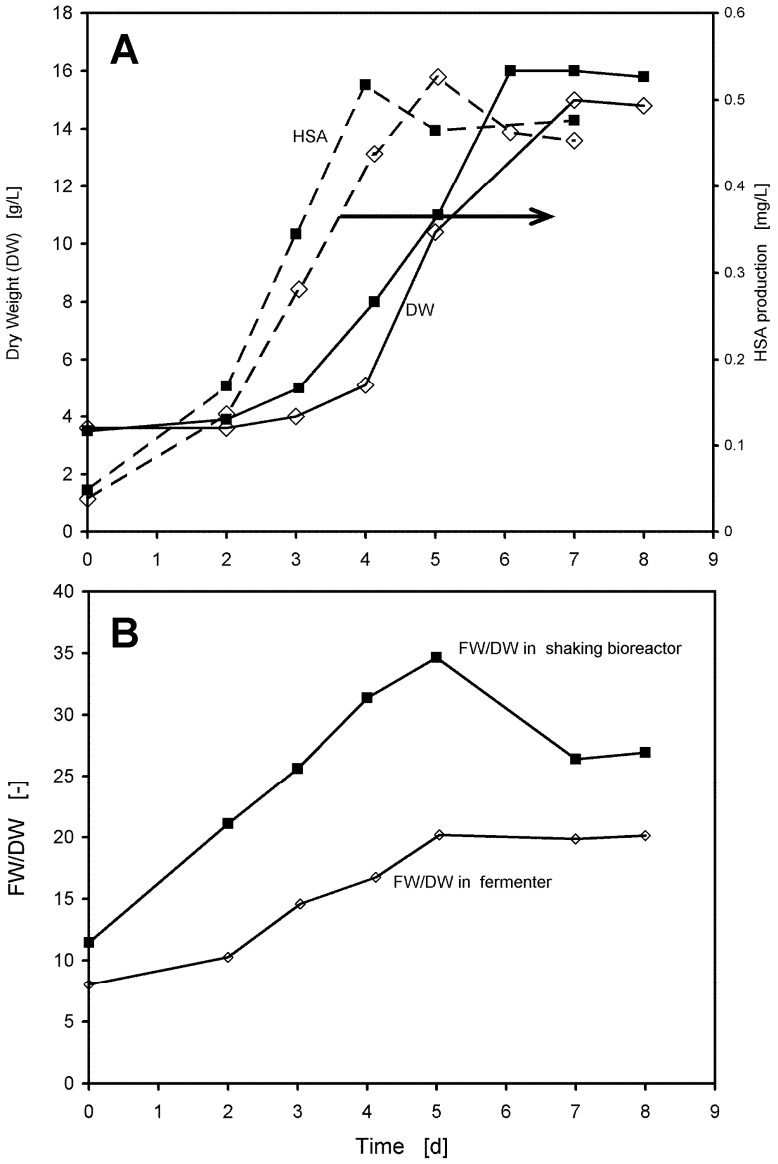

Figure 5.27: (A) Comparison of cell growth and HSA production in (■) 20L disposable bioreactor (10L filling volme) and (◇) a 10L stirred tank fermentor (7L filling volume). The shaking frequency and impeller speed were 190 rpm and 100 rpm, respectively. The aeration was 0.1 vvm. Figure (B) represents fresh weight to dry weight (FW/DW) ratio.

Air is passed through the culture medium in the fermentor which causes excessive foaming at high impeller speed. Although *N. tabacum* cells are less sensitive to hydro-mechanical stresses as compared to animal cells and other plant cell cultures, excessive levels of hydro-mechanical stress near the impeller region could cause the cells to shrink in size. Because of these two important reasons, the stirrer speed was kept at 100 rpm which may not be enough for thorough mixing of a cell culture. On contrary, the hydro-mechanical stress is evenly distributed in shaking bioreactors and is almost one magnitude lower than that generated in stirred tank reactors (13). Air is passed in the head space of the disposable shaking bioreactor which causes

significantly low foaming. Therefore, thorough mixing is achieved at low hydro-mechanical stress which favors “healthy” cell growth.

5.7.1.2.3. Scale-up to 50L disposable shaking bioreactor

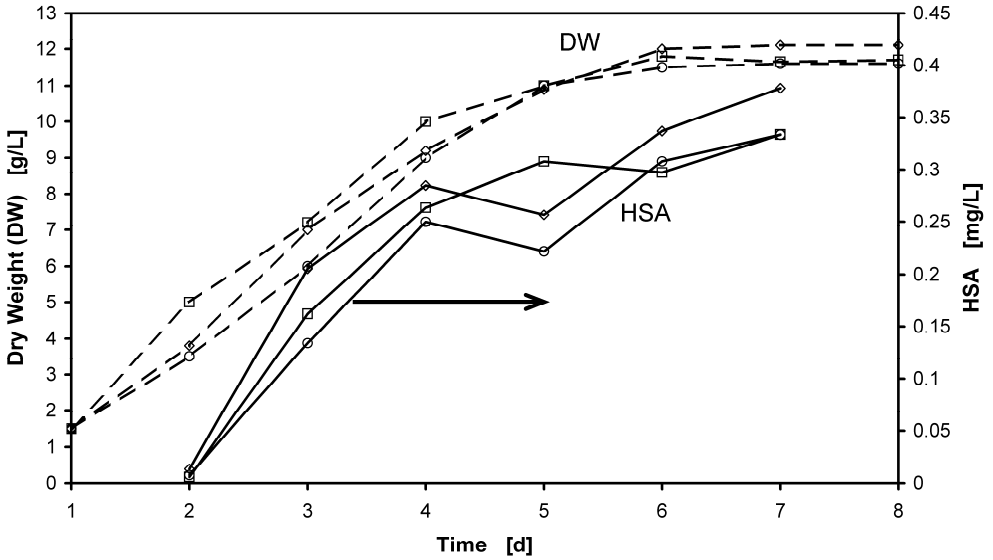

Figure 5.28: Growth and production profile in (◇) 250 mL shake flask (50 mL filling volume, 180 rpm), (□) 20L bioreactor (10L filling volume, 180 rpm) and (○) 50L bioreactor (35L filling volume, 200 rpm). Dashed lines indicate cell growth and solid lines represent HSA production profiles.

The HSA production process was further scaled-up to a 50L shaking bioreactor with 35L filling volume. Figure 5.28 compares the growth and HSA production profile in a 250 mL shake flask, 20L and 50L shaking bioreactor. The identical patterns of cell growth and HSA production in all bioreactors shows the successful applicability of disposable shaking bioreactors for plant cell culture system.

5.7.2. Scale-up of animal and insect cell culture

A hybridoma-cmyc cell culture was successfully cultivated in a 2L disposable shaking bioreactor with 1L filling volume. The live cell counts are shown in Figure 5.29. The live cell count increased from $1 \cdot 10^5$ cells/ml to almost $7 \cdot 10^5$ cells /ml. The pH and pO_2 level of the medium were maintained by 5% CO_2 enriched air in the head space. The shaking bioreactor was not aerated with the 5% CO_2 enriched air continuously but aeration was started manually when the pH value decreased less than 7 or the pO_2 value decreased less than 19% saturation. Because of the manual control of air flow, several small peaks were observed in the pH and pO_2 profile as shown in Figure 5.29. The hybridoma-cmyc cells were obtained from the Institute of Molecular Biotechnology, RWTH Aachen. The given hybridoma-cmyc cells were not grown to

large-scale to date in the Institute of Molecular Biotechnology, RWTH Aachen. Therefore, the cell growth medium as well as the operating conditions were not optimized and were chosen intuitively because the purpose of the experiment was to observe the growth pattern of animal cell culture system in disposable shaking bioreactor. The live cell count increased to almost 7 times which is comparable with cell growth observed by Liu et al. in cylindrical shaking bioreactors of size 20L (31, 32) and cell growth observed in Wave bioreactors (11). However, a detailed optimization of operating conditions and growth medium is mandatory for successful scale-up of the animal cell culture process.

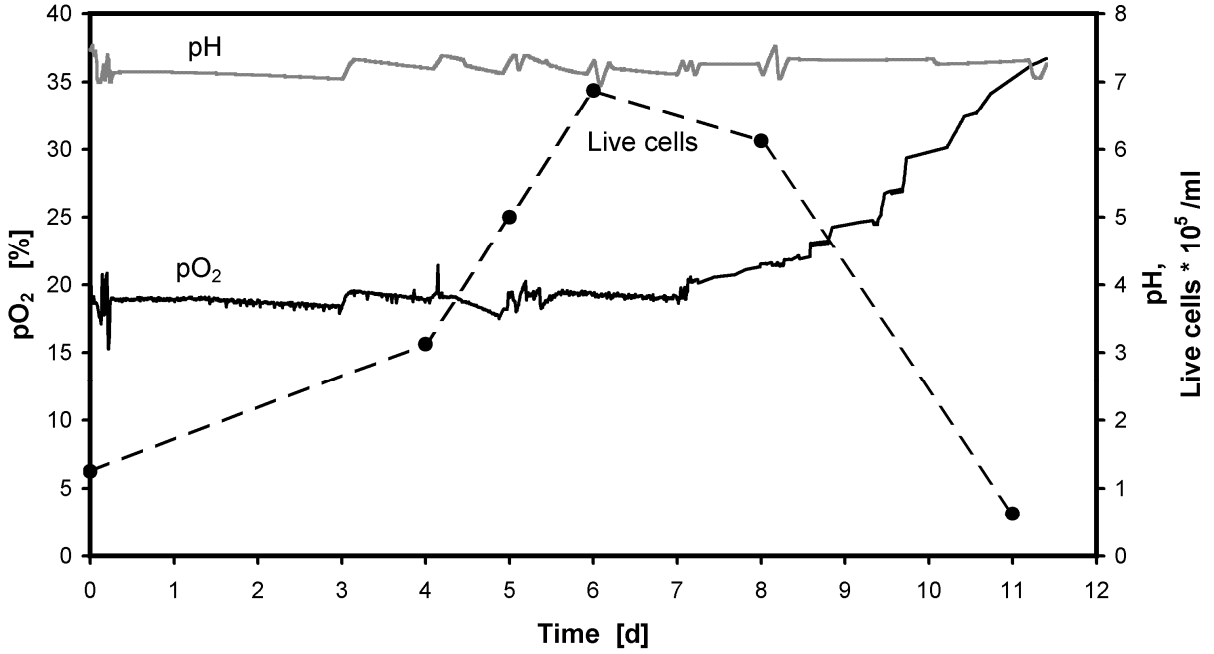

Figure 5.29: Hybridoma-cmyc cell cultivation in a 2L disposable shaking bioreactor with 1L filling volume, 95 rpm and 5 cm shaking diameter. An RPMI medium developed by Moore et al. (45) at Rosswell Park Memorial Institute (RPMI) was used for cultivation.

6. Conclusion

Shaking technology is not limited to lower volumes like µL and ml scale only. Large disposable shaking bioreactors are a promising alternative for high throughput recombinant protein production using plant, animal and insect cell cultures from laboratory scale to pilot scale.

Thorough mixing was achieved at low shaking frequencies. Hence, hydro-mechanical stress sensitive cell lines can be readily grown at mild operating conditions. However, some of the operating conditions observed in 50L bioreactor may lie between “in-phase” and “out-of-phase” condition, indicating the use of shaking diameter larger than 50 mm. The heat of mixing was enormous, especially at shaking frequencies higher than 250 rpm. Thorough ventilation is mandatory for high cell density cultivation of relatively fast growing plant cells and microbial cells. Measurement of oxygen transfer rate revealed that not only slow growing animal and insect cells but relatively fast growing plant cells can be easily grown in large disposable shaking bioreactors. The oxygen transfer rate was correlated with the power consumption. The seamless process scale-up based on one of the fastest growing *N. tabacum* plant cell suspension cultures shows the potential of this simple though highly efficient bioreactor system.

7. References

1. Gamerman, G., and Mackler, B., Winning in today's biopharmaceutical marketplace, *ChemTech, 24*, 37 (1994).
2. Basu, P., Quaadgras, J., Mack, R., and Noren, A., Achieve the right balance in pharmaceutical pilot plants, *Chemical Engineerig Progress, 94* (1998).
3. Burnett, M., Santamarina, V., and Omstead, D., Design of a multipurpose biotech pilot and production facility, *Annals of New York Academy of Sciences, 646*, 357-366 (1991).
4. Hamers, M., Multiuse biopharmaceutical manufacturing, *Biotechnlology, 11*, 561 (1993).
5. Savage, C., Scale-up and bioproduction, in *Genetic Engineering News*, Vol. 65, pp. 80 (2000).
6. Clemento, A., New and Integrated Approaches to Successful Accelerated Drug Development., *Drug Information Journal, 33*, 699 (1999).
7. Struck, M., Biopharmaceutical R&D success rates and development times, *Biotechnlology, 12*, 674 (1994).
8. Ernst, S., Garro, O., Winkler, S., Venkataraman, G., Langer, R., Cooney, C., and Sasisekaran, R., Process simulation for recombinant protein production: Cost estimation and sensitivity analysis for Heparinase I expressed in Escherichia Coli, *Biotechnology and Bioengineering, 53*, 575 (1997).
9. Novais, J. L., Economic comparison between conventional and disposable-based technology for the production of pharmaceuticals, *Biotechnology and Bioengineering, 75*, 143 (2001).
10. Falch, E. A., and Heden, C. G., Disposable shaker flasks, *Biotechnology and Bioengineering, 5*, 211 (1963).
11. Singh, V., Disposable bioreactors for cell culture using wave-induced agitation, *Cytotechnology, 30*, 149 (1999).
12. Eibl, R., Rutschmann, K., Lisica, L., and Eibl, D., Kosten reduzieren durch Einwegbioreaktoren, *Bio World, 5*, 22 (2003).
13. Büchs, J., Introduction to advantages and problems of shaken cultures, *Biochemical Engineering Journal, 7*, 91 (2001).
14. Sumino, Y., Akiyama, S. I., and Fukuda, H., Performance of the shaking flask, *Journal of Fermentation Technology, 50*, 203 (1972).
15. Sumino, Y., and Akiyama, S. I., Measurement of the overall volumetric coefficient of heat transfer of a shake flask, *Journal of Fermentation Technology, 65*, 285 (1987).
16. Büchs, J., Lotter, S., and Milbrandt, C., Out-of-phase operating conditions, a hetherto unknown phenomenon in shaking bioreactors, *Biochemical Engineering Journal, 7*, 135 (2001).
17. Büchs, J., Maier, U., Milbradt, C., and Zoels, B., Power consumption in shaking flasks on rotary shaking machines, II: Non-dimensional description of the

specific power consumption and flow-Regimes in unbaffled flasks at elevated liquid viscosity, *Biotechnology and Bioengineering, 68*, 594 (2000).

18. Büchs, J., Maier, U., Milbrandt, C., and Zoels, B., Power consumption in shaking flasks on rotary shaking machines: I. Power consumption measurement in unbaffled flasks at low liquid viscosity, *Biotechnology and Bioengineering, 68*, 589 (2000).

19. Büchs, J., and Zoels, B., Evaluation of maximum to specific power consumption ratio in shaking bioreactors, *Journal of Chemical Engineeing of Japan, 34*, 647 (2001).

20. Kato, Y., Hiraoka, S., Tada, Y., Koh, S. T., and Lee, Y. S., Mixing time and power consumption for a vertical cylindrical vessel, shaken in a horizontal circle, *Institution of Chemical Engineers, 74*, 451 (may 1996).

21. Maier, U., and Büchs, J., Characterisation of the gas-liquid mass transfer in shaking bioreactors, *Biochemical Engineering Journal, 7*, 99 (2001).

22. Haarde, W., and Zehner, P., Leistungseintrag und Stoffübertragung in Schüttelkolben., in *GVC Fachausschusstagung "Mischen"* (1992).

23. Henzler, H., and Schedel, M., Suitability of the shaking flask for oxygen supply to microbial cultures, *Bioprocess Engineering, 7*, 123 (1991).

24. Suijdam, J. v., Kossen, N., and Joha, A., Model for oxygen transfer in a shake flask, *Biotechnology and Bioengineering, XX*, 1695 (1978).

25. Veglio, F., Beolchini, F., and Ubaldini, S., Empirical models for oxygen mass transfer: a comparison between shake flask and lab-scale fermentor and application to manganiferous ore bleaching, *Process Biochemistry, 33*, 367 (1998).

26. Veljkovic, V., Nikolic, S., Lazic, M., and Engler, C., Oxygen transfer in flasks shaken on orbital shakers, *Chemistry and Industry, 49*, 265 (1995).

27. Kato, Y., Hiraoka, S., Tada, Y., Sato, K., and Ohishi, T., Measurement of mass transfer rate from free surface in shaking vessel type bioreactor, *Journal of Chemical Engineeing of Japan, 30*, 362 (1997).

28. Mrotzek, C., Anderlei, T., Henzler, H.-J., and Buechs, J., Mass transfer resistance of sterile plugs in shaking bioreactors, *Biochemical Engineering Journal, 7*, 107 (2001).

29. Millard, C., Stols, L., Quartey, P., Kim, Y., Dementieva, I., and Donnelly, M., A less laborious approach to the high-throughput production of recombinant proteins in Escherichia coli using 2-liter plastic bottles, *Protein Expression and Purification, 29*, 311 (2003).

30. Muller, N., Girard, P., Hacker, D., Jordan, M., and Wurm, F., Orbital shaker technology for the cultivation of mammalian cells in suspension, *Biotechnology and Bioengineering, 89*, 400 (2005).

31. Liu, C.-M., and Hong, L.-N., Development of shaking bioreactor system for animal cell cultures, *Biochemical Engineering Journal, 7*, 121 (2000).

32. Raval, K., Liu, C.-M., and Büchs, J., Large-Scale Disposable Shaking Bioreactors: A Promising Choice, *Bioprocess International, 4*, 34 (2006).

33. Perry, R. H., and Green, D. W., *Perry's Chemical Engineers' handbook*, McGraw-Hill (1997).

34. Chen, Y.-M., and Pearlstein, A. J., Viscosity-temperature correlation for glycerol-water solutions, *Industrial and Engineeirng Chemistry Research, 26*, 1670 (1987).

35. Linek, V., and Vacek, V., Chemical engineering use of catalyzed sulfite oxidation kinetics for the determination of mass transfer characteristics of gas-liquid contactors, *Chemical Engineering Science, 36*, 1747 (1981).

36. Hermann, R., Walther, N., Maier, U., and Büchs, J., Optical Method for the determination of the oxygen-transfer capacity of small bioreactors based on sulfite oxidation, *Biotechnology and Bioengineering, 74*, 355 (2001).

37. Anderlei, T., and Büchs, J., Device for sterile online measurement of the oxygen transfer rate in shaking flasks, *Biochemical Engineering Journal, 7*, 157 (2001).

38. Anderlei, T., Mrotzek, C., Bartsch, S., Amoabediny, G., Peter, C. P., and Buchs, J., New method to determine the mass transfer resistance of sterile closures for shaken bioreactors, *Biotechnology and Bioengineering* (2007).

39. Amoabediny, G., and Büchs, J., Modelling and advanced understanding of unsteady-state gas transfer in shaking bioreactors, *Biotechnol Appl Biochem, 46*, 57 (2007).

40. Amoabediny, G., A New Method to Quantify the CO2 Sensitivity of Micro-organisms in Shaken Bioreactors and Scale up to Stirred Tank Fermentors, in *Biochemical Engineering, Aachenerverfahrenstechnik*, RWTH Aachen Technical University, Aachen, pp. 150 (2007).

41. Buechs, J., Maier, U., Milbrandt, C., and Zoels, B., Power consumption in shaking flasks on rotary shaking machines: I. Power consumption measurement in unbaffled flasks at low liquid viscosity, *Biotechnology and Bioengineering, 68*, 589 (2000).

42. Kato, Y., Hiraoka, S., Tada, Y., Takafumi, U. E., and Saito, T., Improvement of a particle dispersion in a shaking vessel with current pole, *Journal of Chemical Engineeing of Japan, 29*, 697 (1996).

43. Murashige, T., and Skoog, F., A revised medium for rapid growth and bioassay with tobacco cell cultures, *Physiology Planta, 15*, 473 (1962).

44. Gamborg, O., Miller, R., and Ojima, K., Nutrient requirements of suspension culture of soyabean root cells, *Experimental Cell Research, 50* (1968).

45. Moore, G. E., and Woods, L. K., Culture media for human cells RPMI-1603, RPMI-1634, RPMI-1640, *Tissue Culture Association Manual, 3*, 503 (1976).

46. Lotter, S., Leistungseintrag und Hydrodynamische Phaenomene in Geshuettelten Bioreaktoren, in *Institute of Biochemical Engineering*, RWTH Technical University, Aachen, pp. 163 (2001).

47. Semena, M., and Khmelev, Y., Hydrodynamic regimes of a liquid in a smooth-walled rotating heat pipe, *Journal of Engineering Physics, 43*, 1235 (1982).

48. Kato, Y., Peter, C., Akgün, A., and Büchs, J., Power consumption and heat transfer in large rotary shaking vessels by temperature method, *Biochemical Engineering Journal, 83*, 83 (2004).

49. Calderbank, P. H., and Moo-Young, M. B., The continuous phase heat and mass-transfer properties of dispersions, *Chemical Engineerig Science, 16*, 39 (1961).

50. Mizushina, T., and Ogino, F., *Transport Phenomena*, Sangyo Tosho, Tokyo, Japan (1981).

51. Stöckmann, C., Maier, U., Anderlei, T., Knocke, C., Gellissen, G., and Büchs, J., The oxygen transfer rate as key parameter for the characterization of Hansenula polymorpha screening cultures, *Journal of Industrial Microbiology and Biotechnology, 30*, 613 (2003).

52. Linek, V., Moucha, T., and Sinkule, J., Gas-liquid mass transfer in vessels stirred with multiple impellers-I: Gas-liquid mass transfer characteristics in individual stage, *Chemical Engineerig Science, 51* (1996).

53. Linek, V., Vacek, V., and Benes, P., A critical review and experimental verification of the correct use of the dynamic method for the determination of oxygen transfer in aerated agitated vessels to water, electrolyte solutions and viscous liquids, *Chemical Engineering Journal, 34*, 11 (1987).

54. Smith, J., Riet, K. v. t., and Middleton, J., Scale-up of agitated gas-liquid reactors for mass transfer, in *Second European Conference on Mixing*, Vol. F4, Cambridge, England, pp. 51 (1977).

55. Zlokarnik, M., Sorption characteristics for gas-liquid contacting in mixing vessels, *Advances in Biochemical Engineering, 8*, 133 (1979).

56. Riet, K. V. t., Review of measuring methods and results in nonviscous gas-liquid mass transfer in stirred vessels, *Industrial and Engineering Chemistry Process Design, Dev, 18*, 357 (1979).

57. Maier, U., Gas/Flüssigkeit Stofftransfer im Schüttelkolben, in *Institute of Biochemical Engineering*, RWTH Technical Universtiy, Aachen, pp. 105 (2002).

58. Akgün, A., Maier, B., Preis, D., Roth, B., Klingelhofer, R., and Büchs, J., A novel parallel shaken bioreactor system for continuous operation, *Biotechnology Progress, 20*, 1718 (2004).

59. Baumchen, C., Knoll, A., Husemann, B., Seletzky, J., Maier, B., Dietrich, C., Amoabediny, G., and Buchs, J., Effect of elevated dissolved carbon dioxide concentrations on growth of Corynebacterium glutamicum on D-glucose and L-lactate, *Journal of Biotechnology, 128*, 868 (2007).

60. Chattopadhyay, S., Srivastava, A. K., Bhojwani, S. S., and Bisaria, V. S., Production of podophyllotoxin by plant cell cultures of Podophyllum hexandrum in bioreactor, *Journal of Bioscience and Bioengineering, 93*, 215 (2002).

61. Hiroyuki Honda, K. H., Eiji Nagamori, Mariko Omote, Yoshihito Kato, Setsuro Hiraoka, Takeshi Kobayashi, Enhanced Anthocyanin production from grape callus in an air-lift type bioreactor using a viscous additive supplemented medium, *Jornal of Bioscience and Bioengineering, 94*, 135 (2002).

62. Pestchanker, L., Roberts, S., and Schuler, M., Kinetics of taxol production and nutrient use in suspension cultures of Taxus cuspidata in shake flasks and a Wilson-type bioreactor, *Enzyme and Microbial Technology, 19*, 256 (1995).

63. Raval, K. N., Hellwig, S., Prakash, G., Ramos-Plasencia, A., Srivastava, A., and Büchs, J., Necessity of a two-stage process for the production of azadirachtin-related limonoids in suspension cultures of Azadirachta indica, *Journal of Bioscience and Bioengineering, 96*, 16 (2003).

64. Hellwig, S., Drossard, J., Twyman, R. M., and Fischer, R., Plant cell cultures for the production of recombinant proteins, *Nature Biotechnology, 22*, 1415 (2004).

65. Schinkel, H., Schiermeyer, A., Soeur, R., Fischer, R., and Schillberg, S., Production of an active recombinant thrombomodulin derivative in transgenic tobacco plants and suspension cells, *Transgenic Research, 14*, 251 (2005).

66. Lee, S., Kim, Y., Roh, Y., Myoung, H., Lee, K., and Kim, D., Bioreactor operation for transgenic Nicotiana tabacum cell cultures and continuous production of recombinant human granulocyte-macrophage colony-stimulating factor by perfusion culture, *Enzyme and Microbial Technology, 35*, 663 (2004).

67. Shibasaki, N., Hirose, K., Yonemoto, T., and Tadaki, T., Suspension culture of Nicotiana tabacum cells in a rotary-drum bioreactor, *Journal of Chemical Technology and Biotechnology, 53*, 359 (1986).

Appendix A: Dimensionless numbers

Fr_a	Axial Froude number	$Fr_a = \frac{(2 \cdot \pi \cdot n)^2 \cdot d_0}{2 \cdot g}$
Fr_r	Radial Froude number	$Fr_r = \frac{(2 \cdot \pi \cdot n)^2 \cdot d}{2 \cdot g}$
GR	Geometric ratio	$GR = \frac{d_0}{d}$
Ha	Hatta number	$Ha = \frac{Reaction\ rate}{Mass\ transfer\ rate}$
Ne	Newton number	$Ne = \frac{P}{\rho \cdot n^3 \cdot d^5}$
Ne'	Modified Newton number	$Ne' = \frac{P}{\rho \cdot n^3 \cdot d^4 \cdot V_L^{\frac{1}{3}}}$
Nu	Nusselt number	$Nu = \frac{h \cdot D}{k}$
Ph	Phase number	$Ph = \frac{d}{d_0} \cdot \left(0.41 + 4.24 \cdot \log\left(\mathrm{Re}_f\right)\right)$
Pr	Prandtl number	$P_r = \frac{c_p \cdot \eta}{k}$
Re	Reynolds number	$\mathrm{Re} = \frac{\rho \cdot n \cdot d^2}{\eta}$
Re_f, Re_{film}	Film Reynolds number	$\mathrm{Re}_f = \frac{\rho \cdot (2 \cdot \pi \cdot n) \cdot f^2}{\eta}$

Appendix B: Symbols

a	Constant	[-]
a	Slope of the calibration curve for oxygen sensor	[V/bar]
A	Heat transfer area	[m^2}
b	Constant	[-]
c	Constant	[-]
c_{O2}	Concentration of oxygen in bulk liquid	[mol/L]
c^*_{O2}	Concentration of oxygen in gas-liquid interface	[mol/L]
c_p	Specific heat capacity	[J/kg/K]
d	Maximum inside diameter of the vessel	[m]
d_0	Shaking diameter	[m], [cm]
D_{AB}	Diffusivity	[m^2/s]
f	Film thickness	[m]
g	Gravitational acceleration	[m/s^2]
h	Heat transfer coefficient	[$W/m^2/K$]
H	Liquid height	[m]
He	Henry's constant	[bar·L/mol]
h_g	Gas side heat transfer coefficient	[$W/m^2/K$]
h_L	Liquid side heat transfer coefficient	[$W/m^2/K$]
k	Thermal conductivity	[W/m/K]
k_1	First order reaction constant for sulfite oxidation	[1/s]
k_La	Volumetric mass transfer coefficient	[1/s]
k_{plug}	Gas transfer coefficient	[1/s]
l	Thickness of vessel wall	[m]
m	Mass of the fluid	[kg]
m	Slope of the voltage signal of oxygen sensor	[V/s]
M	Torque	[N·m]
n	Shaking frequency	[1/s]
$\dot{n}$	Molar flow rate	[mol/s]

Symbols

n_c	Critical shaking frequency	[1/s]
n_{crit}	Critical shaking frequency	[1/min]
$\dot{n}^{in/out}$	Molar flow rate of air entering and leaving the system, respectively	[mol/s]
$\dot{n}^{\alpha}$	Molar flow rate of oxygen transferred from the gas phase to the liquid phase	[mol/s]
OTR_{flow}	Oxygen transfer rate because of aeration of flask	[mol/L/s]
OTR_m	Oxygen transfer rate corresponding to slope m	[mol/L/s]
OTR_{max}	Maximum oxygen transfer rate	[mol/L/s], [mol/L/h]
OTR_{plug}	Oxygen transfer rate through the flask closure	[mol/L/s]
p	Total pressure	[bar]
P	Power consumption	[W]
p_{abs}	Absolute pressure	[bar]
p_i	Partial pressure of component i	[bar]
p^N	Normal pressure	[bar]
p_{O2}	Partial pressure of oxygen in gas phase	[bar]
p_{O2}	Partial pressure of oxygen in the head space of shake flask	[bar]
p_{O2out}	Partial pressure of oxygen in surrounding atmosphere	[bar]
P_v	Volumetric power consumption	[W/m^3]
q_{in}	Specific aeration rate	[L/L/s], [L/L/m]
R	Ideal gas constant	[bar·L/mol/K]
t	Time	[s]
T	Temperature	[K]
T_f	Fluid temperature	[K]
T^N	Normal temperature	[K]
T_o	Surrounding temperature	[K]
U	Sensor signal	[Volt]
U	Overall heat transfer coefficient	[W/m^2/K]
UA	Overall heat transfer coefficient	[W/K]

Symbols

u_g	Superficial gas velocity	[m/s]
v_{air}	Air velocity	[m/sec]
V_F	Vessel volume	[m^3]
V_G	Head space volume	[L]
V_L	Filling volume	[m^3]
V_m	Molar volume of a gas	[L/mol]
$\dot{V}^{in}$	Volumetric flow rate entering the system	[L/s]
y_i	Mole fraction of component i	[-]
$y_{O2}^{in/out}$	Mole fraction of oxygen in the gas phase entering and leaving the system, respectively	[-]
Z_k	Number of flasks	[-]

Appendix C: Greek symbols

η	Dynamic viscosity	[Pa·s]
ν	Kinematic viscosity	[m^2/s]
ρ	Density	[kg/m^3]
ε	Energy dissipation	[W/kg]

Appendix D: Proposed level of hydro-mechanical stress generation

Following Figure describes proposed level of hydro-mechanical stress generation in a 20L shaking bioreactor. The experiment was carried out as described by Büchs et al. (19). An aqueous/organic well defined coalescence inhibited two phase system was used. The membrane filtered water was buffered with 40 mM TRIS buffer (analytical grade, Merck, Germany). The pH was adjusted to 7.5 by addition of concentrated hydrochloric acid. Coalescence was inhibited by addition of LEO 30 (Lauryl ethylene oxide, BASF AG, Germany). A mixture of toluene (analytical grade, Merck, Germany) and carbon tetrachloride (analytical grade, Merck, Germany) (4:1) was used as organic phase. The relative volume of organic phase was 3% in aqueous phase. This mixture was poured into the vessel. The solution was mixed at any given operating condition and samples were taken after every hour to measure droplet diameter. The droplet diameter was measured by a Fraunhofer laser diffraction spectrometer (LS100Q, Coulter, Florida USA). The maximum droplet diameter was used as a measure of maximum power consumption obtained at given operating conditions. However, after 4 hours polymer particles could be seen in the sample. The polypropylene material of the cylindrical vessel was dissolved in the carbon tetrachloride. Therefore, the measurements could not be performed further and the data could not be incorporated into the thesis. Hence they are represented in this appendix.

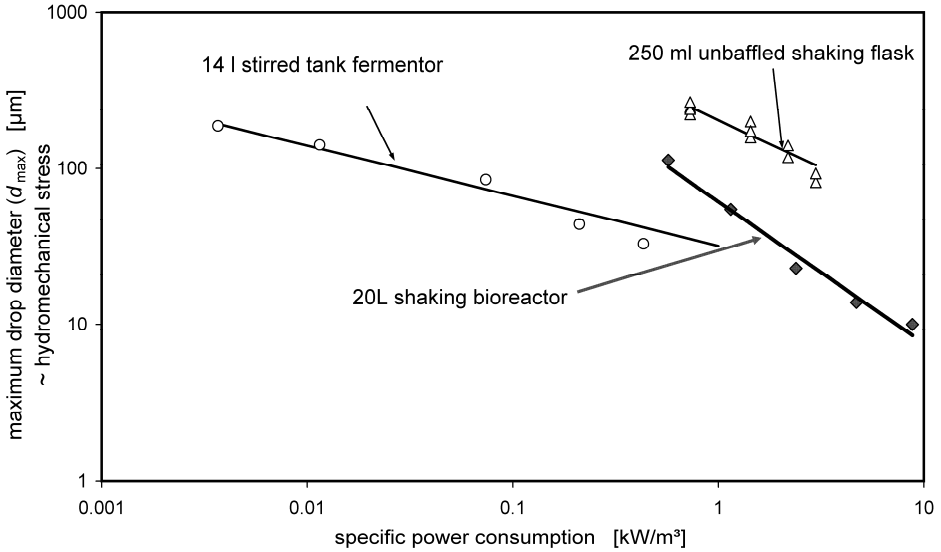

Fig D.1: Maximum drop diameter in (○) stirred tank fermentor, (△) 250 mL shake flask with 10% filling volume, 2.5 cm shaking diameter and (◆) 20L disposable shaking bioreactor with 5 cm shaking diameter.

Resume

Name	Keyur Raval
Birthdate	08.09.1977 in Rajkot, India

Schooling

07.1984 - 06.1985	St. Xaviours School, Rajkot, India
07.1985 - 06.1995	S. V. Virani School, Rajkot, India

University

07.1995 – 06.1999	Chemical Engineering from L. D. College of Engineering, Gujarat University, India
07.2000 – 07.2002	M.S. in Biochemical Engineering from Indian Institute of Technology Delhi, India

Professional Experience

10.2002 – 03.2006	Research associate at Institute of Biochemical Engineering, RWTH Aachen

Lebenslauf

Name	Keyur Raval
Geburtsdatum	08.09. 1977 in Rajkot, Indien

Schulausbildung

07.1984 - 06.1985	St. Xaviours School, Rajkot, Indien
07.1985 - 06.1992	S. V. Virani School, Rajkot, Indien
07.1992 - 06.1995	Gymnasium, S. V. Virani School, Rajkot, Indien

Studium

07.1995 - 06.1999	Verfahrenstechnik am L. D. College of Engineering, Gujarat Universität, Indien
07.2000 - 07.2002	M. S. in Bioverfahrenstechnik am Indian Institute of Technology Delhi, Indien

Berufstätigkeit

10.2002 – 03.2006	Wissenschaftlicher Mitarbeiter Lehrstuhl für Bioverfahrenstechnik der RWTH Aachen